

PhD PROCEEDINGS

ANNUAL ISSUES OF THE DOCTORAL SCHOOL

FACULTY OF INFORMATION TECHNOLOGY & BIONICS

2020

PhD PROCEEDINGS

ANNUAL ISSUES OF THE DOCTORAL SCHOOL

FACULTY OF INFORMATION TECHNOLOGY & BIONICS
PÁZMÁNY PÉTER CATHOLIC UNIVERSITY

PhD PROCEEDINGS

ANNUAL ISSUES OF THE DOCTORAL SCHOOL
FACULTY OF INFORMATION TECHNOLOGY & BIONICS
2020



PÁZMÁNY *1635*
— s i n c e

PÁZMÁNY UNIVERSITY *e*PRESS
BUDAPEST, 2020

© PPKE Információs Technológiai és Bionikai Kar, 2020

HU ISSN 2064-7271

Kiadja a Pázmány Egyetem eKiadó
Budapest, 2020

Felelős kiadó
Rev. Mons. Dr. Kuminetz Géza
a Pázmány Péter Katolikus Egyetem rektora

The publication of this volume was supported by the European Union,
co-financed by the European Social Fund (EFOP-3.6.3-VEKOP-16-2017-00002)
and by the New National Excellence Program of the Ministry for Innovation and Technology

Cover image by Barnabás Kocsis: *Project workflow for creating a simple model to simulate rhythm generation in the medial septum*

Contents

Introduction	9
PROGRAM 1: BIONICS, BIO-INSPIRED WAVE COMPUTERS, NEUROMORPHIC MODELS	10
Neural networks for EEG signal classification and brain-computer interfacing	11
<i>András ADOLF</i>	
Modulation of brain exposure of an intranasal P-glycoprotein substrate in rats	12
<i>Luca Anna BORS</i>	
Feed forward loops towards potential noise reduction	13
<i>Suchana CHAKRAVARTY</i>	
IGF-1 regulates GnRH neurons in prepubertal male mice	14
<i>Veronika CSILLAG</i>	
Classification of Motor Imagery EEG Signals Using Image-Based Deep Neural Network	15
<i>Ward FADEL</i>	
Mechanical unfolding of the CFTR chloride channel NBD1 domain using force probe simulations	16
<i>Bianka Vivien FARKAS</i>	
Immunomodulatory properties of stromal cells	17
<i>Anna HAJDARA</i>	
Development and Optimization of a Pipeline to build Structural Ensemble Models of Intrinsically Disordered Protein Segments	18
<i>Zita HARMAT</i>	
Scalable pipeline for high throughput metagenomic data	19
<i>Regina KALCSEVSZKI</i>	
Effect of disease-causing germline mutations on coiled-coil structures	20
<i>Zsófia Etelka KÁLMÁN</i>	
Microfluidic particle separation methods: Pinched flow fractionation	21
<i>Máté KÁLOVICS</i>	
Predicting molecular effects of hypoxia on kidney cells	22
<i>Bence Márk KEÖMLEY-HORVÁTH</i>	
A new technique for a better autofocus	23
<i>Márton Zsolt KISS</i>	

A simple model to simulate rhythm generation in the medial septum	24
<i>Barnabás KOCSIS</i>	
Multiple SVM based Brain Computer Interface for Cybathlon 2020	25
<i>Csaba Márton KÖLLŐD</i>	
Particle separation by inertial microfluidic devices	26
<i>Dániel Zoltán KOLPASZKY</i>	
A review of protein separation and detection methods in microfluidics	27
<i>Adrienn Lilla MÁRTON</i>	
Opening the genetic toolbox in cats	28
<i>Gergely MÉSZÁROS</i>	
Analyses of protein-protein interactions in the PSD by stochastic simulations	30
<i>Marcell MISKI</i>	
Comparing the performance of global search algorithms in tuning the parameters of a morphologically and biophysically detailed model neuron	31
<i>Máté MOHÁCSI</i>	
Structural characterization of the postsynaptic density scaffold protein GKAP with NMR spectroscopy	32
<i>Eszter NAGY-KANTA</i>	
Development of machine learning algorithms and decision pipelines on medical multimodal databases	33
<i>Bence NÉMETH</i>	
Structural characterization and interactions of Shank, a post-synaptic scaffold protein	34
<i>Anna SÁNTA</i>	
How do astroglia cells react to structured SU-8 thin films?	35
<i>Ágnes SZABÓ</i>	
Microfluidic possibilities of viral tests based on nucleic acid amplification	36
<i>Mihály SZŰCS</i>	
Data-driven developing of a PV basket cell and CA3 pyramidal neuron	37
<i>Luca TAR</i>	
Drug delivery through physiological barriers: investigation of the permeability of blood-brain barrier, nasal- and dermal-barriers	38
<i>Zsófia VARGA-MEDVECZKY</i>	
Bio-stability study of liquid crystal polymer (LCP) / Polydimethylsiloxane (PDMS) coated implants	39
<i>Moutz WAHDOW</i>	
PROGRAM 2: COMPUTER TECHNOLOGY BASED ON MANY-CORE PROCESSOR CHIPS, VIRTUAL CELLULAR COMPUTERS, SENSORY AND MOTORIC ANALOG COMPUTERS	40
Effect of solar panels ratio on the thermal behaviour of a CubeSat	41
<i>Nawar AL-HEMEARY</i>	
Algorithmic Differentiation of Structured Mesh Applications	42
<i>Gábor Dániel BALOGH</i>	

Evaluation of FPGA based SIFT implementation by using real-life examples	43
<i>Attila FEJÉR</i>	
Light Field Camera	44
<i>Mary GUINDY</i>	
Emulation of a single fault-tolerant memristor with memristor networks	45
<i>Dániel HAJTÓ</i>	
Accelerating Charged Single alpha-helix Detection on FPGA	46
<i>Sam KHOZAMA</i>	
Physiological Signal Extractor Algorithms Optimized for Embedded System	47
<i>Ádám NAGY</i>	
Domain of attraction computation of a unique non-zero equilibrium point of a Lotka-Volterra system	48
<i>Péter POLCZ</i>	
FPGA Based Onboard Visual Horizon Detection with Partial Camera Lens Distortion Correction	49
<i>Levente Márk SÁNTHA</i>	
Bitwise reproducible execution of unstructured mesh applications	50
<i>Bálint SIKLÓSI</i>	
Reachability Analysis of Structurally Bounded Reaction Networks	51
<i>Gergely SZLOBODNYIK</i>	
PROGRAM 3: FEASIBILITY OF ELECTRONIC AND OPTICAL DEVICES, MOLECULAR AND NANOTECHNOLOGIES, NANO-ARCHITECTURES, NANOBIONIC DIAGNOSTIC AND THERAPEUTIC TOOLS	52
Optimization Techniques in Neural Network Architectures	53
<i>András FÜLLÖP</i>	
A Summary of Tensor Factorisation Techniques for 3D Image Processing	54
<i>Janka HATVANI</i>	
Automated lesion classification on ultrasound images	55
<i>Péter MAROSÁN</i>	
Two-photon microscopical measurement of navigation integration in mouse brain	56
<i>Zsolt MEZRICZKY</i>	
Two-way logical gates based on nanomagnetic logic devices	57
<i>Tamás RUDNER</i>	
PROGRAM 4: HUMAN LANGUAGE TECHNOLOGIES, ARTIFICIAL UNDERSTANDING, TELEPRESENCE, COMMUNICATION	58
Investigation of open-set recognition techniques	59
<i>András Pál HALÁSZ</i>	
Deep Learning Algorithms for Intelligent Named Entity Recognition.	60
<i>Kamran IBIYEV</i>	
Abstractive Arabic Text Summarization	61
<i>Mram KAHLA</i>	

State Space Reconstruction with Generative Models	62
<i>András Attila SÜLYÖK</i>	
PROGRAM 5: ON-BOARD ADVANCED DRIVER ASSISTANCE SYSTEMS	63
The effect of outlier activations in neural networks	64
<i>Mohammad Jalal ALAFANDI</i>	
Solving K-SAT Problems with Continuous Time Neural Networks	65
<i>Dóra Eszter BABICZ</i>	
A Masonry Wall Image Inpainting Method with Adversarial Learning	66
<i>Yahya IBRAHIM</i>	
Evaluating the quality of medical images using artificial intelligence	67
<i>Ákos KOVÁCS</i>	
Change detection in Lidar point clouds	68
<i>Lóránt KOVÁCS</i>	
On-the-Fly Camera and Lidar Calibration	69
<i>Balázs NAGY</i>	
Different aspects of learning in biological and mathematical systems	70
<i>Franciska Sára RAJKI</i>	
Improving 3D Object Detection in Lidar Point Clouds	71
<i>Örkény Ádám H. ZOVÁTHI</i>	
Appendix	72

Introduction

It is our pleasure to publish this Annual Proceedings again to demonstrate the genuine multidisciplinary research done at the Jedlik Laboratories by young talents working in the Roska Tamás Doctoral School of Sciences and Technology of the Faculty of Information Technology and Bionics at Pázmány Péter Catholic University. The scientific results of our PhD students show the recent main research directions in which our faculty is engaged. We also appreciate the support of the supervisors and consultants, as well as that of the five collaborating National Research Laboratories of the Loránd Eötvös Research Network, Semmelweis University and the University of Pannonia. The collaborative work with the partner universities, especially Katolieke Universiteit Leuven, Politecnico di Torino, Technische Universität München, University of California at Berkeley, University of Notre Dame, Universidad de Sevilla, Università di Catania, Université de Bordeaux, Universidad Autonoma de Madrid is gratefully acknowledged.

We acknowledge the support of numerous institutes, organizations and companies, namely

- Loránd Eötvös Research Network (ELKH),
- National Research, Development and Innovation Office (NKFIH),
- Hungarian Academy of Sciences (MTA),
- UNKP Programme, Ministry for Innovation and Technology, Hungarian Government,
- Gedeon Richter Co.,
- Office of Naval Research (ONR) of the US,
- NVIDIA Ltd.,
- Verizon Computer Vision Group (Eutecus Inc.), Berkeley, CA,
- MorphoLogic Ltd., Budapest,
- Analogic Computers Ltd., Budapest,
- AnaFocus Ltd., Seville,

and several other companies and individuals.

Needless to say, the resources and support of the Pázmány Péter Catholic University are gratefully acknowledged.

Budapest, June 2020.

GÁBOR PRÓSZÉKY

Chairman of the Board of the Doctoral School

GÁBOR SZEDERKÉNYI

Head of the Doctoral School

PROGRAM 1

BIONICS, BIO-INSPIRED WAVE COMPUTERS, NEUROMORPHIC MODELS

Heads: Tamás FREUND, György KARMOS, Zsolt LIPOSITS, Sándor PONGOR

Neural networks for EEG signal classification and brain-computer interfacing

András ADOLF

(Supervisor: István ULBERT)

Pázmány Péter Catholic University, Faculty of Information Technology and Bionics
50/a Práter street, 1083 Budapest, Hungary
adolf.andras@itk.ppke.hu

Abstract—One of the most essential parts of brain-computer interfaces (BCI) is the classification of EEG signals. In this work I have focused on testing neural networks and applying methods for increasing the efficiency of the machine-learning. The main objective is a successful participation in the Cybathlon 2020 competition, for which our group strives to achieve higher and higher classification accuracies.

Keywords—brain-computer interfaces; neural networks; transfer learning; data augmentation

I. SUMMARY

The main motivation of brain-machine interfaces is to help those, whose severe neuromuscular disabilities prevent them from using particular devices, computers for instance. [1]

The classification of EEG signals is an essential part of a non-invasive brain-computer interface (BCI). To achieve this, different machine learning algorithms are used. One of the most widely used techniques is learning via neural networks.

In this work I have implemented convolutional neural network structures, and tested them over our measurements. These measurements were performed with 3 paradigms (A, B and C) on 2 tetraplegic patients from the Rehabilitation Centre for Physically Disabled People, the EEG signals of different imaginary movements were classified and used for giving commands in the Cybathlon competition environment.

The structure of the mainly used convolutional neural network can be seen in the figure below: it consist of 3 two-dimensional convolution layers and fully connected layers, these are responsible for classification. As a preprocessing step, I have reorganized the structure of the data into a spatial arrangement, resulting a 3-dimensional tensor. The first two dimensions are related to the arrangement of the actual electrodes, the third one is the time. This method was described in the work of Dhalin Zhang et al. and it proved useful. [2] Because of we have a limited amount of EEG signals to build a well performing classification system above them, I have used techniques such as data augmentation and transfer learning, to enhance performance.

For A and B paradigms with 5 class classification the average accuracy was 37.9%, but with using transfer learning, we could improve it to 42.6%. For the classification of active/passive states the original accuracy was 83.3%, with data augmentation it was improved by 1%, but with using even transfer-learning, an average of 88.8% was reached, which is quite a good result.

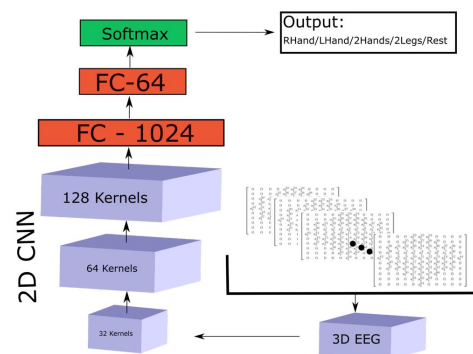


Fig. 1. The structure of the implemented neural network

The system was tested on the more limited dataset of the C paradigm, and the effect of the window length was examined. It turned out that over 3s windows this network performs better than over the ones with 2s length - 60.5% and 72.6%, the average difference is around 12%, so it seems the longer the intervals, the better the system performs. After performing artefact rejection, the accuracy drops down by around 10%, which might be because of the unintentional filtering of some important features. To increase efficiency, it is recommended to try new networks and/or use other attributes, such as Fourier analysis.

ACKNOWLEDGEMENTS

I would like to express my sincere gratitude to my consultant, István ULBERT, who supported me during my work. I would also like to say thank you to the group working on the Cybathlon project with me, in particular Csaba KÖLLÖD, Gergely MÁRTON and Bálint FILE.

REFERENCES

- [1] Jonathan R Wolpaw, Niels Birbaumer, William J Heetderks, Dennis J McFarland, P Hunter Peckham, Gerwin Schalk, Emanuel Donchin, Louis A Quatrano, Charles J Robinson, and Theresa M Vaughan. Brain-computer interface technology: a review of the first international meeting. *IEEE transactions on rehabilitation engineering*, 8(2):164–173, 2000.
- [2] Dalin Zhang, Lina Yao, Xiang Zhang, Sen Wang, Weitong Chen, Robert Boots, and Boualem Benatallah. Cascade and parallel convolutional recurrent neural networks on eeg-based intention recognition for brain computer interface. In *Thirty-Second AAAI Conference on Artificial Intelligence*, 2018.

Modulation of brain exposure of an intranasal P-glycoprotein substrate in rats

Luca Anna BORS

(Supervisor: Franciska ERDŐ)

Pázmány Péter Catholic University, Faculty of Information Technology and Bionics

50/a Práter street, 1083 Budapest, Hungary

bors.luca.anna@itk.pke.hu

Statement of originality - *This proceeding report describes the work of the doctoral student during the academic year 2019/2020. Parts of this work might be under submission to scientific conferences and journals.*

SUMMARY

In our research we have investigated intranasal delivery of a model drug to the brain with microdialysis. First we tried to find an optimal vehicle to study the intranasal (IN) absorption and distribution of P-gp substrate quinidine (QND). The distribution of intranasal solution was examined on a representative rat, with an 1% Evans blue dye treatment, then its skull was sectioned. The result of the dye showed that intranasal administration reaches the most caudal areas in the nasal cavity. However, the further tests with the nasal solution were discontinued, due to the high mortality rate. It was also complicated to apply this formulation with the dual-probe microdialysis we used to collect samples without losing the first and most critical 30-minute of pharmacokinetic data, therefore the study was continued with the gel formulation. Hereinafter a silicon based gel was used as vehicle for IN QND, PSC-833 (as P-gp inhibitor) and epinephrine (as sympathomimetic). Five different experimental groups were created: 1) control (IN QND), 2) IN QND + IN PSC-833 pre-treatment, 3) IN QND + IV PSC-833 pre-treatment, 4) IN QND + ADR (50 ng) co-administration and 5) IN QND + ADR (20 μ g) co-administration. The bioavailability of IN QND in the brain was successfully increased after IV P-gp inhibitor pretreatment as well as with IN epinephrine co-administration. The blood concentration of QND also decreased with PSC-833 treatment. This can be considered as an indicator of P-gp presence in the nasal cavity and that the modulation of P-gp transporter in the BBB can also be responsible for interactions between IN drugs and peripherally administered drugs.

METHODS

The distribution of the nasal solution was tested in one representative rat, with 1% Evans blue. To identify parts of the histological sections haematoxylin and eosin staining was also used on every second sections. In the further studies only the gel formulation was used. IN QND was tested in presence of a P-gp inhibitor Valsopodar (PSC-833). Both intravenous (IV) and IN PSC-833 administration was investigated. The brain exposure modulatory effect of IN epinephrine was also tested, at low (50 ng) and high (20 μ g) dose, inspired by the publication of Hada and co-workers [1]. Dual-probe (brain and venous probes) microdialysis was used to collect samples from anesthetized rats similarly to as it was described by Sziráki and co-workers [2].

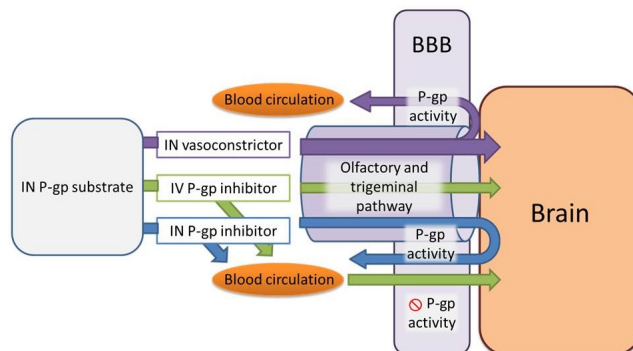


Fig. 1. Schematic illustration of the different modulations that were observed in this study. The vasoconstrictor (purple) decreases absorption into the blood stream through the capillary of the nasal mucosa. The intravenous P-gp inhibitor (green) makes the P-gp substrate able to pass the blood-brain barrier (BBB) even through the blood circulation. The intranasal P-gp inhibitor (blue) showed similar results to the control.

DISCUSSION AND CONCLUSION

In conclusion, the modulation of the efflux transporters is a complex interaction system. Our results showed that drug-drug interactions can occur and can lead to adverse effects, when intranasal drug administration is given simultaneously with another peripherally administered (intravenous, per os etc.) drug. We assumed that in our formulation the inhibitor given IN had only local effect and only if it was given intravenously had effect on striatal QND level, on those molecules which had already reached the brain tissue via direct nasal route. The presence of P-gp in nasal tissue may challenge the local treatment of allergic or infectious diseases as well as the intranasal administration of drugs with systemic action.

REFERENCES

- [1] N. Hada, W. J. Netzer, F. Belhassan, L. P. Wennogle, and S. Gizurarson, "Nose-to-brain transport of imatinib mesylate: A pharmacokinetic evaluation," *Eur. J. Pharm. Sci.*, vol. 102, pp. 46–54, 2017.
- [2] Sziráki I, Erdő F, Beéry E, Molnár PM, Fazakas C, Wilhelm I, Makai I, Kis E, Herédi-Szabó K, Abonyi T, Krizbai I, Tóth GK, Krajcsi P., "Quinidine as an ABCB1 probe for testing drug interactions at the blood-brain barrier: An in vitro in vivo correlation study," *J. Biomol. Screen.*, vol. 16, no. 8, pp. 886–894, 2011.

Feed forward loops towards potential noise reduction

Suchana CHAKRAVARTY

(Supervisor: Attila CSIKÁSZ-NAGY)

Pázmány Péter Catholic University, Faculty of Information Technology and Bionics

50/a Práter street, 1083 Budapest, Hungary

chakravarty.suchana@itk.ppke.hu

Abstract—The stochasticity in cells arises due to cellular noise. The cellular noise has great impact on functional cellular biology. Due to the presence of noise cellular behavior can be defined in terms of probability. The dynamical behavior of cells can be represented by mathematical modeling and captured by computer simulations. Feed forward loops could serve as noise filters. Here, we introduce coupled feed forward loops that can work as a better noise filtering module compared to the simple feed forward loop. We performed simulations on all possible coupled feed forward loop combinations and quantified their noise reducing properties.

Keywords—cellular noise; feed forward loop; coupled feed forward loop; computational simulation.

DISCUSSION

Random variability in cells arise due to cellular noise. Often metabolites of genetically identical cells, get expressed to different levels, due to presence of noise. The origin of intrinsic noise is due to low copy number of proteins between cells. Whereas, extrinsic noise appears because of interactions with neighboring cells. Substantial changes of behavior between cells is the combinatorial effects of extrinsic and intrinsic noise [1].

Feed forward is a pathway where a controlled signal gets transduced from a source to downhill components in one direction. Gene regulatory networks can follow the feed forward pathway. In biology, feed forward loops are three node motifs. In a feed forward loop, a source species regulates a second species and they together act upon the third species through direct and indirect arms. Coherent feed forward loop is obtained when direct arms and indirect arms have similar sign. When the direct arm and indirect arms are different in sign, then it is called incoherent feed forward loop [2]. Earlier reports suggests that, incoherent feed forward loop can accelerate the response time and coherent feed forward loop can show sign sensitive delay in time [2], furthermore feed forward loops can reduce noise as well. Recent studies support the fact that co-expressed species can reduce the biological noise if they can degrade simultaneously. It has been also reported that negative feed back loops have noise reducing property [3].

We have created models for all possible combinations of couple feed forward loops. We have tested the noise reducing capabilities of these models by linear noise approximation [4]. We applied a step-like signal as input to our system **Fig1.**, and found that feed forward loops where each molecule are regulated by two step modifications perform worse in noise reduction than systems where there is a direct conversion between the inactive and active forms. On the contrary, models with intermediate state show a better signal

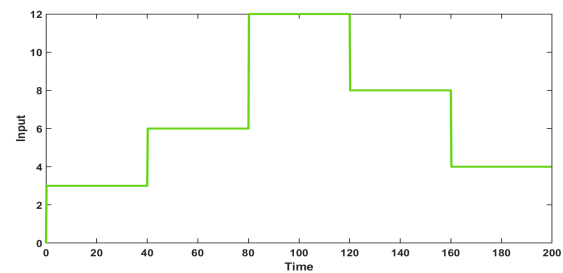


Fig. 1. The variation of a step-like input signal

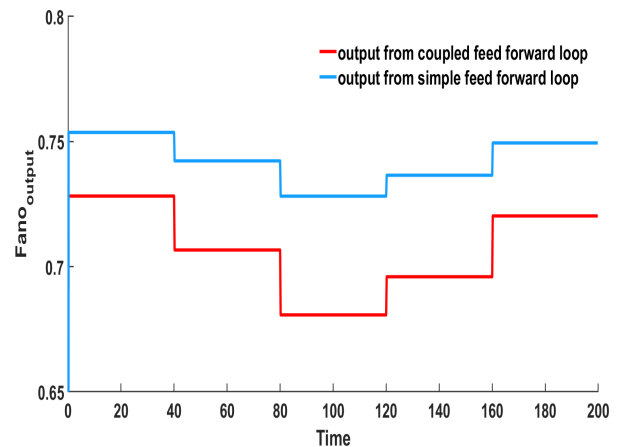


Fig. 2. The Fano factor (measuring the noise reducing capability of a network, with lower numbers, showing better control on noise) of output of simple (blue)(C_1) and coupled (red)(C_1C_1) feed forward loop are provided for a step-like increase and decrease of input.

transduction capacity, than models with direct conversion.

REFERENCE

- [1] P. Thomas, “Intrinsic and Extrinsic Noise of Gene Expression in Lineage Trees.”, *Scientific Reports*, vol.9, no. 474, pp. 1–16, 2019.
- [2] S. Mangan and U. Alon, “Structure and Function of the Feed-Forward Loop Network Motif.”, *PNAS*, vol. 100, no. 21, pp. 11980–11985, 2003.
- [3] L. Laurenti, A. Csikász-Nagy, M. Kwiatkowska, L. Cardelli, “Molecular Filters for Noise Reduction.”, *Biophysical Journal*, vol.114, no. 12, pp. 3000–3011, 2018.
- [4] L. Cardelli, “The Kaemika Approach to Integrated Modeling of Reaction Networks and Protocols.”, pp. 1-18, 2019.

IGF-1 regulates GnRH neurons in prepubertal male mice

Veronika CSILLAG

(Supervisors: Imre FARKAS, Zsolt LIPOSITS)

Pázmány Péter Catholic University, Faculty of Information Technology and Bionics

50/a Práter street, 1083 Budapest, Hungary

csillag.veronika@itk.ppke.hu

Reproduction is controlled by the hypothalamo-pituitary-gonadal (HPG) axis in mammals and its main central regulators, the hypophysiotropic gonadotropin-releasing hormone (GnRH)-expressing neurons.

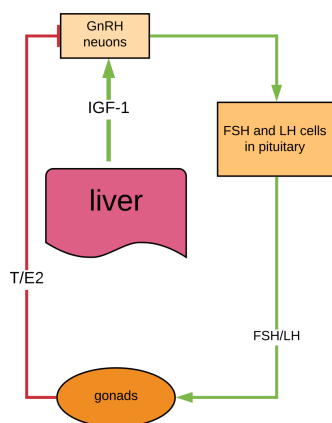


Fig. 1. Schematic figure of HPG axis in male mice. Fusiform GnRH neurons are located in the mPOA of the hypothalamus and their axons terminate in the median eminence (ME) where they secrete GnRH into the portal circulation. GnRH can reach FSH and LH cells in the anterior pituitary. Green arrows show the stimulatory relationships.

The preoptic area in the hypothalamus is considered as the center of the neuroendocrine control of the reproduction in the brain. In mammals, the gonadotropin-releasing hormone (GnRH) neurons located here have a key role in synchronizing numerous events, leading to the onset of puberty. Growth hormones, however, can influence this timing by modulating function of GnRH neurons. One of these substances, the insulin-like growth factor-1 (IGF-1) originating both from peripheral and central sources, is abundant in the hypothalamus at the time of puberty. Earlier data have shown that IGF-1 administration during this developmental period can act centrally by inducing GnRH secretion and accelerating the onset of puberty in female rats [1]. These data suggest that IGF-1 may regulate the HPG axis by modulating the function of GnRH neurons directly. Therefore, responsiveness of GnRH neurons to IGF-1 and the molecular pathways acting downstream to IGF-1 receptor were investigated. In vitro electrophysiological experiments were carried out on GnRH-GFP neurons of acute brain slices from prepubertal (23-29 days) male mice. We found that application of IGF-1 (13 nM) significantly increased the frequency of the spontaneous postsynaptic currents (sPSCs) compared to the control in 42% of the neurons, and that of the excitatory GABAergic miniature postsynaptic currents (mPSCs) in 40% of the measured

neurons. The increase in the mPSC frequency was prevented by the usage of the IGF-1 receptor antagonist, JB1 showing the involvement of IGF-1 receptor in the mechanism. Literature data suggest that binding of IGF-1 to its receptor activates a phosphoinositide-3 kinase (PI3K)-dependent pathway and the intracellularly applied PI3K blocker (LY294002) indeed inhibited the effect of IGF-1. Changes in the mPSC frequency, but not in the amplitude indicated that IGF-1 acts through various retrograde pathways we described earlier in GnRH neurons[2,3,4]. The elevation of the frequency suggested the involvement of retrograde nitric oxide (NO) signaling pathway, but the NO synthase blocker NPLA failed to abolish the effect of IGF-1 demonstrating that the NO retrograde machinery was not involved in this process. Therefore, we examined the retrograde endocannabinoid pathway which has a tonic inhibition on GnRH neurons via reducing frequency of excitatory GABAergic mPSCs, and blockade of this tonic endocannabinoid pathway can lead to excitation. The transient receptor potential vanilloid 1 (TRPV1) is one of the components of this endocannabinoid pathway and the TRPV1 receptor blocker (AMG9810) abolished the frequency elevating effect of IGF-1 on GnRH neurons. To further examine the involvement of the retrograde endocannabinoid pathway, we applied a cannabinoid receptor type-1 (CB1) blocker (AM251) in the ACSF, which also prevented the IGF-1-related frequency elevation of the mPSCs. Our results, therefore, show that IGF-1 can block the tonic retrograde endocannabinoid pathway in GnRH neurons and this disinhibition increases the release of excitatory GABA from the presynaptic terminals.

ACKNOWLEDGEMENTS

The author wishes to acknowledge Dr. Imre Farkas and Prof. Zsolt Liposits for their excellent supervision. The research presented in this paper was conducted in cooperation with and the paper was co-authored by Flóra Bálint.

REFERENCES

- [1] Hiney JK, Srivastava VK, Pine MD, Les Dees W: Insulin-like growth factor-I activates KiSS-1 gene expression in the brain of the prepubertal female rat. *Endocrinology* 2009;150:376-384.
- [2] Farkas I, Vastagh C, Sarvari M, Liposits Z: Ghrelin decreases firing activity of gonadotropin-releasing hormone (GnRH) neurons in an estrous cycle and endocannabinoid signaling dependent manner. *PloS one* 2013;8:e78178.
- [3] Farkas, I., et al., Glucagon-Like Peptide-1 Excites Firing and Increases GABAergic Miniature Postsynaptic Currents (mPSCs) in Gonadotropin-Releasing Hormone (GnRH) Neurons of the Male Mice via Activation of Nitric Oxide (NO) and Suppression of Endocannabinoid Signaling Pathways. *Front Cell Neurosci*, 2016. 10: p. 214.
- [4] Csillag V, Vastagh C, Liposits Z, Farkas I: Secretin Regulates Excitatory GABAergic Neurotransmission to GnRH Neurons via Retrograde NO Signaling Pathway in Mice. *Frontiers in cellular neuroscience* 2019;13

Classification of Motor Imagery EEG Signals Using Image-Based Deep Neural Network

Ward FADEL

(Supervisors: István ULBERT, Lucia WITTNER)

Pázmány Péter Catholic University, Faculty of Information Technology and Bionics

50/a Práter street, 1083 Budapest, Hungary

fadel.ward@itk.pke.hu

Abstract—Classification of EEG signals is the main part of the Motor-Imagery (MI) based Brain Computer Interface (BCI) systems. EEG signals differ from one subject to another and even for the same subject among different trials, and this is why designing a general classification model is still debated. Deep learning is dominant in so many fields like computer vision and natural language processing but it is still under investigation for EEG signals classification. We followed a new trend in EEG signals classification in which these signals are transformed into images, and so classifying such signals become an image classification problem where Deep learning can work well. The Physionet dataset for EEG motor movement/imagery tasks was used which consists of 109 subjects and the motor imagery EEG signals for three frequency bands (Delta [0.5-4 Hz], Mu [8-13 Hz], and Beta [13-30 Hz]) was transformed into 3-channel images (one channel for each band) using the Azimuthal equidistant projection and Clough-Tocher algorithm for interpolation. These 2-D images represent the input data to our model which consists of Deep Convolutional Neural Network (DCNN) to extract the spatial and frequency features followed by Long Short Term Memory (LSTM) to extract temporal features and then finally to be classified into 5 different classes (4 motor imagery tasks and one rest). Our results were promising (70.64 % average accuracy) and 5% better than the results of Support Vector Machine (SVM) method over the same dataset. We noticed that taking Delta band into account increases the classification accuracy by 2.51%.

Keywords—Brain-Computer Interface (BCI); Classification; Motor Imagery; Convolutional Neural Networks (CNN); Long Short Term Memory (LSTM).

I. SUMMARY

Classification of the EEG features is the main part of BCI systems. The classification of motor imagery activity is a challenging task due to the low signal-to-noise ratio of EEG signals and their non-stationary nature for the same subject and among subjects, the high sensitivity for artifacts, the limited number of training data, and the low reliability of current BCI systems. Therefore, classification algorithms mainly aim to overcome one or more of the previously mentioned challenges. The goal in [1] was to classify memory/cognitive load. The EEG data gathered from 64 electrodes was transformed into colored images using 3 frequency bands, and these images were fed to a CNN followed by LSTM in order to keep the spatial, frequency and temporal features of the EEG signals. We used a similar approach for MI-EEG classification. In our approach, we used CNN followed by LSTM and we used Physionet dataset with 109 subjects taken from 64 electrodes and by transforming the MI-EEG signals into images that preserve the spatial-frequency dimensions of the signals. LSTM was used to extract the temporal information between consecutive images that were classified into 5 different classes. the motor imagery EEG signals activity is mainly dominant

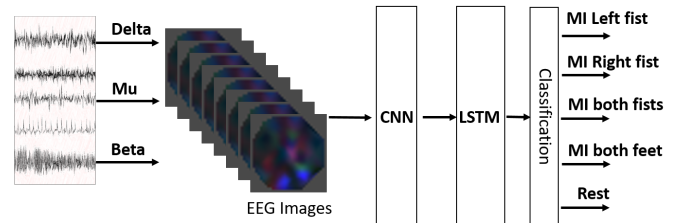


Fig. 1. The proposed approach for MI-EEG signals classification.

in two bands; Mu [8-13 Hz] and Beta [13-30 Hz], so for the first scenario, the signals for each subject were bandpass filtered into two bands. Then, for the second scenario, we also band pass filtered Delta band [0.5-4 Hz] to add another option to the selected bands for feature extraction. Next, we applied Fast Fourier Transform (FFT) on the time series with a window equals to 0.4 second (this means we have 10 different measures per each 4 seconds trial for every electrode), and then the sum of the squared absolute values was calculated for each band, then the measurements for 64 electrodes were transformed into 2-D images, and thus the problem of EEG signal classification becomes an image classification task. In order to project the 3-D electrodes space into a 2-D plane, we applied the Azimuthal Equidistant Projection (AEP) and then Clough-Tocher interpolation was applied over 32 x 32 mesh and thus we got the 2-D topology-preserving unicolor images for each band (red refers to Delta, green refers to Mu and blue refers to Beta) which represents the average activity for motor imagery EEG signals over the scalp for 0.4 seconds, then we added the resulting images for each band together to form either 2-channel images for the 2 band scenario or 3-channel images for the 3 bands scenario. The average classification accuracy is 70.64% after adding Delta band to the image generation process, which is usually ignored in MI-EEG signals classification approaches, and this is 5% improvement compared to SVM.

REFERENCES

- [1] Pouya Bashivan, Irina Rish, Mohammed Yeasin, Noel Codella, *Learning Representations from EEG with Deep Recurrent-Convolutional Neural Networks*, ICLR Conference, 2016.
- [2] Reza Abiri et al, *A comprehensive review of EEG-based brain-computer interface paradigms*, *J. Neural Eng.* 2019, 16, 011001 ,
- [3] F Lotte , L Bougrain, A Cichocki, M Clerc, M Congedo, A Rakotomamonjy and F Yger, *A review of classification algorithms for EEG-based brain-computer interfaces: a 10 year update*, *J. Neural Eng.* 2018, 15, 031005 ,

Mechanical unfolding of the CFTR chloride channel NBD1 domain using force probe simulations

Bianka Vivien FARKAS

(Supervisors: Tamás HEGEDŰS, Zoltán GÁSPÁRI)

Pázmány Péter Catholic University, Faculty of Information Technology and Bionics

50/a Práter street, 1083 Budapest, Hungary

farkas.bianka.vivien@itk.ppke.hu

SUMMARY

Cystic fibrosis (CF) is a monogenic disease with high mortality. It is caused by mutations in the gene of the CFTR/ABCC7 (cystic fibrosis transmembrane conductance regulator) protein, an ATP-Binding Cassette (ABC) protein. CFTR is a chloride channel in the apical membrane of epithelial cells. CF-causing mutations can impair the channel function in various ways, such as altering the protein folding, domain-domain assembly, trafficking to the cell membrane or the stability of the mature protein. Mutations with the lack of functional CFTR expression cause imbalanced salt and water homeostasis leading to the CF symptoms. [1]

The currently used CF drugs mainly stabilize the mature protein; however, correcting folding during the early steps of maturation may result in more efficient therapies. For this purpose, precise knowledge of the folding-unfolding pathway at the atomic resolution is required. As simulations are a powerful tool to describe protein dynamics in atomic details, we performed steered pulling molecular dynamics with the structure of CFTR first nucleotide binding domain (NBD1, PDBID:2BBO [2]) without the regulatory insertion (Δ RI) using all-atom $G\ddot{o}$ model [3]. We characterized the unfolding of the domain identifying pathways and intermediate states. The most frequent mutation, the deletion of phenylalanine 508 (Δ F508) is localized in the first nucleotide binding domain (NBD1). To investigate whether the Δ F508 influences the mechanical unfolding of NBD1 we executed simulations with the NBD1 carrying the F508 deletion. To validate our simulation results, we performed single-molecule force spectroscopy experiments with the NBD1 and with the Δ F508 mutant NBD1. Our results suggest that the S6- α -S8-Core region of the NBD1 (a.a. 487 to 604), where the F508 is localized, may have a central role in the unfolding-folding process.

To investigate the unfolding of the S6- α -S8-Core region more accurately, we performed additional force probe simulations with the NBD1 S6- α -S8-Core using GROMACS with CHARMM36m force field [4]. These all-atom simulations with the S6- α -S8-Core region enabled us to study not only the native but the non-native interactions during the pulling simulations and to identify intermediate structures describing the unfolding steps of the NBD1 more accurately.

The unfolding events calculated with force probe MD simulations and the ones measured by *in vitro* experiments show similar pattern. The simulations help to interpret the experiments and understand the atomic details of the unfolding process. This approach may help to understand the mechanics of the protein unfolding-folding processes and to design more efficient drug molecules for Cystic fibrosis therapies.

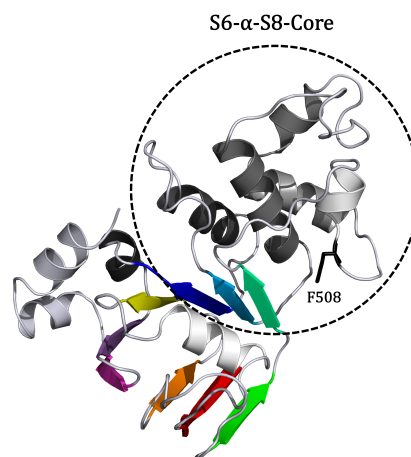


Fig. 1. Structural organization of the CFTR chloride channel first nucleotide binding domain (NBD1) is shown by cartoon representation. β -strands are colored, α -helices are marked in grey shade. Dashed black circle marks the S6- α -S8-Core region. Phenylalanine 508 is highlighted (F508, stick representation).

ACKNOWLEDGEMENTS

The support of NKFIH K127961, Cystic Fibrosis Foundation (CFE HEGEDU1810), Grubmüller laboratory at Max Planck Institute, NIIF/KIFÜ HPC, MTA Wigner GPU Laboratory, Semmelweis Infrastructure Funding is greatly acknowledged.

REFERENCES

- [1] J. R. Riordan, J. M. Rommens, B. Kerem, N. Alon, R. Rozmahel, Z. Grzelczak, J. Zielenski, S. Lok, N. Plavsic, and J. L. Chou, "Identification of the cystic fibrosis gene: cloning and characterization of complementary DNA," *Science (New York, N.Y.)*, vol. 245, pp. 1066–1073, Sept. 1989.
- [2] H. Lewis, C. Wang, X. Zhao, Y. Hamuro, K. Conners, M. Kearins, F. Lu, J. Sauder, K. Molnar, S. Coales, P. Maloney, W. Guggino, D. Wetmore, P. Weber, and J. Hunt, "Structure and Dynamics of NBD1 from CFTR Characterized Using Crystallography and Hydrogen/Deuterium Exchange Mass Spectrometry," *Journal of Molecular Biology*, vol. 396, pp. 406–430, Feb. 2010.
- [3] J. K. Noel, M. Levi, M. Raghunathan, H. Lammert, R. L. Hayes, J. N. Onuchic, and P. C. Whitford, "SMOG 2: A Versatile Software Package for Generating Structure-Based Models," *PLOS Computational Biology*, vol. 12, p. e1004794, Mar. 2016.
- [4] R. B. Best, X. Zhu, J. Shim, P. E. M. Lopes, J. Mittal, M. Feig, and A. D. MacKerell, "Optimization of the additive CHARMM all-atom protein force field targeting improved sampling of the backbone ϕ , ψ and side-chain χ_1 and χ_2 dihedral angles," *Journal of chemical theory and computation*, vol. 8, pp. 3257–3273, Sept. 2012.

Immunomodulatory properties of stromal cells

Anna HAJDARA

(Supervisors: Balázs MAYER, Miklós GYÖNGY)

Pázmány Péter Catholic University, Faculty of Information Technology and Bionics

50/a Práter street, 1083 Budapest, Hungary

hajdara.anna@itk.ppke.hu

Abstract—Bone marrow stromal cells (BMSCs) are a heterogeneous population of multipotent stromal cells with the ability of multilineage-differentiation and immunoregulatory functions [1]. Stromal cells/fibroblasts of the dermal connective tissue not only share similar cell surface markers with BMSCs, but they also have immunomodulatory properties and are able to differentiate into adipocytes, chondrocytes and osteoblasts. Many studies have focused on the effect of BMSCs on inflammatory responses of primary macrophages - a mononuclear cell population among innate immune cells. BMSCs have been a great tool for different cell based therapies, however several complications limited their use in clinical trials [1]. Dermal fibroblasts are abundant within the skin, and their isolation is relatively easier than those of BMSCs. Their shared characteristics with BMSCs make them potential candidates in immunomodulatory studies. We have developed an assay with macrophage cells polarized into inflammatory (M1) and anti-inflammatory (M2) immunophenotypes and with dermal fibroblasts. Their immunomodulatory effect was evaluated by measuring an anti-inflammatory cytokine, IL-10 from co-culture supernatants using enzyme-linked immunosorbent assays (ELISA).

I. RESULTS

An in-house differentiation method for primary M1 and M2 macrophage cells was established and we used these cells in co-cultures with dermal fibroblasts. Fibroblasts increased IL-10 production both in M1 and M2 macrophages. Pre-conditioning of dermal fibroblasts with pro-inflammatory cytokines enhanced the IL-10 response, indicating that inflammatory reactions could be influenced in vitro. Fibroblasts also impacted the cell surface marker expression of macrophage cells and made a shift towards the anti-inflammatory, M2 immune-phenotype.

II. CONCLUSION

Dermal fibroblast isolation

Dermal fibroblasts can substitute BMSCs in in vitro immunomodulatory assays and could be alternative cell type in future in vivo studies as well.

III. MATERIALS AND METHODS

Cell isolation

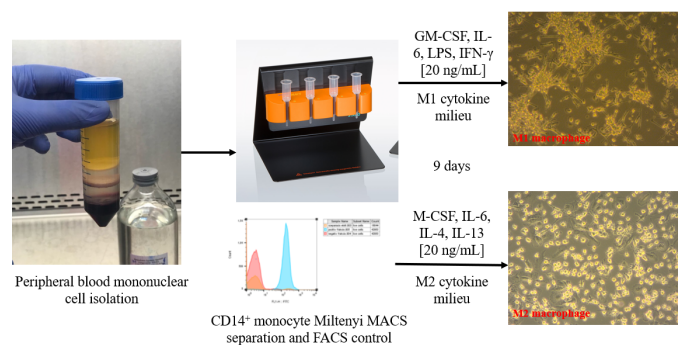


Fig. 1. Isolation of monocytes and differentiation of macrophages

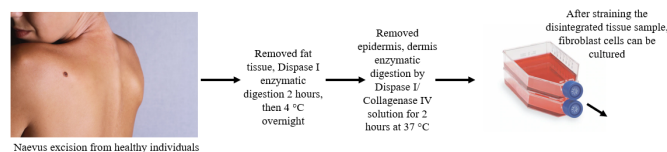


Fig. 2. Isolation of dermal fibroblasts

Both dermal fibroblasts and peripheral blood mononuclear cells were isolated from healthy individuals.

Immuno-modulatory assay

Pro-inflammatory M1 and anti-inflammatory M2 macrophage cells were co-cultured with dermal fibroblasts, followed by bacterial LPS stimulus. Cell supernatants were collected and measured by ELISA (OD at 405 nm).

Immuno-staining

CD14-FITC, CD206-PE, CD80-FITC fluorescent antibodies and 7AAD dye were used. All antibodies were from Biolegend. For flow cytometry analysis, a BD FACS CaliburTM flow cytometer and FlowJo software was used.

REFERENCES

- [1] N. D. C. Noronha Nc et al., "Priming approaches to improve the efficacy of mesenchymal stromal cell-based therapies," *Stem Cell Research and Therapy*, vol. 10, no. 1. BioMed Central Ltd., p. 131, 02-May-2019.

Development and Optimization of a Pipeline to build Structural Ensemble Models of Intrinsically Disordered Protein Segments

Zita HARMAT

(Supervisor: Zoltán GÁSPÁRI)

Pázmány Péter Catholic University, Faculty of Information Technology and Bionics

50/a Práter street, 1083 Budapest, Hungary

3in Research Group, Faculty of Information Technology and Bionics, Pázmány Péter Catholic University, Esztergom, Hungary

harmat.zita@itk.ppke.hu

One of the main research areas of our group is the Postsynaptic Density (PSD), a dense region in the membrane of dendrites, consisting of proteins, which form a complex network taking part in neurotransmission [1]. To understand the structure of the constituting proteins and the functioning of the network at a molecular level would be a great advancement in understanding the mechanisms of molecular neurobiology. The Guanylate Kinase Associated Protein (GKAP) is a scaffold protein and an important part of this network, being involved in the regulation and trafficking of glutamate receptors and the majority of its structure is intrinsically disordered and not yet experimentally determined [2], [3]. The human SH3 and multiple ankyrin repeat domains protein 1 (SHANK1) is similarly a scaffold protein and it is interacting with GKAP, its structure is also mostly intrinsically disordered and not yet experimentally determined [4]. The Homer protein homolog 3 (HOMER) protein is also a scaffold protein, mainly interacting with glutamate receptors, but in the case of this protein, only one region is intrinsically disordered and not yet experimentally determined [5].

Experimental determination of the three-dimensional structure of proteins is a very time-consuming and resource demanding process. Therefore, the structure of most of the proteins, especially the ones with intrinsically disordered parts have not been experimentally determined to date. This gave rise to *in silico* protein structure prediction methods.

The task to predict the three-dimensional structure of a protein based on its sequence alone is a daunting one, because the number of possible conformations of a protein is astronomical, as Levinthal's paradox clearly states [6]. This is even more profound in the case of an intrinsically disordered part of a protein, where alpha helical and beta strand regions do not pose constraints of the possible ϕ and ψ angles. Narrowing down the number of possible conformations is an obvious requirement especially in this case.

There has been many protein structure prediction methods made to model intrinsically disordered proteins (IDP-s), to mention some of them: Flexible Meccano [7], ENSEMBLE [8] and the method of Estaña et al. [9]. Flexible Meccano uses potentials specific to each amino acids and volume exclusion, and generates a structural ensemble model. The ENSEMBLE approach incorporates NMR experimental parameters to generate a structural ensemble. Estaña and coworkers use a method which builds up IDP-s from the building blocks of coil and

loop regions of experimentally determined structures.

Unfortunately, most of these methods seem to be outdated, not keeping up with the changing software environment (operation system version, Java version, etc.) and therefore we could not use them. This is why we have developed a protein structure prediction method which is based on local interactions.

We have applied the method for the intrinsically disordered parts of the rat GKAP, the repeat region of the human SHANK1, and the disordered parts of the human HOMER protein. For each protein region we have generated 50 structures, and so creating a small ensemble for each. The analysis of the structural model and the selection of the appropriate conformations is still ongoing.

Acknowledgement

The research has been supported by the European Union, co-financed by the European Social Fund (EFOP-3.6.2-16-2017-00013, Thematic Fundamental Research Collaborations Grounding Innovation in Informatics and Infocommunications)

REFERENCES

- [1] W. Feng and M. Zhang, "Organization and dynamics of PDZ-domain-related supramodules in the postsynaptic density," *Nat. Rev. Neurosci.*, vol. 10, pp. 87–99, Feb 2009.
- [2] A. H. Rasmussen, H. B. Rasmussen, and A. Silahtaroglu, "The dlga family: neuronal expression, function and role in brain disorders," *Molecular Brain*, vol. 10, p. 43, Sep 2017.
- [3] S. M. Shin, N. Zhang, J. Hansen, N. Z. Gerges, D. T. Pak, M. Sheng, and S. H. Lee, "GKAP orchestrates activity-dependent postsynaptic protein remodeling and homeostatic scaling," *Nat. Neurosci.*, vol. 15, pp. 1655–1666, Dec 2012.
- [4] M. Sheng and E. Kim, "The Shank family of scaffold proteins," *J. Cell. Sci.*, vol. 113 (Pt 11), pp. 1851–1856, Jun 2000.
- [5] B. Xiao, J. C. Tu, R. S. Petralia, J. P. Yuan, A. Doan, C. D. Breder, A. Ruggiero, A. A. Lanahan, R. J. Wenthold, and P. F. Worley, "Homer regulates the association of group 1 metabotropic glutamate receptors with multivalent complexes of homer-related, synaptic proteins," *Neuron*, vol. 21, pp. 707–716, Oct 1998.
- [6] Levinthal, Cyrus, "Are there pathways for protein folding?," *J. Chim. Phys.*, vol. 65, pp. 44–45, 1968.
- [7] V. Ozenne, F. Bauer, L. Salmon, J. R. Huang, M. R. Jensen, S. Segard, P. Bernadó, C. Charavay, and M. Blackledge, "Flexible-meccano: a tool for the generation of explicit ensemble descriptions of intrinsically disordered proteins and their associated experimental observables," *Bioinformatics*, vol. 28, pp. 1463–1470, Jun 2012.
- [8] M. Krzeminski, J. A. Marsh, C. Neale, W. Y. Choy, and J. D. Forman-Kay, "Characterization of disordered proteins with ENSEMBLE," *Bioinformatics*, vol. 29, pp. 398–399, Feb 2013.
- [9] A. Estaña, N. Sibille, E. Delaforge, M. Vaisset, J. Cortés, and P. Bernadó, "Realistic Ensemble Models of Intrinsically Disordered Proteins Using a Structure-Encoding Coil Database," *Structure*, vol. 27, pp. 381–391, 02 2019.

Scalable pipeline for high throughput metagenomic data

Regina KALCSEVSZKI

(Supervisor: Sándor PONGOR)

Pázmány Péter Catholic University, Faculty of Information Technology and Bionics

50/a Práter street, 1083 Budapest, Hungary

kalcsevszki.regina@itk.ppke.hu

I. INTRODUCTION

In recent years more and more scientific study is written about the connection of human microbiome and diseases. The human microbiome contains the organisms which are living inside and on human. While the human genome contains about 20,000 genes, in the human microbiome this number is larger by a factor of ten. To investigate the connections we have to sequence and analyse the sequences. Microbiome sequencing results tremendous amount of data that bioinformatics has to process, understand, and draw conclusions from them.

In this paper, we provide a solution for microbiome data analysis, a semi-automatized pipeline for metagenomic data, that guide through the steps from the raw reads till the biomarkers, based on one can classify the patients to different medical conditions.

With the pipeline we improved the quality of sixteen different dataset, during this step more than 8.8 thousands of gigabytes of data were preprocessed. We chose two colorectal carcinoma dataset for further analysis with the pipeline and identified biomarkers on genus level, based on the samples can be classified to the health conditions. Running multiple taxonomic classifiers and biomarker search tools, we conclude that the method or tool choice heavily influences the results.

II. SUMMARY

The presented scalable pipeline for high throughput metagenomic data consists of four parts. In the first part we improve the quality of the raw reads, based on a generated quality profile. In the second part, we generate the taxonomic profile of the sequences. These methods differ in the databases and the comparing methods that results different speed and accuracy, as well as different number of assigned reads. In the third part we concatenate the profiles of the different samples to one table and apply transformations to get the final relative abundance table. In the last part we use different feature selection methods to find biomarkers, that can be the input of a classifier, that predicts the health condition of the patient, the sample was derived from.

Running the quality control pipeline on sixteen different dataset accessible through curatedMetagenomicData from Bioconductor [1], altogether more than 8.8 thousands of gigabytes of data, it is proven that the quality control pipeline is scalable.

With the presented tools, we managed to find biomarkers on genus level which could reach adequate ROC AUC values, thus the pipeline is able to find biomarkers. However, the results heavily depend on the choice of the tools, including the taxonomic classifier and the biomarker search tool.

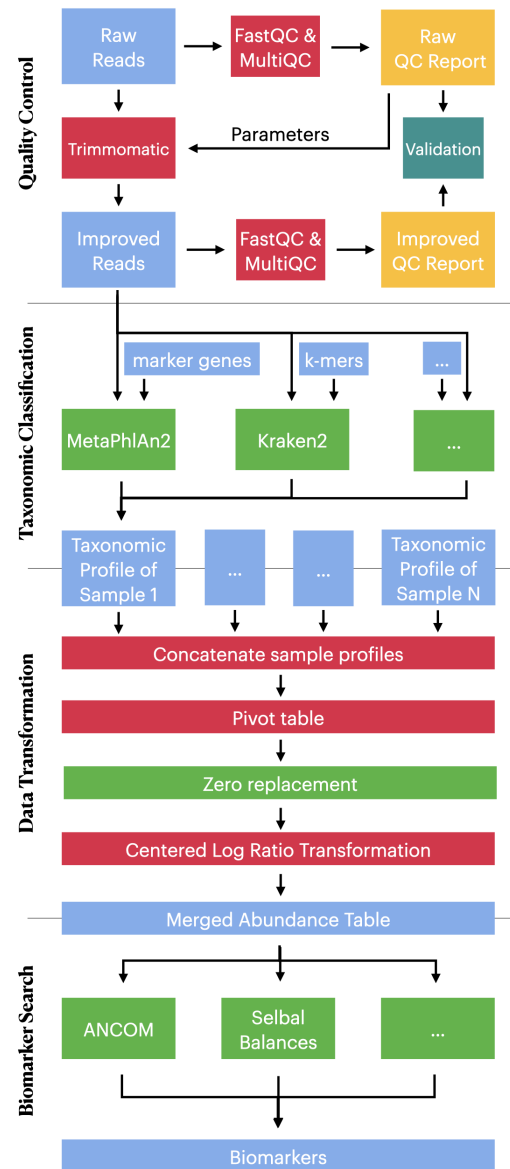


Fig. 1. Scalable pipeline for high throughput metagenomic data. The pipeline consists of four parts. In the first part we improve the quality of the raw reads, based on a generated quality profile. In the second part, we generate the taxonomic profile of the sequences. In the third part we concatenate the profiles of the different samples to one table and apply transformations to get the final relative abundance table. In the last part we use different feature selection methods to find biomarkers that can be used for disease classification.

REFERENCES

- [1] E. Pasolli et al., *Accessible, curated metagenomic data through ExperimentHub*, Nature Methods, 2017

Effect of disease-causing germline mutations on coiled-coil structures

Zsófia KÁLMÁN

(Supervisor: Zoltán GÁSPÁRI)

Pázmány Péter Catholic University, Faculty of Information Technology and Bionics
50/a Práter street, 1083 Budapest, Hungary
kalman.zsofia.etelka@itk.ppke.hu

I. INTRODUCTION

The advancement of sequencing methods resulted in enormous genomic data, not only revealing the nucleotide sequence of the human genome, but also resulted in the identification of many natural variants. These variants range from harmless polymorphisms to serious lethal mutations (causing cancer for example). Disease-causing germline mutations are somewhere in between neutral and deadly variations, as they can be passed down through generations, but they result in weak phenotype changes, but they lead to the emerge of diseases.

Coiled-coils are alpha-helical structures, where two or more helices are twisted around each other. They represent one of the most diverse folds - which appears in the orientation and composition of the helices and in their formation into supercomplexes. Coiled-coils exhibit characteristic interhelical interactions, usually referred as 'knobs-into-holes', that have a repetitive periodicity in which different amino acids help to hold the structure together [1]. Their structure supports the diverse range of processes coiled-coils participate in: they serve as molecular spacers, they are essential for chromosomal segregation and for DNA recognition in transcriptional activation and they help with the oligomerization and the formation of macromolecular complexes [2].

In the past several years, several studies investigated how disease-causing germline mutations perturb different segment of proteins e.g. for disordered and transmembrane proteins. Although coiled-coils were one of the earliest studied protein structures, yet the effect of disease-causing germline mutations on them is highly understudied. In our research we describe how disease-associated mutations affect coiled-coil structures and the functional consequences these changes might have. For our investigation we used comprehensive sequential coiled-coil data from different predictions. To further strengthen our results, we also used available structures containing coiled-coil domains.

II. MATERIALS AND METHODS

Non-synonym Single Nucleotide Variations were collected from the Humsavar [3] database. The protein sequences were downloaded from Uniprot [3] and the protein structures from PDB [4]. Coiled-coil regions and register positions in the human proteome were determined using a variety of prediction algorithms with their default settings. Furthermore, for coiled coil identification from structure we used Socket [5].

III. RESULTS

Our dataset contained 30 432 disease-causing mutations and 38 984 polymorphisms. We detected 17 503 proteins

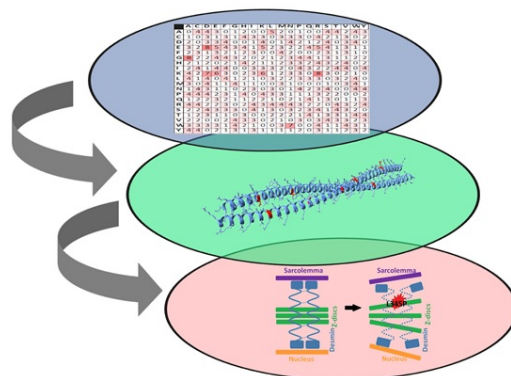


Fig. 1. The tree level of protein structure

- A. at sequence level (blue) - amino acid changes
- B. at structure level (green) - mutational effect in different positions in the coiled-coil and their distribution along coiled-coil segment
- C. at function level (red) - functional consequences of variations. For example, the L345P mutation in the coiled-coil regions of desmins disrupt the superhelix structure eventually leading to the disorganization of Z discs and affecting the integrity of the cellular filament network.

with coiled-coil domain, supported by at least one prediction method. According to the sequence-structure-function paradigm the amino acid sequence determines the structure of the protein, which is responsible for its function. Here we show how mutations affect the different aspects of coiled-coil structures and functions by mapping a high amount of polymorphisms and disease-causing mutations to the human coiled-coil proteome (Figure 1).

REFERENCES

- [1] A. N. Lupas and J. Bässler, "Coiled coils—a model system for the 21st century," *Trends in biochemical sciences*, vol. 42, no. 2, pp. 130–140, 2017.
- [2] L. Truebestein and T. A. Leonard, "Coiled-coils: The long and short of it," *Bioessays*, vol. 38, no. 9, pp. 903–916, 2016.
- [3] U. Consortium *et al.*, "Uniprot: the universal protein knowledgebase," *Nucleic acids research*, vol. 46, no. 5, p. 2699, 2018.
- [4] H. Berman, K. Henrick, H. Nakamura, and J. L. Markley, "The worldwide protein data bank (wwpdb): ensuring a single, uniform archive of pdb data," *Nucleic acids research*, vol. 35, no. suppl_1, pp. D301–D303, 2007.
- [5] J. Walshaw and D. N. Woolfson, "Socket: a program for identifying and analysing coiled-coil motifs within protein structures," *Journal of molecular biology*, vol. 307, no. 5, pp. 1427–1450, 2001.

Microfluidic particle separation methods: Pinched flow fractionation

Máté KÁLOVICS

(Supervisor: Kristóf IVÁN)

Pázmány Péter Catholic University, Faculty of Information Technology and Bionics

50/a Práter street, 1083 Budapest, Hungary

kalovics.mate@itk.ppke.hu

Abstract—The miniaturized, low-cost, portable devices with reduced sample volumes and analysis time, reduced contamination chance and high sensitivity makes microfluidic particle separation and manipulation techniques are in demand both industry and research.

The aim of this PhD research is to highlight and understand the effects that influence particle separation in pinched flow fractionation. There will be a world about the effect of the width of the pinched segment, the effect of the inlet flow rate ratio, the effect of the pinched segment length, the effect of the boundary angle, and the effect of the fluid properties. To understand and study these kind of devices in operation, computational fluid dynamics simulations were modelled with COMSOL Multiphysics 5.2a (COMSOL, Inc., PaloAlto, CA, USA). Channels were designed with AutoCAD 2019. (Autodesk Inc., San Rafael, CA, USA).

Keywords—pinched flow fractionation, microfluidics, particle separation, CFD

I. SUMMARY

Pinched flow fractionation (PFF) was first introduced by Yamada *et. al* [1] in 2004 by separating micrometer sized particles by size. The very first equation was based on the laminar flow properties and the phenomenon that the particles are following the streamlines was [1]:

$$y = \frac{(W_p - \frac{d_p}{2})W_b}{W_p}, \quad (1)$$

where W_p and W_b are the width of the pinched and the broadened segments, respectively, and d_p is the particle diameter. This equation is about the position of the particles in the outlets based on a relation between the pinched and the broadened segment with completely pinched round shaped and same sized particles. This equation does not take into consideration internal forces, particle rotation, attraction to the wall.

Since this invention many groups were working on this topic to improve and achieve the best separation resolution. Jain *et. al* [2] defined an equation which describes how to set the flow ratios the reach perfect alignment of the particles. Sai *et. al* [3] suggested an ideal channel width depending on particle sizes you want to separate. Maenaka *et. al* [4] realised that the particles are migrating away from the channel wall on its length. Shardt *et. al* [5] determined the reason for attraction to the channel wall and suggested why specific geometries are better.

Since then there is no review of this topic which makes the understanding of the working principle of these devices better. It could grant new ideas to improve the performance and new application fields.

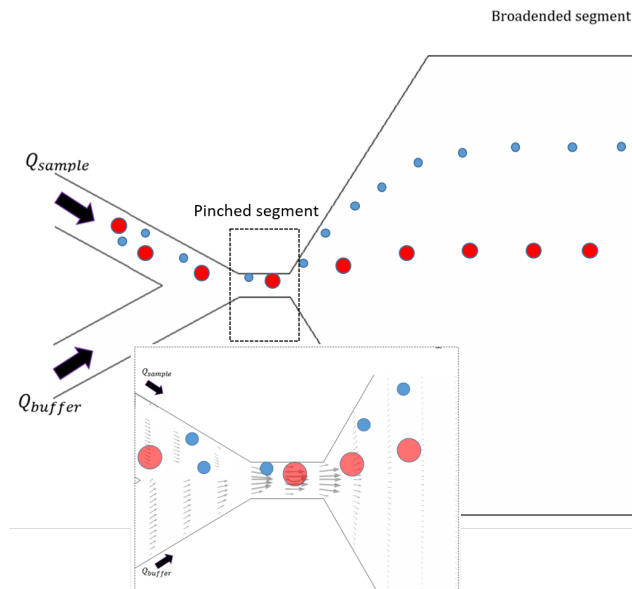


Fig. 1. Working principle of basic pinched flow fractionation devices. The sample (particle containing liquid) enters the device in the first inlet with a flow rate of Q_{sample} and a buffer solution on the second inlet with a flow rate of Q_{buffer} where $Q_{sample} \ll Q_{buffer}$. In the pinched segment the particles are pushed to the channel wall by the buffer liquid independent to size. The opening angle rapidly spreads the streamlines and significantly increases the differences in particle positions in the broadened segment. Separates particles perpendicular to flow direction based on size [1].

REFERENCES

- [1] M. Yamada, M. Nakashima, and M. Seki, "Pinched flow fractionation: continuous size separation of particles utilizing a laminar flow profile in a pinched microchannel," *Analytical chemistry*, vol. 76, no. 18, pp. 5465–5471, 2004.
- [2] A. Jain and J. D. Posner, "Particle dispersion and separation resolution of pinched flow fractionation," *Analytical chemistry*, vol. 80, no. 5, pp. 1641–1648, 2008.
- [3] Y. Sai, M. Yamada, M. Yasuda, and M. Seki, "Continuous separation of particles using a microfluidic device equipped with flow rate control valves," *Journal of chromatography A*, vol. 1127, no. 1-2, pp. 214–220, 2006.
- [4] H. Maenaka, M. Yamada, M. Yasuda, and M. Seki, "Continuous and size-dependent sorting of emulsion droplets using hydrodynamics in pinched microchannels," *Langmuir*, vol. 24, no. 8, pp. 4405–4410, 2008.
- [5] O. Shardt, S. K. Mitra, and J. Derksen, "Lattice boltzmann simulations of pinched flow fractionation," *Chemical engineering science*, vol. 75, pp. 106–119, 2012.

Review of proteomics databases for protein complex simulations

Bence Márk KEÖMLEY-HORVÁTH

(Supervisors: Attila CSIKÁSZ-NAGY, István REGULY)

Pázmány Péter Catholic University, Faculty of Information Technology and Bionics

50/a Práter street, 1083 Budapest, Hungary

keomley-horvath.bence.mark@itk.ppke.hu

Abstract—Using our whole-cell protein complex simulation tool, we want to identify essential proteins in ischemia-reperfusion. We work together with a research lab from Semmelweis, where they identified some vital proteins using multiple wet-lab proteomics experiments. Our tasks to validate it using our pipeline, and with this experience, further develop our methods.

Keywords—Proteomics; Whole-cell simulation; Protein-Protein Interactions; Complexome

I. INTRODUCTION

In previous years our group developed a whole-cell protein complex prediction tool called Cytocast. With that tool, we can simulate how the proteins bind and unbind and forming different kinds of complexes, which can help us to understand how the cell behaves in different conditions.

II. CYTOCAST

Based on the input data, our model can simulate any cell in any state. The input file describes the cell's geometrical structure, the proteins, and its localization and abundances. The interactions are described on the level of the proteins' binding sites. These binding sites do not have any structure, and they are referred to as point-like objects. The cell is divided into ten thousand sub-volumes (SVs). Thus the reaction simulation can run separately, and the particles are mixed through the diffusions.

The output of this simulation is a list of proteins and protein complexes with their abundance, structure, and localization. In the post-processing, we analyze these data based on what our goal was with the experiment.

III. INVESTIGATING ACUTE RENAL FAILURE

We are working in collaboration with a team from Semmelweis University. They are doing proteomics experiments to identify possible protein targets to treat Acute Renal Failure, which is caused by kidney ischemia-reperfusion injury (I/R injury). Using proteomics experiments they measured the abundance changes of several proteins.

IV. USING OUR PIPELINE TO IDENTIFY ESSENTIAL PROTEINS

First of all, we need a baseline protein abundance data, because we only got data about how it changed. For this, we used the PaxDB database [1]; unfortunately, there is no rat kidney data; therefore, we had to decide between whole rat sample or human kidney. We chose the latter because it was more important to make it tissue-specific, then specie specific. We checked how much of 108 protein has a human variant, and almost 96 % of the investigated proteins are in the human kidney data. We created two different input files from these

data, one with the baseline abundance data, and one was that we applied the measured changes.

For the PPI data, we used the Hippie database [2] with a 0.75 quality score threshold. We found this value optimal for the simulation performance and for good coverage. A smaller number would have decreased the simulation performance higher would decrease the coverage.

V. RESULTS

The comparative analysis of the simulations had two directions. One is when we analyzed the predicted complexes, the other where we compared the interactions of the proteins.

We ran all simulations three times, to be able to average out the noise from the system. We merged the similar complexes and clustered them to corresponding real complexes that we downloaded from the CORUM database [3]. Then we averaged the abundances of these refined complexes. Thus we can compare their numbers across multiple experiments. We listed them based on their fold change. Most of the refined complexes are a cluster of multiple raw complexes.

Another approach of the analysis would be to compare which interactions changed the most. We can use the raw data directly in this case. Therefore we can efficiently perform statistical tests. We use t-tests on the three-three identical runs of the different conditions, and we run it for every interaction. It will result in cleaner results than the fold change because it factors out the variance of the data, which can be crucial for low abundance interactions.

VI. FUTURE TASKS

We found thousands of significantly changed interactions and hundreds of complexes. Our goal is to develop a method that can predict cell behavior changes based on this data. So far, we experimented with GO enrichment analysis, which can lead to good results. We want to improve it using clusterings and machine learning. We also want to improve the general pipeline by further automatize it.

REFERENCES

- [1] M. Wang, C. J. Herrmann, M. Simonovic, D. Szklarczyk, and C. von Mering, "Version 4.0 of PaxDb: Protein abundance data, integrated across model organisms, tissues, and cell-lines," *PROTEOMICS*, vol. 15, no. 18, pp. 3163–3168, Mar. 2015.
- [2] Gregorio Alanis-Lobato, Miguel A. Andrade-Navarro, Martin H. Schaefer, *HIPPIE v2.0: enhancing meaningfulness and reliability of protein-protein interaction networks*, *Nucleic Acids Research*, Volume 45, Issue D1, January 2017, Pages D408–D414
- [3] M. Giurgiu et al., "CORUM: the comprehensive resource of mammalian protein complexes—2019," *Nucleic Acids Research*, vol. 47, no. D1, pp. D559–D563, Oct. 2018.

A new technique for a better autofocus

Márton Zsolt KISS

(Supervisor: Ákos ZARÁNDY)

Pázmány Péter Catholic University, Faculty of Information Technology and Bionics

50/a Práter street, 1083 Budapest, Hungary

kismal@itk.ppke.hu

Abstract—Digital holographic imaging is a good tool for automatic particle size and morphology measurements. Now, we present a new way to increase the accuracy of the autofocus. It is not another autofocus algorithm, but it can be used with different autofocus algorithms. This new method was tested with different autofocus algorithms, and its efficiency can be clearly observed. We used it in an in-line holographic setup, which was built to observe algae from algae cultures.

Keywords-digital holography, autofocus, microscopy, real time measurements

I. INTRODUCTION

Our aim was to have a better autofocus result to have a proper focus distance. With our approach we observe flowing samples that contain many point-like objects which are algae. From a captured hologram we can numerically reconstruct the images of the different objects that are in different depths.

Our idea was to modify the input images of the autofocus algorithm instead of the algorithm to have a better autofocus result. In the case of holography we apply numerical wave field propagation. It is known that rays connected to a higher numerical aperture have higher divergence angle. So we tested that if imaging is done only with these rays the accuracy of the focus distance measurement can be increased or not. We have to emphasize that these modified images are used only to determine the proper focus distance of an object. The original hologram and the proper focus distance are used to reconstruct the full image of an object for sample analyzes.

II. THE THEORETICAL BACKGROUND

First let observe an imaging using ray optics. Figure 1 a)-b) shows that if the numerical aperture (NA) is increased then the depth of field (δ) is decreased. They are in inverse proportion: $\delta \approx \frac{1}{NA}$. The numerical aperture is defined by the extremal rays diverging half angle (Θ). $NA = n * \sin(\Theta)$. So drawing extremal rays the focus point can be pointed out more clearly as it can be seen comparing Figure 1. a) to c). Leaving the focal point the extremal rays will spread more than the central rays. It is also known that the waist of a beam is smaller when the numerical aperture is bigger.

Because there is no way to increase the numerical aperture we decided to make the extremal rays more dominant, so we filter out the central rays that have usually higher intensity also as it can be seen in Figure 1 c). Without the central rays the image biased considerably, but the difference and so the contrast between the in focus and out of focus images will be bigger. Imaging without the central rays is imaging with a gappy wavefront.

We used holography for our measurements. The object's wavefront is captured as a thin digital hologram. We used angular spectrum method to emulate the propagation of the wave field. To make the reconstruction using only the extremal

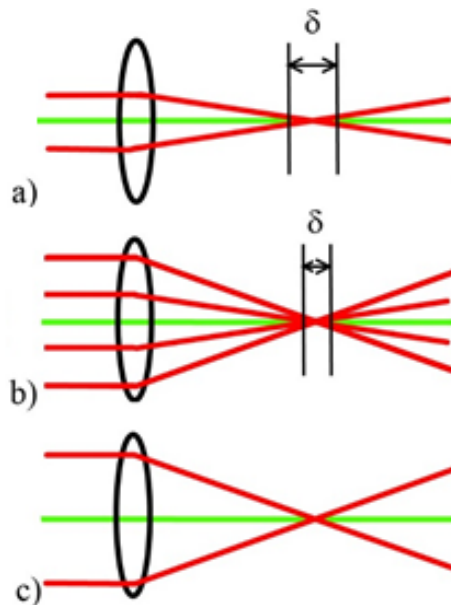
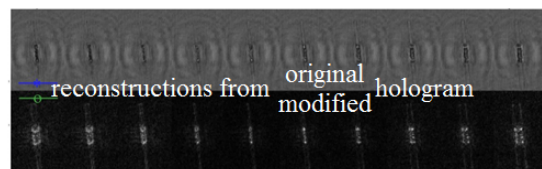


Fig. 1. a)-b) The connection between the numerical aperture (NA) and the depth of field. c) Cutting out the central rays, the effect of the extremal rays can be more dominant.



$z = 6.384, 6.451, 6.517, 6.564, 6.65, 6.717, 6.783, 6.85, 6.915, 6.983$ mm

Fig. 2. Making the imaging without the central rays -the images that have a black background - will define more clearly where the focus is.

rays we can cut out the middle of the hologram of every object or also we can make a low frequency filtering. We chose the second solution. It is easier, and making on the full captured hologram it will be done on every holograms of the objects.

III. RESULTS AND CONCLUSION

Using this filtering it is more obvious for human and for autofocus algorithms where the focus is. In Figure 2. we can see the reconstructions at different distances of an original and a modified holograms.

ACKNOWLEDGEMENT

This article was fully presented in: SPIE, Photonoc West 2019. Conference, Proceedings Volume 10944, Practical Holography XXXIII: Displays, Materials, and Applications; 109440I (2019) <https://doi.org/10.1117/12.2508896>

A simple model to simulate rhythm generation in the medial septum

Barnabás KOCSIS

(Supervisor: István ULBERT)

Pázmány Péter Catholic University, Faculty of Information Technology and Bionics
50/a Práter street, 1083 Budapest, Hungary
kocsis.barnabas@itk.ppke.hu

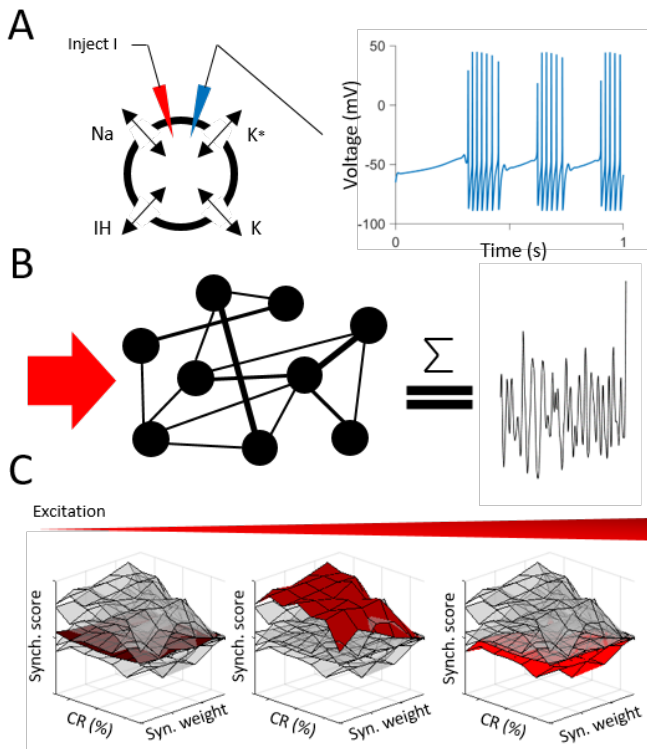


Fig. 1. Project workflow. A: The one-compartment model neuron with 4 channels fires rhythmic bursts [1]. B: Randomly connected minimal network, and theoretical output. C: Exploration of the parameter space.

Abstract—Hippocampal theta oscillation was extensively studied in the past years. Several experiments were conducted and computational models [2][3] were suggested to decipher the neural mechanisms underlying theta generation. Here we submitted a minimal network model, that is capable of transforming tonic excitation to a rhythmic signal. Autonomous dynamical properties of one-compartment neurons [1] drove the synchronization process across the model circuits. This network design was tuned based on our anaesthetized rodent data. Optimal model parameters were selected after a parameter space exploration. Formerly written algorithms for *in vivo* projects enabled us a comprehensive analysis of the model output. Simulations revealed significant similarities of the model and *in vivo* results. Both data sets' neurons exhibited similar bursting dynamics and pacemaker synchronization trends were also in accordance with each other.

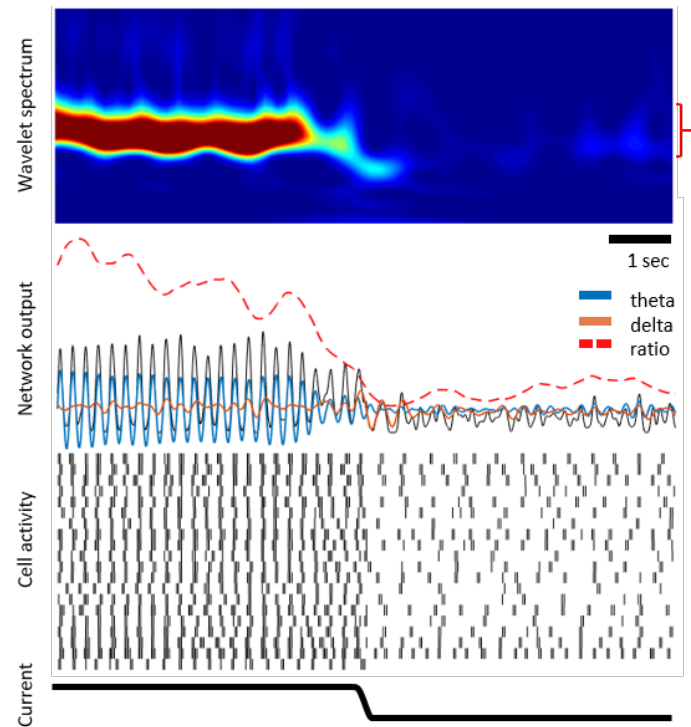


Fig. 2. Optimal network, theta-delta transition. Neurons desynchronize to a weaker excitation, theta disappears from dynamic wavelet spectrum (red curly brackets).

Keywords—neuronal oscillations, theta rhythm, hippocampus, medial septum, pacemaker, synchronization, network model, parameter space

REFERENCES

- [1] D. Golomb, K. Donner, L. Shacham, D. Shlosberg, Y. Amitai, and D. Hansel, "Mechanisms of firing patterns in fast-spiking cortical interneurons," *PLoS Computational Biology*, vol. 3, no. 8, 2007.
- [2] B. Ujfalussy and T. Kiss, "How do glutamatergic and gabaergic cells contribute to synchronization in the medial septum?," *Journal of computational neuroscience*, vol. 21, no. 3, pp. 343–357, 2006.
- [3] I. E. Mysin, V. F. Kitchigina, and Y. Kazanovich, "Modeling synchronous theta activity in the medial septum: key role of local communications between different cell populations," *Journal of computational neuroscience*, vol. 39, no. 1, pp. 1–16, 2015.

Multiple SVM based Brain Computer Interface for Cybathlon 2020

Csaba Márton KÖLLŐD

(Supervisor: István ULBERT)

Pázmány Péter Catholic University, Faculty of Information Technology and Bionics

50/a Práter street, 1083 Budapest, Hungary

kollod.csaba@itk.ppke.hu

Abstract—This report describes the start of the HUN BCI project. The aim of the project is to develop a Brain-Computer Interface System, which can classify the brain signals and control a computer game.

I. INTRODUCTION

Brain-Computer Interfaces (BCI) are integrated software and hardware systems which record the bio-electrical signals of the brain. And by classifying the signals it controls an external device. (Fig. 1.)

Our research team, lead by István ULBERT, aims to create a BCI system, which will be challenged by other BCI devices of other research groups, in 2020 at the international Cybathlon competition. <https://cybathlon.ethz.ch/>

II. DATASET

Our dataset is recorded similarly according to the Schalk database [1], which is available on <https://physionet.org/> [2]. For signal recording, 64 channeled ActiChamp+ EEG system were used, which is produced by Brain Products. In our initial paradigm, four motor movements and the resting activity were imagined by the subjects, which concluded overall five imaginary classes. However, during the resting phase, subjects were allowed to blink, swallow and do many different short movements in purpose to avoid artefact appearance under motor movement imagination. Therefore later on the resting activity were avoid in EEG signal classification.

III. METHODS

Raw EEG data is recorded and send to the Signal Processing part of the BCI System. With a given window length data is cut and for each window the Power Spectral Density (PSD) is calculated. Two different methods are created for feature extraction and classification. One of them is the FFT POWER method, where the average FFT of a well known EEG band is calculated for each channel. This resulted a *number of channel* \times *I* feature vector which is used as train and test data for a Support Vector Machine (SVM). The other is the FFT RANGE method, which further utilizes the FFT Power method, by creating feature vectors form distinct 2 Hz wide parts of the PSD. These features are fed to separate SVMs with respect to the frequency range. The final classification result is calculated as the max vote of the individual SVMs.

IV. RESULTS

The FFT Range method outperformed the FFT Power method on the alpha range. However the FFT Power method on beta brain waves resulted similar accuracy as the FFT Range method. The accuracy of the classifications were calculated and tested with n-fold crossvalidation.

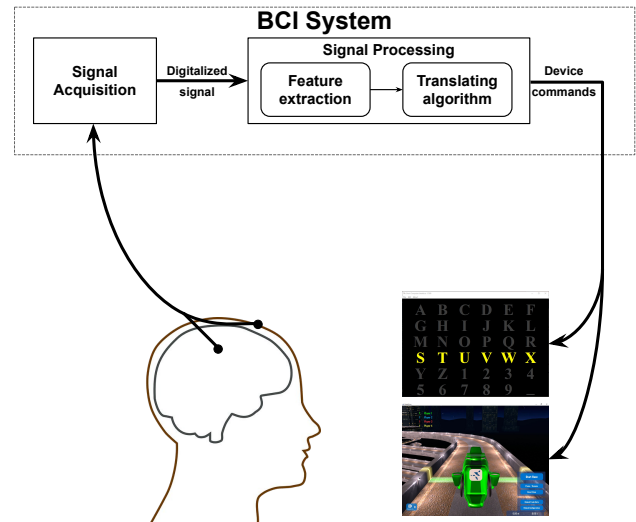


Fig. 1. BCI System workflow, based on J. R. Wolpaw et al. [3]

With the help of these methods the prototype BCI System is created, which now works and can be used for pilot training. This system will be further developed with new feature extraction and classification algorithms.

V. ACKNOWLEDGEMENT

Our research was founded by the Hungarian Brain Research Program Grant (Grant No. 2017-1.2.1-NKP-2017-00002).

REFERENCES

- [1] G. Schalk, D. J. McFarland, T. Hinterberger, N. Birbaumer, and J. R. Wolpaw, "Bci2000: a general-purpose brain-computer interface (bci) system," *IEEE Transactions on biomedical engineering*, vol. 51, no. 6, pp. 1034–1043, 2004.
- [2] A. L. Goldberger, L. A. Amaral, L. Glass, J. M. Hausdorff, P. C. Ivanov, R. G. Mark, J. E. Mietus, G. B. Moody, C.-K. Peng, and H. E. Stanley, "Physiobank, physiokit, and physionet: components of a new research resource for complex physiologic signals," *Circulation*, vol. 101, no. 23, pp. e215–e220, 2000.
- [3] J. R. Wolpaw, N. Birbaumer, D. J. McFarland, G. Pfurtscheller, and T. M. Vaughan, "Brain-computer interfaces for communication and control," *Clinical neurophysiology*, vol. 113, no. 6, pp. 767–791, 2002.

Particle separation by inertial microfluidic devices

Dániel KOLPASZKY

(Supervisor: Kristóf IVÁN)

Pázmány Péter Catholic University, Faculty of Information Technology and Bionics

50/a Práter street, 1083 Budapest, Hungary

kolpaszky.daniel@itk.ppke.hu

Abstract—An increasing research field today is the cells and particles separation and focusing in microfluidics. These processes are useful in biomedical applications and basic cell biology research as they offer cost-effective and miniaturized point-of-care (POC) diagnostic tools and replication of rare cells.

The aim of this PhD research is to highlight fluid flow conditions above the generally prevalent low Stokes range, where the hydrodynamic inertial effects arising. The most common and best flow index for characterization is the Reynolds number, which gives the ratio of viscous to inertia forces. Inertial microfluidics works in laminar flow regime, between Stokes ($Re < 1$) and turbulent ($Re > \sim 2300$) flow. To better understand the operation of these devices in this region, flow physics was followed by a review of the devices exploiting these effects, followed by modeling of different microchannel geometries using AutoCAD 2018 (Autodesk Inc., San Rafael, CA, USA) vector-graphing program and simulating their hydrodynamic properties with computational fluid dynamics program, COMSOL Multiphysics 5.2a (COMSOL, Inc., PaloAlto, CA, USA).

Keywords-microfluidics; inertial microfluidics; particle separation; MEMS; Computational Fluid Dynamics;

I. SUMMARY

In the case of a straight channel of circular cross-section, the particles enroll equilibrium positions near the channel wall approximately 0.6 times the radius of the channel. These positions changes if in a straight rectangular channel. Determination of the equilibrium positions becomes much more complex, for a channel with square cross-section four symmetrical positions can be observed, in the center of each channel wall 0.6 times from the center. In rectangular channels, only two positions can be observed at the center of the wider channel walls. The particles to reach these positions, a certain length is required, which is in dependence of the flow rate. [1], [2], [3]

However with straight channels, a high rate particle separation cannot be achieved, only a certain degree of concentration can be solved for bigger particles, because they are focused after a certain length due to the inertial effects, while the smaller particles in the medium scatter across the channel. [3], [4], [5]

This is why devices with different channel structures have been appeared, such as the spiral, serpentin, microvortex manipulating (MVM), deterministic lateral displacement (DLD) and devices with contraction and expansion array (CEA) channels, of which I focused on CEA, because it has the best theoretical separation ratio. [6]

II. FIGURES

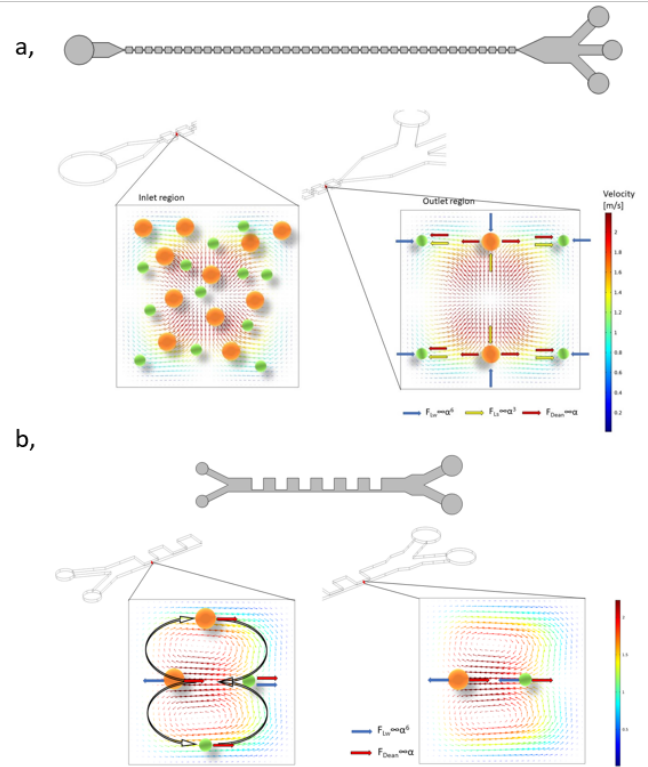


Fig. 1. Working principle and a cross section from the contraction chamber of symmetric (a.) and asymmetric (b.) CEA device. (a.) Smaller particles (green) following streamlines near the channel walls, inertial forces pushes bigger particles (orange) at the center of the channel. Due to the sudden narrowing at the contraction region vortices generating with opposite orbiting direction with four center. (b.) Smaller particles (green) takes up positions near the straight channel wall, inertial forces pushes bigger particles (orange) away from the straight channel wall, in this structure only two facing vortices arising at the contraction region due to the asymmetric expansion and contraction.

REFERENCES

- [1] B. Ho and L. Leal, "Inertial migration of rigid spheres in two-dimensional unidirectional flows," *Journal of fluid mechanics*, vol. 65, no. 2, pp. 365–400, 1974.
- [2] D. Di Carlo, J. F. Edd, K. J. Humphry, H. A. Stone, and M. Toner, "Particle segregation and dynamics in confined flows," *Physical review letters*, vol. 102, no. 9, p. 094503, 2009.
- [3] E. S. Asmolov, "The inertial lift on a spherical particle in a plane poiseuille flow at large channel Reynolds number," *Journal of Fluid Mechanics*, vol. 381, pp. 63–87, 1999.
- [4] J.-P. Matas, J. F. Morris, and E. Guazzelli, "Inertial migration of rigid spherical particles in poiseuille flow," *Journal of Fluid Mechanics*, vol. 515, pp. 171–195, 2004.
- [5] A. T. Ciftlik, M. Etori, and M. A. Gijs, "High throughput-per-footprint inertial focusing," *Small*, vol. 9, no. 16, pp. 2764–2773, 2013.
- [6] J. Zhang, W. Li, and G. Alici, "Inertial microfluidics: mechanisms and applications," in *Advanced Mechatronics and MEMS Devices II*, pp. 563–593, Springer, 2017.

A review of protein separation and detection methods in microfluidics

Adrienn Lilla MÁRTON

(Supervisor: Kristóf IVÁN)

Pázmány Péter Catholic University, Faculty of Information Technology and Bionics

50/a Práter street, 1083 Budapest, Hungary

marton.adrienn.lilla@itk.ppke.hu

Thanks to the impressive technological advances of the last few decades, great progress has been made in the technologies of microfabrication and micro-electromechanical systems (MEMS), which have a major impact on diagnostics. Devices such as Lab-on-a-Chip are already widely used tools in this field. These multi-laboratory devices offer the possibility to detect and analyze proteins, while integrating all the steps within the same chip itself. Testing proteins plays a crucial role in diagnostics, as they are the most common biomarkers for diseases, infections and many types of cancer. Therefore, their separation and identification are essential for healthcare. The efficiency of these analyzes depends heavily on a fundamental part of the device, namely the sensor. Sensors are usually characterized by 3 parameters, namely sensitivity, specificity and the limit of the detection. [1] Microfluidic particle separation can be carried out with various active and passive methods on the microscale. On the nanoscale, however, the sorting resolution is greatly reduced due to the smaller size of the particles. Rapid Brownian motions occur, and it is also necessary to take into account surface interaction forces such as electrostatics, hydrophobic, and Van der Waals forces [2]. When these effects become more dominant, the sorting resolution is more negatively influenced in this case, as the separation behavior depends strongly on the properties of the environment. This can be improved with so-called affinity-based binding separation, in which micro- or nano-beads selectively bind to the target particles. [3] It is often used for protein separation. In addition, further positive effects can be achieved by using an active method that implies an external source of the driving force. These separation techniques can improve the result obtained during the detection phase. The beads can also be used during the detection phase, e.g. Surface Plasmon Resonance (SPR) [4] and Surface Enhanced Raman spectrometry (SERS). [5] Both methods are based on optical detection, whereby variations in light intensity or refractive index sensitivity are measured by optical sensors [6]. Electrochemical detection is based on the measurement of various electrical properties such as potential changes, current, conductance, impedance and capacitance. [6] Mechanical detection, in which the surface tension or resonance frequency is measured using optical technique. These sensors use cantilevers for signal amplification [6]. As we can see, there are many great solutions, but still many challenges also. This is because proteins are extremely diverse in both their physical and chemical properties. Today, improving existing equipment and techniques is one of the most researched areas because they have a profound impact on health and everyday life not only of humanity but of all living beings.

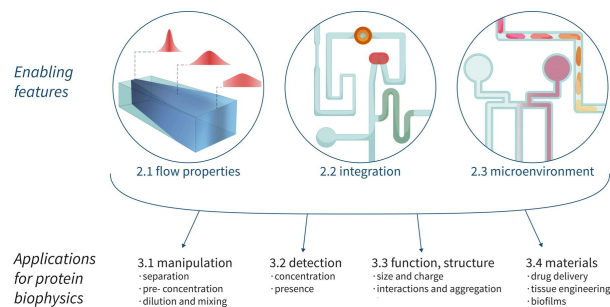


Fig. 1. Representation of the essential features of microfluidics and in addition, the methods can be used for analysing test sample properties which could be e.g. the protein biophysical properties [7]

REFERENCES

- [1] A. Gencoglu and A. R. Minerick, "Electrochemical detection techniques in micro- and nanofluidic devices" *Microfluidics and Nanofluidics* vol. 17, pp. 781–807. 25 March 2014.
- [2] T. M. Squires and S. R. Quakek, "Microfluidics: Fluid physics at the nanoliter scale" *Rev. Mod. Phys* vol. 77, no. 3, pp. 977. 6. Oct 2005.
- [3] M. Tsushima, S.i Sato, and H. Nakamura, "Selective purification and chemical labeling of a target protein on ruthenium photocatalyst-functionalized affinity beads" *Cheml Commun* vol. 53 no. 35 pp. 977. 27. Apr 2017.
- [4] D. G. Drescher, D. Selvakumar 2, M. J Drescher, "Analysis of Protein Interactions by Surface Plasmon Resonances" *Adv Protein Chem Struct Biol* vol. 110, pp. 1-30. 12 Sep 2017.
- [5] A. Gencoglu and A. R. Minerick, "Surface Enhanced Raman Spectroscopy for Single Molecule Protein Detection" *Sci Rep* vol. 9,12356. 26 Aug 2019.
- [6] N. M. Matos Pires, T. Dong, U. Hanke, and N. Hoivik, "Recent Developments in Optical Detection Technologies in Lab-on-a-Chip Devices for Biosensing Applications" *Sensors* vol. 14 no 8, pp. 15458–15479. 21 Aug 2014
- [7] S. Abdullah et al. "Microfluidics for Protein Biophysics" *J Mol Biol* vol. 430 no. 5 pp.565-580 2 March 2018.

Opening the genetic toolbox in cats

Gergely MÉSZÁROS

(Supervisors: István ULBERT, Dániel HILLIER)

Pázmány Péter Catholic University, Faculty of Information Technology and Bionics
50/a Práter street, 1083 Budapest, Hungary
meszaros.gergely@itk.ppke.hu

AAV is a widely used tool to explore unknown or not well characterized connections and relations between neurons, nuclei and cortical areas in the brain. Local injections of engineered viral vectors can be delivered into different areas of the nervous system.

Investigation of the visual system by targeting retinal cells is of high interest due to successful gene delivery targeting genetically determined diseases of the retina. A successful gene delivery into the retina could be achieved by subretinal [1]–[3] intravitreal[4]–[6] or even by suprachoroidal [7] injections. Several animal models were used including rodents[4], [5], [8]–[11], cats[6], [12], dog[1], [2], [13], [14] and primates[7], [15]–[19].

However there are limitations of the retinal gene delivery method. Genetically encoded obstacles in the body might cause the limited effectiveness of the AAV-mediated gene delivery. One factor hindering efficient delivery is the vitreal body, which might be a strong barrier to infect effectively the whole retina and its layers[20]. Solving the problem vitrectomy is used not only in animal models[21], [22], but also translated into human medical use[23], [24]. Although this method should be used carefully, due to the possibility to get just the opposite result causing significantly worse gene-expression pattern in the retinal cells compared with the untreated animal controls[13].

The other barrier inside the retina is the inner limiting membrane (ILM) set up by Müller cells. To effectively improve the delivered gene expression ILM removal (peel) was applied in several researches[17], [20], [25].

There are other engineered solutions for enhanced retinal gene delivery like microcatheter[21], electric current stimulation[26] or MR-assisted focused ultrasound[27].

A less invasive and minimally harmful treatment option could be via intravenous administration of the viral vector, however the blood-brain and blood-retina barrier may block or reduce the effectiveness of the treatment. It has been shown in mice, that this method may work with conventional or non-conventional engineered viral vectors in rodent[13], [27], [28], however whether these approaches could work in larger animal models and ultimately humans remain to be seen.

Our objective is to develop and validate in preclinical species non-invasive, efficient and targeted gene delivery strategies to the retina and the brain. We will reach this objective by testing synthetic capsid variants, promoter sequences and genes for neuronal response monitoring and modulation. Our preliminary experiment already demonstrated that one selected capsid-promoter combination yields non-invasive, stable, long-term functional neuronal targeting in preclinical species.

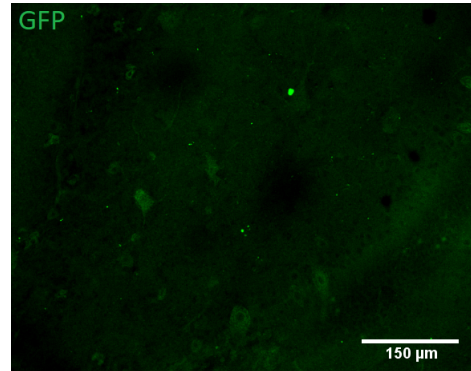


Fig. 1. Successful AAV gene delivery into the retina of cat (ganglion cell side) without any invasive treatment referred in the main text

REFERENCES

- [1] A. V. Cideciyan, R. Sudharsan, V. L. Dufour, M. T. Massengill, S. Iwabe, M. Swider, B. Lisi, A. Sumaroka, L. F. Marinho, T. Appelbaum, B. Rossmiller, W. W. Hauswirth, S. G. Jacobson, A. S. Lewin, G. D. Aguirre, and W. A. Beltran, “Mutation-independent rhodopsin gene therapy by knockdown and replacement with a single AAV vector,” *Proceedings of the National Academy of Sciences*, vol. 115, pp. E8547–E8556, Sept. 2018.
- [2] K. E. Guziewicz, B. Zangerl, A. M. Komáromy, S. Iwabe, V. A. Chiodo, S. L. Boye, W. W. Hauswirth, W. A. Beltran, and G. D. Aguirre, “Recombinant AAV-Mediated BEST1 Transfer to the Retinal Pigment Epithelium: Analysis of Serotype-Dependent Retinal Effects,” *PLoS ONE*, vol. 8, p. e75666, Oct. 2013.
- [3] Q. Li, A. M. Timmers, J. Guy, J. Pang, and W. W. Hauswirth, “Cone-specific expression using a human red opsin promoter in recombinant AAV,” *Vision Research*, vol. 48, pp. 332–338, Feb. 2008.
- [4] S. H. S. Lee, H. J. Kim, O. K. Shin, J.-S. Choi, J. Kim, Y.-H. Cho, J. Ha, T. K. Park, J. Y. Lee, K. Park, and H. Lee, “Intravitreal Injection of AAV Expressing Soluble VEGF Receptor-1 Variant Induces Anti-VEGF Activity and Suppresses Choroidal Neovascularization,” *Investigative Ophthalmology & Visual Science*, vol. 59, p. 5398, Nov. 2018.
- [5] Y.-F. Liu, S. Huang, T. K. Ng, J.-J. Liang, Y. Xu, S.-L. Chen, C. Xu, M. Zhang, C. P. Pang, and L.-P. Cen, “Longitudinal evaluation of immediate inflammatory responses after intravitreal AAV2 injection in rats by optical coherence tomography,” *Experimental Eye Research*, vol. 193, p. 107955, Apr. 2020.
- [6] S. Wassmer, L. Carvalho, B. György, L. Vandenberghe, and C. Maguire, “Exosome-associated aav2 vector mediates robust gene delivery into the murine retina upon intravitreal injection,” *Scientific Reports*, vol. 7, p. 45329, 03 2017.
- [7] G. Yiu, S. H. Chung, I. N. Mollhoff, U. T. Nguyen, S. M. Thomasy, J. Yoo, D. Taraborelli, and G. Noronha, “Suprachoroidal and Subretinal Injections of AAV Using Transscleral Microneedles for Retinal Gene Delivery in Nonhuman Primates,” *Molecular Therapy - Methods & Clinical Development*, vol. 16, pp. 179–191, Mar. 2020.
- [8] J. J. Alexander, Y. Umino, D. Everhart, B. Chang, S. H. Min, Q. Li, A. M. Timmers, N. L. Hawes, J.-j. Pang, R. B. Barlow, and W. W. Hauswirth, “Restoration of cone vision in a mouse model of achromatopsia,” *Nature Medicine*, vol. 13, pp. 685–687, June 2007.
- [9] R. Ali, “Gene transfer into the mouse retina mediated by an adeno-associated viral vector,” *Human Molecular Genetics*, vol. 5, pp. 591–594, May 1996.
- [10] M. S. Dias, V. G. Araujo, T. Vasconcelos, Q. Li, W. W. Hauswirth, R. Linden, and H. Peters-Silva, “Retina transduction by rAAV2 after in-

- travitreal injection: comparison between mouse and rat,” *Gene Therapy*, vol. 26, pp. 479–490, Dec. 2019.
- [11] D. L. Simons, S. L. Boye, W. W. Hauswirth, and S. M. Wu, “Gene therapy prevents photoreceptor death and preserves retinal function in a Bardet-Biedl syndrome mouse model,” *Proceedings of the National Academy of Sciences*, vol. 108, pp. 6276–6281, Apr. 2011.
- [12] K. A. Hansen, I. K. Sugino, F. Yagi, H. Wang, I. Tsukahara, V. Gullapalli, J. Bennett, and M. A. Zarbin, “Adeno-Associated Virus Encoding Green Fluorescent Protein as a Label for Retinal Pigment Epithelium,” *Investigative Ophthalmology & Visual Science*, vol. 44, p. 772, Feb. 2003.
- [13] R. F. Boyd, S. L. Boye, T. J. Conlon, K. E. Erger, D. G. Sledge, I. M. Langohr, W. W. Hauswirth, A. M. Komáromy, S. E. Boye, S. M. Petersen-Jones, and J. T. Bartoe, “Reduced retinal transduction and enhanced transgene-directed immunogenicity with intravitreal delivery of rAAV following posterior vitrectomy in dogs,” *Gene Therapy*, vol. 23, pp. 548–556, June 2016.
- [14] V. Pichard, N. Provost, A. Mendes-Madeira, L. Libeau, P. Hulin, K.-T. Tshilenge, M. Biget, B. Ameline, J.-Y. Deschamps, M. Weber, G. Le Meur, M.-A. Colle, P. Moullier, and F. Rolling, “AAV-mediated Gene Therapy Halts Retinal Degeneration in PDE6-deficient Dogs,” *Molecular Therapy*, vol. 24, pp. 867–876, May 2016.
- [15] L. C. Byrne, T. P. Day, M. Visel, C. Fortuny, D. Dalkara, W. H. Merigan, D. V. Schaffer, and J. G. Flannery, “In vivo directed evolution of AAV in the primate retina,” preprint, Neuroscience, Nov. 2019.
- [16] L. S. Carvalho, R. Xiao, S. J. Wassmer, A. Langsdorf, E. Zinn, S. Pacouret, S. Shah, J. I. Comander, L. A. Kim, L. Lim, and L. H. Vandenberghe, “Synthetic Adeno-Associated Viral Vector Efficiently Targets Mouse and Nonhuman Primate Retina *In Vivo*,” *Human Gene Therapy*, vol. 29, pp. 771–784, July 2018.
- [17] K. Y. C. Teo, S. Y. Lee, A. V. Barathi, S. B. B. Tun, L. Tan, and I. J. Constable, “Surgical Removal of Internal Limiting Membrane and Layering of AAV Vector on the Retina Under Air Enhances Gene Transfection in a Nonhuman Primate,” *Investigative Ophthalmology & Visual Science*, vol. 59, p. 3574, July 2018.
- [18] A. M. Timmers, J. A. Newmark, H. T. Turunen, T. Farivar, J. Liu, C. Song, G.-j. Ye, S. Pennock, C. Gaskin, D. R. Knop, and M. S. Shearman, “Ocular Inflammatory Response to Intravitreal Injection of Adeno-Associated Virus Vector: Relative Contribution of Genome and Capsid,” *Human Gene Therapy*, vol. 31, pp. 80–89, Jan. 2020.
- [19] L. H. Vandenberghe, P. Bell, A. M. Maguire, R. Xiao, T. B. Hopkins, R. Grant, J. Bennett, and J. M. Wilson, “AAV9 Targets Cone Photoreceptors in the Nonhuman Primate Retina,” *PLoS ONE*, vol. 8, p. e53463, Jan. 2013.
- [20] D. Dalkara, K. D. Kolstad, N. Caporale, M. Visel, R. R. Klimczak, D. V. Schaffer, and J. G. Flannery, “Inner Limiting Membrane Barriers to AAV-mediated Retinal Transduction From the Vitreous,” *Molecular Therapy*, vol. 17, pp. 2096–2102, Dec. 2009.
- [21] M. C. Peden, J. Min, C. Meyers, Z. Lukowski, Q. Li, S. L. Boye, M. Levine, W. W. Hauswirth, R. Ratnakaram, W. Dawson, W. C. Smith, and M. B. Sherwood, “Ab-Externo AAV-Mediated Gene Delivery to the Suprachoroidal Space Using a 250 Micron Flexible Microcatheter,” *PLoS ONE*, vol. 6, p. e17140, Feb. 2011.
- [22] K.-T. Tshilenge, B. Ameline, M. Weber, A. Mendes-Madeira, P. Pichard, and F. Rolling, “Vitreotomy Before Intravitreal Injection of AAV2/2 Vector Promotes Efficient Transduction of Retinal Ganglion Cells in Dogs and Nonhuman Primates,” *Hum Gene Ther Methods*, June 2016.
- [23] I. J. Constable, C. M. Pierce, C.-M. Lai, A. L. Magno, M. A. Degli-Esposti, M. A. French, I. L. McAllister, S. Butler, S. B. Barone, S. D. Schwartz, M. S. Blumenkranz, and E. P. Rakoczy, “Phase 2a Randomized Clinical Trial: Safety and Post Hoc Analysis of Subretinal rAAV.sFLT-1 for Wet Age-related Macular Degeneration,” *EBioMedicine*, vol. 14, pp. 168–175, Dec. 2016.
- [24] K. Xue, M. Groppe, A. P. Salvetti, and R. E. MacLaren, “Technique of retinal gene therapy: delivery of viral vector into the subretinal space,” *Eye*, vol. 31, pp. 1308–1316, Sept. 2017.
- [25] K. Takahashi, T. Igarashi, K. Miyake, M. Kobayashi, C. Yaguchi, O. Iijima, Y. Yamazaki, Y. Katakai, N. Miyake, S. Kameya, T. Shimada, H. Takahashi, and T. Okada, “Improved Intravitreal AAV-Mediated Inner Retinal Gene Transduction after Surgical Internal Limiting Membrane Peeling in Cynomolgus Monkeys,” *Molecular Therapy*, vol. 25, pp. 296–302, Jan. 2017.
- [26] H. Song, R. A. Bush, Y. Zeng, H. Qian, Z. Wu, and P. A. Sieving, “Trans-ocular Electric Current *In Vivo* Enhances AAV-Mediated Retinal Gene Transduction after Intravitreal Vector Administration,” *Molecular Therapy - Methods & Clinical Development*, vol. 13, pp. 77–85, June 2019.
- [27] Y. Touahri, R. Dixit, R. H. Kofoed, K. Miloska, E. Park, R. Raeesossadati, K. Markham-Coultes, L. A. David, H. Rijal, J. Zhao, M. Lynch, K. Hynynen, I. Aubert, and C. Schuurmans, “Focused ultrasound as a novel strategy for noninvasive gene delivery to retinal Müller glia,” *Theranostics*, vol. 10, no. 7, pp. 2982–2999, 2020.
- [28] E. Hudry, E. Andres-Mateos, E. P. Lerner, A. Volak, O. Cohen, B. T. Hyman, C. A. Maguire, and L. H. Vandenberghe, “Efficient Gene Transfer to the Central Nervous System by Single-Stranded Anc80L65,” *Molecular Therapy - Methods & Clinical Development*, vol. 10, pp. 197–209, Sept. 2018.

Analyses of protein-protein interactions in the PSD by stochastic simulations

Marcell MISKI

(Supervisor: Attila CSIKÁSZ-NAGY)

Pázmány Péter Catholic University, Faculty of Information Technology and Bionics

50/a Práter street, 1083 Budapest, Hungary

miski.marcell@itk.ppke.hu

Abstract—The postsynaptic density is an elaborate network of proteins involved in intraneuronal information transmission. My goal is to model the occurrence and distribution of complexes with stochastic simulations. I have parametrized and performed a number of test simulations in order to set up a protocol suitable for calculations with realistic molecule numbers.

Keywords—keyword;postsynaptic density; CytoCast; Synaptic Theory;

I. INTRODUCTION

Modeling synaptic signal transduction is key to understanding neuronal function and dysfunction. In my work I have focused on some key known complexes of the postsynaptic density (PSD), a key component in transmitting signals towards the neuronal body. I have used computer simulations allowing the inspection of protein complexes within the PSD.

II. ABOUT THE SIMULATIONS

I put the experimental data into the agent based Gillespie-simulations similar to those described in [SiComPre][1] where I got complexes as a graph (nodes are the proteins, edges are the contacts). I have set up, run and evaluated about 1,000 simulations with different parameters. I have included only the most abundant PSD proteins in these and focused on whether experimentally described complexes emerge using the various settings.

III. DISCUSSION

I conclude that carefully parametrized simulations can give rise to complexes that have been described/suggested by literature data. The next step is to scale up these simulation for realistic protein abundance data.

ACKNOWLEDGEMENTS

I would like to thank to supervisor Attila Csikász-Nagy and Zoltán Gáspári for their guidance and to Bence Márk Keömley-Horváth and Simone Rizetto the developers of CytoCast. The authors acknowledge the support of the National Research, Development and Innovation Office – NKFIH through grant no. NN124363. The research was funded by the European Union and co-financed by the European Social Fund under grant number EFOP-3.6.2-162017-00013.

REFERENCES

- [1] S. Rizzetto, P. Moyses, B. Baldacci, C. Priami, and A. Csikász-Nagy, "Context-dependent prediction of protein complexes by SiComPre," *npj Systems Biology and Applications*, vol. 4, Sept. 2018.

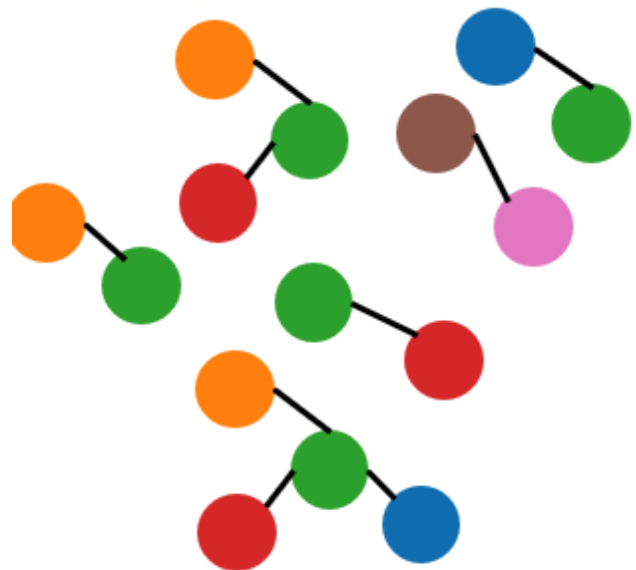


Fig. 1. The schematic diagram of possible complexes in a system.

Comparing the performance of global search algorithms in tuning the parameters of a morphologically and biophysically detailed model neuron

Máté MOHÁCSI

(Supervisors: Szabolcs KÁLI, Tamás FREUND)

Pázmány Péter Catholic University, Faculty of Information Technology and Bionics

50/a Práter street, 1083 Budapest, Hungary

mohacsi.mate@itk.ppke.hu

Keywords-neuronal modeling; model fitting; algorithms; performance

I. INTRODUCTION

Automated parameter search has become a standard method in the modeling of neural systems [1], [2], [3]. These studies could potentially take advantage of recent developments in nonlinear optimization, and the availability of software packages containing high-quality implementations of algorithms that proved useful in other domains. However, a systematic comparison of the available algorithms for problems that are typical in neuroscience has not been performed.

Our starting point was our previously developed software (Optimizer; <https://github.com/KaliLab/optimizer>), which was already shown to be a useful tool for neuronal optimization. [4] We developed a software tool for fitting the parameters of neural models, which provides intuitive, uniform access to a variety of state-of-the-art optimization algorithms implemented by four different Python packages. We also established a set of benchmark problems of different complexity that involve a variety of widely used neuronal models. We then used our optimization tool to systematically evaluate the performance of the algorithms on our set of benchmark problems.

We found that several evolutionary and related algorithms consistently provided good solutions for all of our benchmarks (Fig. 1). However, the relative performance of the different methods, both in terms of the quality of the final result and in terms of convergence speed, depended substantially on the nature of the problem. We hope that our software tool and benchmarking results will facilitate the choice and application of the best parameter-fitting methods in neuroscientific research.

ACKNOWLEDGEMENTS

I would like to thank to my supervisor Szabolcs Káli, Sára Sáray, Márk Patrik Török and Luca Tar for their help and support. We received funding from the European Union's Horizon 2020 Framework Programme for Research and Innovation under the Specific Grant Agreements No. 720270 and No. 785907 (Human Brain Project SGA1 and SGA2), from the Széchenyi 2020 Program of the Human Resource Development Operational Program, and from the Program of Integrated Territorial Investments in Central-Hungary (EFOP-3.6.2-16-2017-00013 and 3.6.3-VEKOP- 16-2017- 00002).

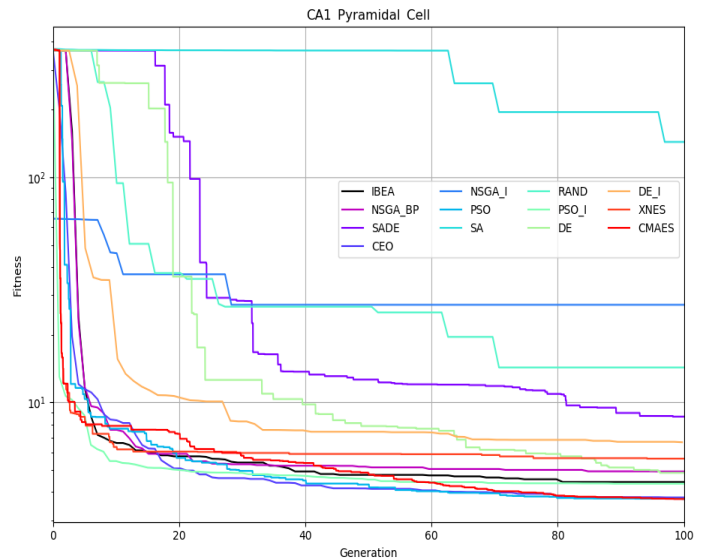


Fig. 1. Generation plot of all the algorithms used to optimize the CA1 pyramidal cell use-case. The figure shows the median over 10 consecutive runs of the cumulative minimum error.

REFERENCES

- [1] S. Druckmann, T. Berger, S. Hill, F. Schürmann, H. Markram, and I. Segev, "Evaluating automated parameter constraining procedures of neuron models by experimental and surrogate data," *Biological cybernetics*, vol. 99, pp. 371–9, 12 2008.
- [2] M. Vanier and J. Bower, "A comparative survey of automated parameter-search methods for compartmental neural models," *Journal of computational neuroscience*, vol. 7, pp. 149–71, 09 1999.
- [3] W. Van Geit, E. De Schutter, and P. Achard, "Automated neuron model optimization techniques: A review," *Biological cybernetics*, vol. 99, pp. 241–51, 12 2008.
- [4] P. Friedrich, M. Vella, A. I. Gulyás, T. F. Freund, and S. Káli, "A flexible, interactive software tool for fitting the parameters of neuronal models," *Frontiers in Neuroinformatics*, vol. 8, p. 63, 2014.

Functional and structural investigation of the post-synaptic scaffold protein GKAP

Eszter NAGY-KANTA

(Supervisor: Zoltán GÁSPÁRI)

Pázmány Péter Catholic University, Faculty of Information Technology and Bionics

50/a Práter street, 1083 Budapest, Hungary

nagy-kanta.eszter@itk.ppke.hu

Keywords-PSD; disordered protein structure; NMR

I. INTRODUCTION

Scaffold proteins of the post-synaptic density (PSD) have been shown to have a high relevance in different neuronal disorders, as they participate in the regulation and modulation of protein-level processes of learning and memory. Detailed structural description of these proteins might lead to the better understanding of their interactions and mechanism of action, and also their contribution to the associated diseases [1]. GKAP is one of the essential scaffold proteins in the PSD, interacting with the GK domain of PSD-95, the dynein light chain (DLC2) motor protein, and the PDZ domain of Shank [2], [3], [4]. Most of GKAP is predicted to be disordered, and its structure is unknown, except for the GH1 domain on the C terminal [5]. Our aim is to explore the structural ensembles and dynamics that characterize the disordered segments of GKAP: the GK binding region, the dynein binding segment, and the first 300 residues with unknown function or interaction partners.

II. METHODS

I was using plasmid vector technology in *E. coli* bacteria for protein expression and affinity chromatography (IMAC and GST-columns) as well as size-exclusion chromatography for the purification of the dynein binding region and the GK-binding region of GKAP. Purity, size and structural control measurements included SDS-PAGE, mass spectrometry, and electronic circular dichroism (ECD) spectroscopy. Protein-protein interaction detection methods that we use are gel filtration, native PAGE, pull-down assay, isothermic titration calorimetry (ITC), Trp fluorescence measurements and titration NMR spectroscopy. NMR measurements were executed at 25°C on a Bruker 800 MHz spectrometer, with the help of Permi Perttu and his colleagues, at the University of Jyväskylä, Finland.

III. RESULTS AND DISCUSSION

Protein production of the designed constructs was successfully accomplished and NMR spectra were acquired for chemical shift assignment. Side chain assignment is planned, as well as titration NMR measurements. The obtained chemical shifts will serve as input for generating ensemble-based structural models of GKAP, which will contribute to a more detailed description of PSD organization.

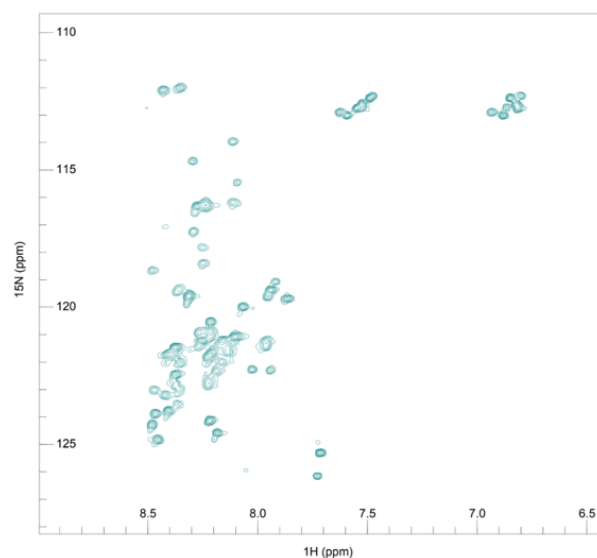


Fig. 1. HSQC NMR spectrum of the ¹⁵N-labeled GKAP-DLC construct

IV. ACKNOWLEDGEMENTS

The research has been supported by the European Union, co-financed by the European Social Fund (EFOP-3.6.2-16-2017-00013), a grant from the Hungarian Scientific Research Fund (NKFI 124363) and the Bolyai Research Fund. The author thanks Zoltán Gáspári, Permi Perttu, Helena Tossavainen, Bálint Ferenc Péterfia, Anna Sánta, József Hegedüs, Mária Steinbach, Melinda Keresztes, Viktor Farkas, Gitta Schlosser and Pál Stráner for their contribution to this work.

REFERENCES

- [1] C. Gao, N. C. Tronson, and J. Radulovic, "Modulation of behavior by scaffolding proteins of the post-synaptic density," *Neurobiology of learning and memory*, vol. 105, pp. 3–12, 2013.
- [2] T. M. Boeckers, C. Winter, K. H. Smalla, M. R. Kreutz, J. Bockmann, C. Seidenbecher, C. C. Garner, and E. D. Gundelfinger, "Proline-rich synapse-associated proteins ProSAP1 and ProSAP2 interact with synaptic proteins of the SAPAP/GKAP family," *Biochem. Biophys. Res. Commun.*, vol. 264, pp. 247–252, Oct 1999.
- [3] A. H. Rasmussen, H. B. Rasmussen, and A. Silahtaroglu, "The dlga family: neuronal expression, function and role in brain disorders," *Molecular brain*, vol. 10, no. 1, p. 43, 2017.
- [4] J. Zhu, Q. Zhou, Y. Shang, H. Li, M. Peng, X. Ke, Z. Weng, R. Zhang, X. Huang, S. S. Li, *et al.*, "Synaptic targeting and function of sapaps mediated by phosphorylation-dependent binding to psd-95 maguks," *Cell reports*, vol. 21, no. 13, pp. 3781–3793, 2017.
- [5] J. Tong, H. Yang, S. H. Eom, C. Chun, and Y. J. Im, "Structure of the gh1 domain of guanylate kinase-associated protein from rattus norvegicus," *Biochemical and biophysical research communications*, vol. 452, no. 1, pp. 130–135, 2014.

Development of machine learning algorithms and decision pipelines on medical multimodal databases

Bence NÉMETH

(Supervisor: András HORVÁTH)

Pázmány Péter Catholic University, Faculty of Information Technology and Bionics

50/a Práter street, 1083 Budapest, Hungary

nemeth.bencze@itk.ppke.hu

Keywords-data mining, multi-source medical data, decision pipelines, machine learning, cardiovascular imaging, personalized medicine

I. INTRODUCTION

Recent developments in high-throughput technologies have accelerated the accumulation of massive amounts of data from multiple sources: EHR patient data, financial data, genome, epigenome, transcriptome, proteome, phenotype, patient records, imaging data etc. Traditionally, data from each source is analyzed in isolation using statistical and machine learning methods. Robust scalable algorithm development and integrative analysis of multi-omics and clinical data is key to new biomedical discoveries and advancements in precision medicine.

Precision or personalized medicine is a clinical approach that strives to customize therapies based on the individual profiles of patients. Development of pipelines are long, complex and depend on numerous factors. Machine learning and Deep learning approaches provide a set of tools that can improve discovery and decision making for well-specified questions with abundant, high-quality data.

Specialized computational approaches are required to effectively and efficiently perform integrative analysis of biomedical data acquired from diverse modalities. We have to cope with the possible arising specific computational challenges associated with integrative analysis such as curse of dimensionality, data heterogeneity, missing data, class imbalance and scalability issues. Joint analysis of high-dimensional imaging, electronic health records and genetic data poses major computational and theoretical challenges.

II. GOAL

The key challenge in developing such approaches is the identification of effective models to provide a comprehensive and relevant systems view. An ideal method can answer a biological or medical question, identifying important features and predicting outcomes, by harnessing heterogeneous data across several dimensions of biological variation. Analyze public and private data with a claim to work with less data, noisier and more biased data. Analyze data from multiple sources collectively such as anamnestic data, patient health records, imaging data, genomics Leverage machine learning and deep learning methods for cancer treatment Suggest preprocessing pipelines for highly deficient, multi modal and multi source databases. Examine actionable factors influencing long term survival and outcomes Examine Long-term Outcomes - death, MI, stroke, re-hospitalization

III. METHODS

I have reviewed and collected publicly available and private data sources from companies. The data collected to date includes 5000+ records of patients who were involved in cardiological examinations. Exploratory data analysis and statistical measurement were performed to investigate the data. Association of radial vs femoral access site with long-term outcomes in patients with ACS (Acute coronary syndrome) undergoing PCI (Percutaneous coronary intervention). Data analysis was performed on 6337 patients with ACS. Exploratory data analysis was performed. Metrics associated with better short term outcomes will be prioritized and highlighted.

Supervised learning is the most common form of machine learning and involves the training of models on pairs of input and expected outputs (“labeled” data) and then their deployment to make predictions in previously unseen data. It includes such approaches as support vector machines, nearest neighbor, decision trees, random forests and naive Bayes classifiers. Unsupervised learning algorithms are used to address clustering or dimensionality reduction problems by detecting patterns and structures within the data without any prior knowledge or constraints. Examples including k-means clustering, t-distributed stochastic neighbor embedding (t-SNE), and association rule learning algorithms.

IV. DISCUSSION

While the use of deep learning (DL) approaches in cardiovascular imaging-genetics have great potential, the limitations and challenges of DL in genetics and imaging are further amplified once these large datasets are combined. In AI imaging-genetics, no single method is universally applicable, and the choice of whether and how to use ML or DL approaches is unresolved. Fully integrated, end-to-end, imaging-genetics DL approaches are theoretically attractive but have yet to be tested.

To confidently implement AI methods in research and clinical practice, challenges regarding standardization of data acquisition and algorithm development and reporting still need to be overcome. Initiatives such as adapting the Transparent Reporting of a Multivariable Prediction Model for Individual Prognosis or Diagnosis (TRIPOD) recommendations to machine learning research [TRIPOD-ML] are often recommended.[1]

REFERENCES

- [1] G. S. Collins, J. B. Reitsma, D. G. Altman, and K. G. Moons, “Transparent reporting of a multivariable prediction model for individual prognosis or diagnosis (tripod): the tripod statement,” *British Journal of Surgery*, vol. 102, no. 3, pp. 148–158, 2015.

Structural characterization and interactions of Shank, a post-synaptic scaffold protein

Anna SÁNTA

(Supervisor: Zoltán GÁSPÁRI)

Pázmány Péter Catholic University, Faculty of Information Technology and Bionics

50/a Práter street, 1083 Budapest, Hungary

santa.anna@itk.ppke.hu

Abstract—Shank proteins are an abundant family of scaffolds in the post-synaptic density with a known connection to autism spectrum disorders. In this study, one of its interaction domains, PDZ, was produced in both non-labelled and isotope-labelled form and NMR (nuclear magnetic resonance) measurements were carried out to characterize structure.

Keywords—post-synaptic density; protein interaction; NMR

I. INTRODUCTION

The post-synaptic density found in glutamatergic synapses is a complex network of proteins responsible for long-term changes in neuron behavior and morphology, allowing processes such as memory formation and learning to occur. Scaffolding proteins in the PSD participate in the formation and maintenance of the organization of supramolecular complexes, while they also contribute to the regulation of signaling and modulating glutamatergic response. They showcase high structural variability and a large number of interactions where structural dynamics play a crucial role. [1]

Shank proteins (aliases ProSAP, SSTRIP or synamon) are a family of scaffolding proteins abundant in the PSD with a significant role in establishing PSD morphology and bridging the various glutamate receptors with the cytoskeleton. Members of the protein family have a characteristic domain composition, consisting of globular domains - including a PDZ domain - connected by disordered regions. Dynamic behaviour of these globular domains is yet to be characterized and disordered segments are suspected to also regulate interaction dynamics. PDZ domains of Shanks have multiple interaction partners, binding the C-terminal motif of GKAP (DLGAP) with a notably higher affinity. [2], [3]

II. METHODS

Recombinant protein constructs corresponding to the PDZ domains (rat Shank1 and Shank3 PDZ, the latter also including a disordered segment towards the N-terminal) were produced in *E. coli* and purified using a protocol of subsequent chromatography steps (immobilized metal ion, ion exchange and gel filtration). NMR and electronic circular dichroism spectroscopy measurements were performed to assess proper folding of each construct and native polyacrylamide gel electrophoresis, gel filtration, pull-down assay, and isothermal titration calorimetry was employed to verify interactions.

III. RESULTS

Constructs appear folded and functional. Preliminary ITC measurements were performed and K_d values were determined but require further experiments to verify. A double isotope-labelled (^{15}N and ^{13}C) Shank1 PDZ construct was produced and 3D NMR measurements were performed. Further NMR

measurements to analyze the dynamical behaviour of the domain structure during interactions are in plan, and new constructs for more detailed experiments are on the way.

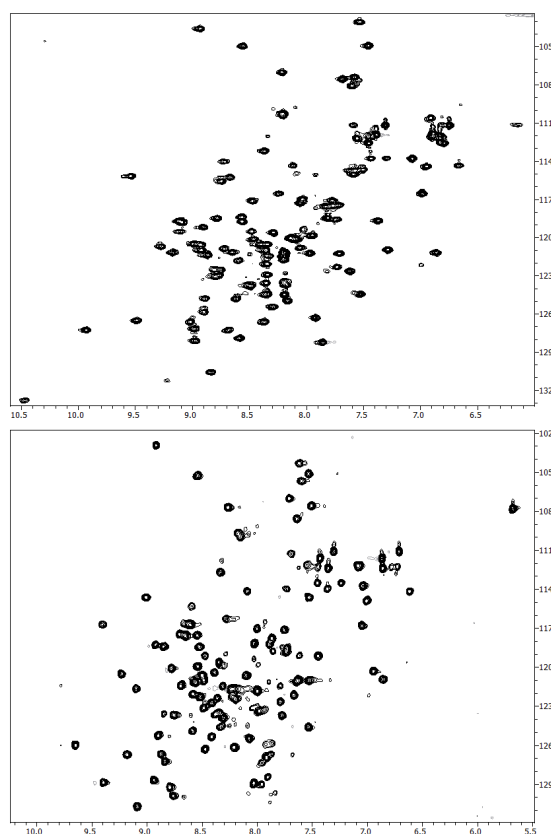


Fig. 1. Preliminary HSQC spectra of Shank1-PDZ (top) and Shank3-PDZ (bottom), exhibiting good dispersion of signals.

ACKNOWLEDGEMENTS

This research had been funded by EFOP-3.6.2-16-2017-00013. The author thanks Zoltán Gáspári, Bálint Ferenc Péterfia, Gyula Batta, József Hegedüs and Melinda Keresztes-Andrei for their contribution to this work.

REFERENCES

- [1] C. Verpelli, C. Heise, and C. Sala, “Structural and functional organization of the postsynaptic density,” *The Synapse: Structure and Function*, pp. 129–153, 12 2013.
- [2] M. Sheng and E. Kim, “The Shank family of scaffold proteins,” *J. Cell. Sci.*, vol. 113 (Pt 11), pp. 1851–1856, Jun 2000.
- [3] C. M. Durand, J. Perroy, F. Loll, D. Perrais, L. Fagni, T. Bourgeron, M. Montcouquiol, and N. Sans, “SHANK3 mutations identified in autism lead to modification of dendritic spine morphology via an actin-dependent mechanism,” *Mol. Psychiatry*, vol. 17, pp. 71–84, Jan 2012.

How do astroglia cells react to structured SU-8 thin films?

Ágnes SZABÓ

(Supervisor: Zoltán FEKETE)

Pázmány Péter Catholic University, Faculty of Information Technology and Bionics

50/a Práter street, 1083 Budapest, Hungary

szabo.agnes@itk.ppke.hu

Abstract—Neuronal implants have an increasing role in clinical settings. The topography of the surface has a great impact on cell survival. The long-term usage of the implant depends on the inflammatory response of the brain tissue. In this study, we examine the astroglial survival on micropatterned SU-8 surface.

Keywords—cell-surface interaction; topography; astroglia

I. INTRODUCTION

The cell survival depends on the environment, the extracellular matrix (ECM). In case of neurons, this environment based on the glial cells. One of the functions of these glial cells is the protection of the neurons. When a foreign body enters the tissue, astrocytes are activated and insulate the implant from the neuronal tissue [?]. The surfaces of biomaterials can be easily patterned by photolithography. This technology allows to design multiple structures with multiple size parameters. The research of surface-cell interaction is a broadly investigated topic. Most of the groups analyze the cytoskeleton of the cell [?], [?]. However, there are only a few studies about the reaction of the nucleus to device topography [?], [?]. The goal of this work is to examine the cell nuclei whether the cell reacts to the topography even in the level of a cell particle.

II. MATERIALS AND METHODS

SU-8, a biocompatible epoxy-based negative photoresist has been formed on a silicon surface. The different microstructures were patterned by standard photolithography. The created patterns are grooves, pillars and meander. The 2 and 5 μm wide patterns are divided by 3, 4, 5, 10 and 20 μm wide spaces in case of grooves and pillars. The meander samples contain 2 and 5 μm wide lines with 2 and 5 μm spacing. Primer mouse astrocytes were seeded to the patterned chip. After the fixation by 24 and 48 hours, the nuclei were stained. The DNA bonded DAPI, fluorescence stain was used. For statistical data collection, a Matlab based program was developed. The program collects the area, orientation and elongation data.

III. DISCUSSION

During this project, we investigated the effects of micropatterned SU-8 surface on astrocytes. The measured data show that the influence of the topography can be captured also on the cell nuclei. The results suggest that the surface-cell interaction can be examined by the developed program.

ACKNOWLEDGEMENTS

This research was supported by the National Science Foundation of Hungary (NKFIH K 120143).

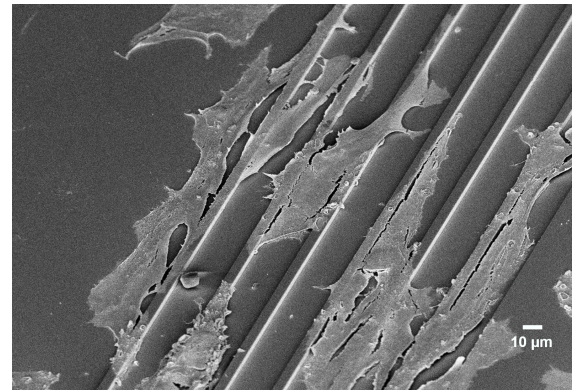


Fig. 1. Scanning electron microscope image on astrocytes on 5 μm wide grooves with 20 μm spacing.

REFERENCES

- [1] Salatino, Ludwig, *Glial responses to implanted electrodes in the brain* Nature biomedical engineering 1.11 (2017): 862-877.
- [2] Johnson, Zuidema, *The Effect of Electrospun Fiber Diameter on Astrocyte-Mediated Neurite Guidance and Protection*. ACS applied bio materials 2.1 (2018): 104-117.
- [3] Katschnig, Maroh, *Cell Morphology on Poly (methyl methacrylate) Microstructures as Function of Surface Energy*. International journal of biomaterials 2019 (2019)
- [4] Pan, Yan, *Control of cell nucleus shapes via micropillar patterns*. Biomaterials 33.6 (2012): 1730-1735.
- [5] Ahmed, Wolfram, *Myoblast morphology and organization on biochemically micro-patterned hydrogel coatings under cyclic mechanical strain*. Biomaterials 31.2 (2010): 250-258

Microfluidic possibilities of viral tests based on nucleic acid amplification

Mihály SZÚCS

(Supervisor: Kristóf IVÁN)

Pázmány Péter Catholic University, Faculty of Information Technology and Bionics

50/a Práter street, 1083 Budapest, Hungary

szucs.mihaly@itk.ppke.hu

Keywords-Coronavirus Disease 2019, SARS-CoV-2, Lab-On-a-Chip, Microfluidics, Loop-mediated isothermal amplification

I. THE COVID-19 VIRUS

Coronavirus disease 2019 (COVID-19) is now a widespread epidemic started in late 2019. It can cause severe pneumonia and is similar in many ways to the 18 years earlier Severe Acute Respiratory Syndrome (SARS).[1]

II. PATIENT TESTING

Since the symptoms of the COVID-19 disease are not clearly distinguishable from other illnesses, like influenza and allergies, specific tests are important in controlling the epidemic.[2] There are some difficulties, which must be overcome to continue testing. As the epidemic is spreading, the demand of reagents may exceed the production, so test distribution strategies should be applied.[3]

Nucleic acid amplification tests (NAAT) are used routinely to confirm cases of COVID-19. These tests amplification and detection unique sequences of the viral RNA.[4]

III. MICROFLUIDIC APPROACH

Using microfluidics could help with the problems of current testing methods. Microfluidic chips uses up low amounts of sample and reagents, while offering precise control of reaction environment.[5]

Microfluidics seems to have answers to some of the major problems of this test method. Portable Point of Care (PoC) devices, which are inexpensive to produce and operate, not necessarily need professional technicians and are capable of high sensitivity detection would be optimal.[6]

In order to overcome the difficulties of temperature control, a simpler amplification protocol can be used. Loop Mediated Isothermal Amplification (LAMP) is an isothermal nucleic acid amplification method.[7]

To detect RNA viruses, like SARS-CoV-2 Reverse transcription loop-mediated isothermal amplification (RT-LAMP) is needed. Here LAMP is combined with a reverse transcription assay, since LAMP can only amplify DNA.[8]

There is evidence that the LAMP method could be successful even without nucleic acid extraction. Reproducible experiments were conducted where LAMP was successful on whole blood, urine and serum samples.[9] This implies that using LAMP as the amplification method could simplify the sample preparation, which greatly beneficial when designing a PoC device.

IV. SUMMARY

Controlling the recent COVID-19 epidemic patient testing is a key factor. Various viable protocols have been researched, however the extent and the high infectivity of the epidemic pose new challenges. Implementing laboratory tests based on nucleic acid amplification on microfluidic devices could be a more cost efficient solution. Based on recent studies RT-LAMP test would be a great choice to be realised on a portable microfluidic test device.

ACKNOWLEDGEMENTS

I would like to thank the support of my supervisor, Kristóf Iván.

REFERENCES

- [1] P. Zhou, X.-L. Yang, X.-G. Wang, B. Hu, L. Zhang, W. Zhang, H.-R. Si, Y. Zhu, B. Li, C.-L. Huang, *et al.*, "A pneumonia outbreak associated with a new coronavirus of probable bat origin," *nature*, vol. 579, no. 7798, pp. 270–273, 2020.
- [2] C. H. Yan, F. Faraji, D. P. Prajapati, C. E. Boone, and A. S. DeConde, "Association of chemosensory dysfunction and covid-19 in patients presenting with influenza-like symptoms," in *International Forum of Allergy & Rhinology*, Wiley Online Library, 2020.
- [3] W. H. Organization *et al.*, "Laboratory testing strategy recommendations for covid-19: interim guidance, 22 march 2020," tech. rep., World Health Organization, 2020.
- [4] W. H. Organization *et al.*, "Laboratory testing for coronavirus disease (covid-19) in suspected human cases: interim guidance, 19 march 2020," tech. rep., World Health Organization, 2020.
- [5] D. J. Beebe, G. A. Mensing, and G. M. Walker, "Physics and applications of microfluidics in biology," *Annual review of biomedical engineering*, vol. 4, no. 1, pp. 261–286, 2002.
- [6] T. Nguyen, D. Duong Bang, and A. Wolff, "2019 novel coronavirus disease (covid-19): paving the road for rapid detection and point-of-care diagnostics," *Micromachines*, vol. 11, no. 3, p. 306, 2020.
- [7] T. Notomi, H. Okayama, H. Masubuchi, T. Yonekawa, K. Watanabe, N. Amino, and T. Hase, "Loop-mediated isothermal amplification of dna," *Nucleic acids research*, vol. 28, no. 12, pp. e63–e63, 2000.
- [8] Y.-P. Wong, S. Othman, Y.-L. Lau, S. Radu, and H.-Y. Chee, "Loop-mediated isothermal amplification (lamp): a versatile technique for detection of micro-organisms," *Journal of applied microbiology*, vol. 124, no. 3, pp. 626–643, 2018.
- [9] J. Song, C. Liu, M. G. Mauk, S. C. Rankin, J. B. Lok, R. M. Greenberg, and H. H. Bau, "Two-stage isothermal enzymatic amplification for concurrent multiplex molecular detection," *Clinical chemistry*, vol. 63, no. 3, pp. 714–722, 2017.

Data-driven developing of a PV basket cell and CA3 pyramidal neuron

Luca TAR

(Supervisors: Szabolcs KÁLI, Tamás FREUND)

Pázmány Péter Catholic University, Faculty of Information Technology and Bionics

50/a Práter street, 1083 Budapest, Hungary

tar.luca@itk.pke.hu

Keywords-hippocampus; pyramidal cell; basket cell

I. SUMMARY

To create a novel network model of the CA3 area of the mouse hippocampus we need new interneuron models. The first in the line is the parvalbumin positive basket cell that fast-spiking behavior is unique in the hippocampus. To capture this behavior we needed to re-evaluate our experimental data and our channel models as well that led to unexpected difficulties. The main problem was the ion channels. We found out after a few optimization that the channels we used in pyramidal cells are not capable of expressing fast spiking behavior so we need other channels. We found a study about the behavior of basket cells [1] that included modelling as well so I wrote to the author and asked for their model. We found out that their ion channels are not working under long current injections only when we give the model pulses so it was a dead end. We also tried out some previous ion channel used in our lab to create a basket cell long time ago [2] but with them we were not be able to fit the fast spiking along with the correct voltage base and steady state voltage. We need to create our own channels which is still in progress.

I got another interesting project from a different group that examines the different types of calcium spikes in the rat CA3 pyramidal cell. For that we needed to create a new, general CA3 pyramidal cell model that shows bursting behavior using our previous experiences with the CA1 pyramidal cell. We had to adjust our methods to the new challenge to explore bursting and the mechanisms behind it. We can confirm the previous findings during channel blocking experiments, that the L-type calcium channel is responsible for bursting and the different type of calcium spikes but we need to have a generalise model to give the most realistic composition of the different ion channel densities.

Our strategy was that we started with the smaller steps and used the CMAES algorithm to get as accurate results as possible to fix the passive parameters like the leak conductance density and the reverse potential of the leak conductance and those parameter that showed very little standard deviation among the 20 model instances. Then we moved onto the higher currents because to our main goal it was the most important to capture the parameters behind the bursts. We also tried to narrow down the parameter space to make easier for the algorithm to find good parameters. For that we found a paper from Kim et al. [3] where they measured the exact channel densities of a CA3 pyramidal cell. We set our boundaries of each parameter keeping in mind that their results should be within the boundaries and we kept the proportions of the different densities. Using these proportions did not lead to

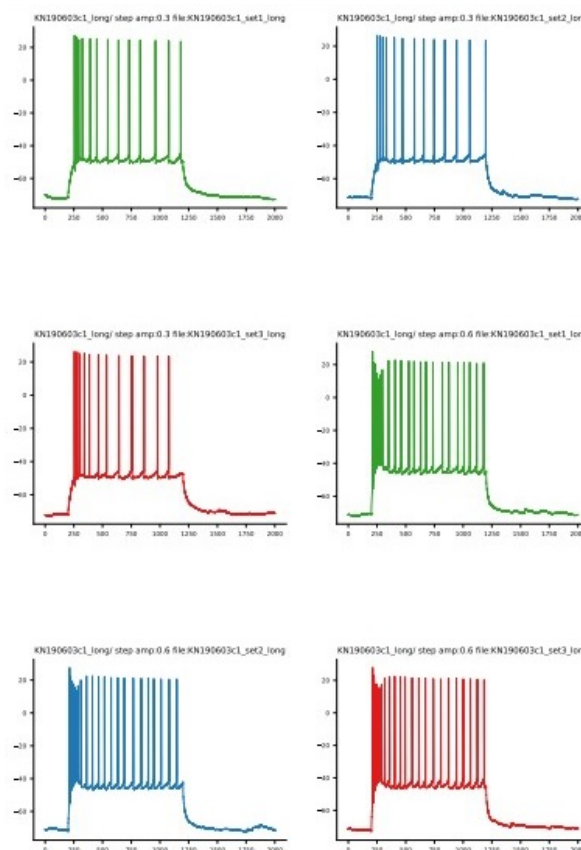


Fig. 1. The general response of a CA3 pyramidal cell for a 0.3 nA current injection and a 0.6 nA current injection. The different colours show different measurements from the same cell. We can see that for the 0.6 nA the cell is bursting. This is the behavior we try to capture with our model.

worse results than those models had when we allowed to freely tune every parameters and resulted in less parameters so we could implement the L-type calcium channel as well.

REFERENCES

- [1] H. Hu, F. C. Roth, D. Vandael, and P. Jonas, “Complementary tuning of Na^+ and K^+ channel gating underlies fast and energy-efficient action potentials in GABAergic interneuron axons,” *Neuron*, vol. 98, no. 1, pp. 156 – 165.e6, 2018. [Online]. Available: <http://www.sciencedirect.com/science/article/pii/S0896627318301454>
- [2] B. Chiovini, G. F. Turi, G. Katona, A. Kaszás, D. Pálfi, P. Maák, G. Szalay, M. F. Szabó, G. Szabó, Z. Szadai, S. Káli, and B. Rózsa, “Dendritic spikes induce ripples in parvalbumin interneurons during hippocampal sharp waves,” *Neuron*, vol. 82, no. 4, pp. 908 – 924, 2014. [Online]. Available: <http://www.sciencedirect.com/science/article/pii/S0896627314002943>
- [3] S. Kim, S. Guzman, and H. e. a. Hu, “Active dendrites support efficient initiation of dendritic spikes in hippocampal CA3 pyramidal neurons.” *Nature Neuroscience*, vol. 15, p. 600–606, 2012.

Drug delivery through physiological barriers: investigation of the permeability of blood-brain barrier, nasal- and dermal-barriers

Zsófia VARGA-MEDVECZKY

(Supervisor: Franciska ERDŐ)

Pázmány Péter Catholic University, Faculty of Information Technology and Bionics

50/a Práter street, 1083 Budapest, Hungary

varga-medveczky.zsofia@itk.ppke.hu

Abstract—This summary focuses on effective drug delivery methods through different physiological barriers: the blood-brain barrier, nasal barrier and dermal barrier. Apart from the structure and physiological functions of these barriers, the basics of drug delivery methods are presented, which are suitable to pass through them.

Keywords—drug delivery; neurodegenerative disorders; blood-brain barrier; intranasal administration; dermal barrier

I. INTRODUCTION

Mental illnesses and neurodegenerative diseases are the most common central nervous system diseases [1]. Most neurodegenerative diseases (e.g. Alzheimer's disease, Parkinson disease, multiple sclerosis etc.) are associated with aging and are partially caused by the dysfunction of the blood-brain barrier [2], [3]. These diseases are serious problems for developed, aging societies, because still there is no proper therapy against them and there are difficulties to send drugs to the target brain area. It requires efficient drug delivery methods where drugs can be targeted directly to the brain, but the passage of molecules through the blood-brain barrier is challenging. The low bioavailability and quick elimination of drugs mean also problems, in addition to the high number of unwanted side effects due to high peripheral doses [1].

II. INVESTIGATION OF THE BLOOD-BRAIN BARRIER

The blood-brain barrier (BBB) is the main interface, which is responsible for separating the cerebral circulatory network from the brain parenchyma [2], [4]. As a bidirectional mediator, the blood-brain barrier plays a key role in maintaining the proper brain function. It ensures the entry of all necessary nutrients and oxygen to brain parenchyma, but at the same time it prevents harmful chemical substances or pathogens from entering which can be toxic for the neurons and may cause neuronal death [2], [3], [4]. This strict regulation of influx and efflux pathways results in the maintenance of the neurochemical homeostasis [4].

For the proper functioning of the BBB, coordinated operation of all the building blocks, such as the cellular elements, the basal lamina and the extracellular matrix is required. However, many changes in the cerebrovascular structure can be observed during physiological aging. Morphological, physiological and biochemical alterations in any components may cause fundamental changes in the permeability of this barrier, which can lead to the development of various diseases [2], [3]. In advanced age, the permeability of the blood-brain barrier

increases as a result of the changed expression of the transport proteins (e.g. P-gp) [2] [3].

III. DRUG DELIVERY ACROSS THE NASAL BARRIER

Intranasal administration is an effective method of drug delivery that provides direct access to the brain parenchyma. This delivery route, in addition to being a non-invasive method, is even easy to self-administer. In contrast to enteral dosage form, lower doses are sufficient, because the pharmacologically active agents avoid the metabolism and absorption in the gastrointestinal (GI) tract. Moreover first-pass metabolism is not to be expected, and the number of unwanted side effects is also significantly lower [1].

IV. DRUG DELIVERY THROUGH THE DERMAL BARRIER

Ointments, creams, gels and patches containing different pharmacologically active molecules are often applied to treat various skin diseases and injuries [5]. These delivery methods of different drugs can also be used for other therapeutic [5] (e.g. nicotine-containing or analgesic patches) or cosmetic purposes [6] (e.g. moisturizers and anti-aging serums). Topical drug administration has mostly local effects, because the drug molecules are utilized directly at the site of the treatment. However, the drug may enter the systemic circulation through the dermal barrier, thereby a systemic effect can also be induced [5]. Compared to oral administration the method is characterized by significantly lower doses, which cause less side effects. First pass metabolism is not expected, because the GI tract is avoided during this type of administration. Another main advantage is that such drugs are easily self-administered [5].

REFERENCES

- [1] F. Erdő, L. A. Bors, D. Farkas, Ágnes Bajza, and S. Gizurarson, "Evaluation of intranasal delivery route of drug administration for brain targeting," *Brain Research Bulletin*, 2018.
- [2] F. Erdő, L. Dénes, and E. de Lange, "Age-associated physiological and pathological changes at the blood-brain barrier: A review," *Journal of Cerebral Blood Flow & Metabolism*, 2016.
- [3] F. Erdő and P. Krajcsi, "Age-related functional and expressional changes in efflux pathways at the blood-brain barrier," *Frontiers in Aging Neuroscience*, 2019.
- [4] C. L. Graff and G. M. Pollack, "Drug transport at the blood-brain barrier and the choroid plexus," *Current Drug Metabolism*, 2004.
- [5] F. Erdő, "3d skin bioprinting: A novel tool for dermato-pharmacology, -toxicology and drug development," *EC Pharmacology and Toxicology*, 2019.
- [6] F. Farner, L. Bors, Ágnes Bajza, G. Karvaly, I. Antal, and F. Erdő, "Validation of an in vitro-in vivo assay system for evaluation of transdermal delivery of caffeine," *Drug Delivery Letters*, 2019.

Bio-stability study of liquid crystal polymer (LCP) / Polydimethylsiloxane (PDMS) coated implants

Moutz WAHDOW

(Supervisor: István ULBERT)

Pázmány Péter Catholic University, Faculty of Information Technology and Bionics

50/a Práter street, 1083 Budapest, Hungary

wahdow.moutz@itk.ppke.hu

Abstract—The production of bioimplants typically involves an understanding of both biomedical science and electromechanical engineering to yield biocompatible products with sufficient lifespans. Selection of the constructional biomaterial is an essential requirement for a long-term and reliable service of the implants, which relies on material properties. Bio-electronic implants are becoming important to us with the goal to improve longevity and quality of human life by restoring bodily functions. Lately there has been increased attention to study polymeric materials such as poly(p-xylylene), polyimide (PI), parylene-C, polydimethylsiloxane (PDMS) and Liquid Crystal Polymer (LCP). Our rule is to investigate the bio-stability and structural performance of the materials that are used now and might be in the future to build Bio-electronic Implants. Reviewing their performance under In-vitro and In-vivo conditions for prolonged durations as for 3, 6, 9 and 12 months time points apart between explanations. Having 18 rats implanted with LCP samples, LCP with PDMS coated samples and two types of bare CMOS chips starting June 2019. The materials are expected to withstand the biological environment and must neither degrade or evoke any counter response from the host biological body. LCP been reported to have the potential to laminate bio-implants as for its physical properties. It has a high resistivity to degrade over time and can provide MRI compatibility and is easy to process and fabricate. Also PDMS silicon rubber is already being used in implantable devices as well.

Our six months data conclude the affirmation of biocompatibility of the investigated materials. Scanning electron microscopy (SEM) analysis was conducted on the samples, Encapsulation and tissue pocket formation was observed on all explanted samples. Surface characteristics of LCP did not change according to the Atomic Force Microscopy (AFM) surface roughness measurements, suggesting negligible deterioration of the coating material and excellent biostability during the first 3 months.

Keywords—Liquid Crystal Polymer (LCP); Polydimethylsiloxane (PDMS); Flexible electronics and Medical Implants.

CONCLUSION

LCPs have an appealing mechanical and chemical properties for neural prostheses applications. Such having chemical stability, low water and gas absorption rate, simultaneous flexibility and rigidity and easiness to process and fabricate. After 3 and 6 months explantation No signs of infection could be observed, Scarring was minimal for all implanted samples. The tissue reactions are sterile and biocompatibility of the used materials was confirmed as per to literature. Pathological and toxicological hallmarks such as inflammation, granulomas or necrosis were not found. LCP is more likely to be encapsulated after 3 months than PDMS.

Future analysis will include Impedance spectroscopy and AFM analysis of PDMS samples and histology of the tissue pockets formulated around the encapsulated samples to evaluate the material reliability and integrity for Medical Implants applications.

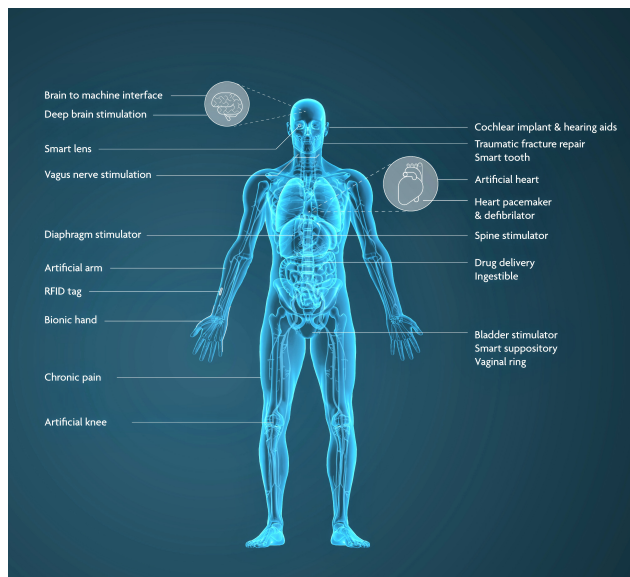


Fig. 1: Patients suffering from neuronal degenerative diseases are increasingly being equipped with neural implants to treat symptoms or restore functions.[imec magazine Apr/2020]

ACKNOWLEDGEMENTS

This research is conducted within POSITION-II. A pilot line for the next generation of smart catheters and implants. Funded by ECSEL Innovation Action contributed with more than 40 partners of research institutes, universities, industrial companies and technology leaders from all across Europe. In this pilot line scalable open technology platforms based on essential technologies will be integrated in one manufacturing network. POSITION-II will enable the electronic industry to take the lead in the development of these live saving instruments and to introduce open technology platforms for: miniaturization, in-tip AD conversion, wireless communication, MEMS transducer technology and encapsulation. These platforms are open to multiple users and for different applications. Open platforms will allow manufacturers to improve the performance of smart catheters at a lower cost. Additionally, it will enable the development of completely new smart minimally invasive instruments. Great thanks to Ulbert István, Iván Kristóf, Nánási Tibor, Köllöd Csaba, Márton Gergely, Ward Fadel, András Adolf, Bálint File, Domokos Meszéna, Richárd Fiáth and Domonkos Horváth, and all staff of PPCU and MTA TTK.

PROGRAM 2

COMPUTER TECHNOLOGY BASED ON MANY-CORE PROCESSOR CHIPS, VIRTUAL CELLULAR COMPUTERS, SENSORY AND MOTORIC ANALOG COMPUTERS

Head: Péter SZOLGAY

Effect of solar panels ratio on the thermal behaviour of a CubeSat

Nawar AL-HEMEARY

(Supervisors: Gábor SZEDERKÉNYI, György CSEREY)

Pázmány Péter Catholic University, Faculty of Information Technology and Bionics

50/a Práter street, 1083 Budapest, Hungary

al.hemeary@itk.ppke.hu

Abstract—The discipline and strategies for designing spacecraft structure depend on the aircraft layout with more emphasis upon the least weight and problems of material selection for space applications. The important objective of minimum mass must be met with limited cost and schedule. A CubeSat presents a cost-effective spacecraft, even though it has fundamental drawbacks such as small surface area, implying that power is always precious on a CubeSat. Thus, one of the most concerning issues beyond CubeSat manufacturing is the design and implementation of solar panels. In this study, the investigations of transition thermal behaviour due to different solar panels ratios have been performed. MATLAB Simulink is used to simulate the temperature reactions for some essential parts of CubeSat under these conditions. Then the unified equivalent model attached to the ratio of a solar panel has been derived and evaluated. The simulation results of the developed model are very similar to the results from the original TMM through passive and active control.

Keywords—CubeSat; Solar panel; TMM; Thermal control system.

I. INTRODUCTION

A CubeSat is an extremely small size satellite with the least payload. One unit (1U) CubeSat is a standard Cubic module, with a size of 10 cm^3 and a mass of close to 1.33 kg. This small satellite's walls offer a small area for solar panels. Such a limited area can not provide a high amount of electric energy. At the point silicon-based solar panels are utilized, due to their low cost, it is beyond the realm of imagination to expect more than 2 W of power[1]. The thermal mathematical model TMM of CubeSat surface and distinct inner part has been derived in the nonlinear input- affine form [2]. To maintain a temperature of the satellite's tank within the reference value, passive and active thermal control systems with the assumption that 30 % of solar panels cover specific faces of a Cubesat have been analyzed and simulated [3]. The linearization method of the nonlinear TMM has also been performed and simulated to eliminate the fuel tank temperature fluctuations at a CubeSat orbit [4]. Throughout the emissivity and absorptivity of materials, solar panels ratios allow significant thermal control of CubeSats. This research has two purposes: review the mechanism of CubeSat surface and tank thermal exchanges by changing solar panels ratios, and simulate the refined thermal model of CubeSat. The developed model is designed to include all equations of TMM in [2] into seven nonlinear equations concerning the ratio of the solar panels. This new model is simulated with 30% of solar panels covering certain faces of the satellite to present the thermal behaviour of the surface and fuel tank during the satellite orbit. The results show a realistic thermal response in agreement with the original thermal model.

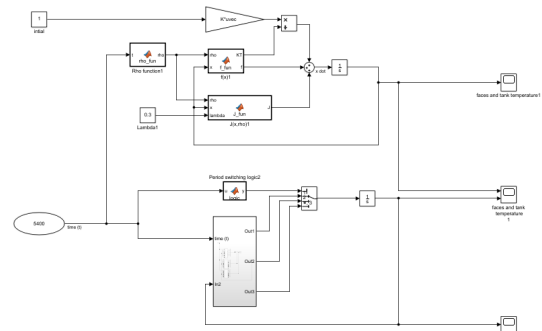


Fig. 1. MATLAB Simulink of the original TMM and the new model synthesis.

REFERENCES

- [1] J. Claricoats and S. M. Dakka, "Design of power, propulsion, and thermal sub-systems for a 3u cubesat measuring earth's radiation imbalance," *Aerospace*, vol. 5, no. 2, p. 63, 2018.
- [2] N. Al-hemeary, M. Jaworski, J. Kindracki, and G. Szederkenyi, "Thermal model development for a cubesat," *Hungarian Journal of Industry and Chemistry*, vol. accepted, to appear, 2018.
- [3] N. Al-hemeary and G. Szederkenyi, "Fuel tank temperature control of a time-varying cubesat model," *IEEE 17th World Symposium on Applied Machine Intelligence and Informatics*, vol. accepted, to appear, 2019.
- [4] N. Al-Hemeary and G. Szederkényi, "Power regulation and linearization-based control design of a small satellite," in *2019 12th International Conference on Developments in eSystems Engineering (DeSE)*. IEEE, 2019, pp. 646–650.

Algorithmic Differentiation of Structured Mesh Applications

Gábor Dániel BALOGH

(Supervisors: István Zoltán REGULY, Péter SZOLGAY)

Pázmány Péter Catholic University, Faculty of Information Technology and Bionics

50/a Práter street, 1083 Budapest, Hungary

3in Research Group, Faculty of Information Technology and Bionics, Pázmány Péter Catholic University, Esztergom, Hungary

balogh.gabor.daniel@itk.ppke.hu

Abstract—Algorithmic (or Automatic) Differentiation (AD) is used to evaluate derivatives of the function which defined by a computer program with respect to some input variables. In other word AD answers the questions like "How sensitive are the values of outputs of my computer program with respect to changes in the values of input variables?". AD shown to be an essential tool to get sensitivity information in multiple areas of science such as Computational Fluid Dynamics (CFD) or finance due to relatively low computational cost and accuracy. Yet there is no sufficient tool to ease the cost of providing performance portable AD codes, especially for modern hardware like GPU clusters. This paper sketches our plans and progress so far to extend the Oxford Parallel library for Structured mesh solvers (OPS) framework with an adjoint tape (storage for descriptors of intermediate steps and intermediate states of variables) to compute derivatives and shows preliminary performance results on CPU nodes. Our work aims to exploit the benefits of OPS to provide performance portable adjoint implementations for future structured mesh stencil applications with minimal modifications.

Keywords—algorithmic differentiation; domain specific language; adjoint methods

I. THE PROBLEM

"How sensitive are outputs of my code with respect to changes in the values of input variables?" Answering this and similar questions are essential to reason about the results of a computer program. Algorithmic Differentiation is used to evaluate derivatives of the function which defined by a computer program. By applying the chain rule repeatedly to the elementary steps in a program, derivatives can be computed automatically, and accurate to machine precision. For more detailed information about AD the reader is referred to [1].

With a tool like OPS we define these computational steps as parallel loops and OPS is generating parallel implementation for the loops. Our goal is to build a directed acyclic graph (DAG) of computational steps and a coarse grained tape (the data structure where the intermediate states and the DAG is stored) inside OPS for the application. Assuming we have derivative function for each loop body, we can evaluate apply the chain rule on using this tape. Moreover due to OPS's code generation we can provide performance portable implementations on a range of hardware.

II. PROPOSED SOLUTION

We extended OPS with a DAG with all the information about the computational loops required for performing the reverse run at runtime. To achieve this we used the kernel descriptors that are used to perform lazy execution in OPS [2] with the difference that we need to perform the adjoint

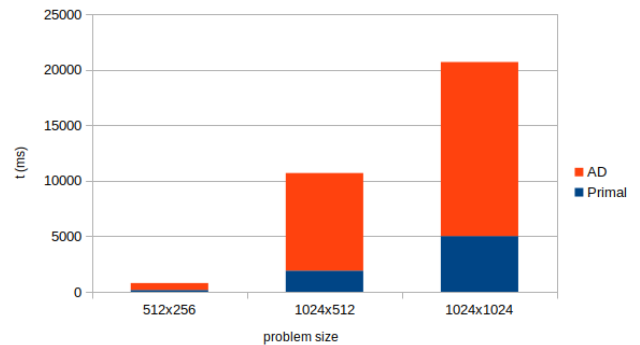


Fig. 1. Runtime of the SLV code for different grid sizes. The forward run of the code noted with blue and the red parts stand for the backward run with the adjoint computations.

version of the kernels. Each loop will automatically register itself to the DAG and save all written data to checkpoints, then the developer can initialise adjoints for the result and interpret adjoints, during which the adjoint for each loop will be executed in reverse order loading all the checkpoints stored during the forward run.

On figure 1 the runtime overhead of computing the derivatives for a stochastic local volatility (SLV) model with OpenMP is shown. The overhead of the backward sweep is around 3-4 times of the time spent on the forward computation. This result means the the total cost of computing the derivatives of this SLV code is five times bigger than computing only the original function, which is a promising (the computation time of adjoints is usually 3-30 times bigger than the evaluation of the original program[1]). However the current implementation has a significant memory overhead since we need to store all intermediate state of the datasets.

ACKNOWLEDGMENT

This research has been carried out partly in the project Thematic Research Cooperation Establishing Innovative Informatic and Info-communication Solutions, which has been supported by the European Union and co-financed by the European Social Fund under grant number EFOP-3.6.2-16-2017-00013.

REFERENCES

- [1] U. Naumann, *The art of differentiating computer programs: an introduction to algorithmic differentiation*, vol. 24. Siam, 2012.
- [2] I. Z. Reguly, G. R. Mudalige, and M. B. Giles, "Loop tiling in large-scale stencil codes at run-time with ops," *IEEE Transactions on Parallel and Distributed Systems*, vol. 29, no. 4, pp. 873–886, 2017.

Evaluation of FPGA based SIFT implementation by using real-life examples

Attila FEJÉR

(Supervisor: Péter SZOLGAY)

Pázmány Péter Catholic University, Faculty of Information Technology and Bionics

50/a Práter street, 1083 Budapest, Hungary

fejer.attila@itk.ppke.hu

Abstract—This paper discusses a way to control a prosthetic arm based on egocentric videos. To control this wearable robotic arm, there are many constraints which necessary to fulfil. This is a portable, wearable, lightweight device, that consume less energy than typical desktop hardware, and real-time processing is also necessary. Taking this into consideration an FPGA (Field-programmable gate arrays) has been chosen for this task. In this paper, a SIFT (Scale-Invariant Feature Transform) keypoint extractor method FPGA version provided which has an energy consumption less then 6 Watt and extracts the same 90% keypoints as a regular CPU implementation.

Keywords-FPGA, SIFT, acceleration

I. INTRODUCTION

In the world, there are some reason for example wars and accidents, or disease why a patient required a prosthetic arm. However, those products are expensive and hard to control them. Our goal in this research to achieve to control a neuroprosthetic arm using, to aim that image processing and computer vision algorithms have been used.

The proposed system for this problem [1] uses three different video camera input in this case two GoPro action-cameras which equipped to the patient shoulder and a Tobii glass camera which is an eye tracker, and this eye tracker recorded an egocentric video. The system has an object recognition part and an object matching part also. This paper is about the object matching part.

The goal of the object matching part is to find the object which the patient tries to grasp with his hand in the three different cameras video frames. The first step to aim that it is required to extract some characteristic points from the video frames. These characteristic points are the keypoints. In this case, SIFT keypoints are extracted. After the keypoints are extracted, the descriptors are calculated. Then a Bruteforce matcher is used between the different GoPro cameras and the Eyetracker frames to find the nearest descriptors in each cameras video frames. Ransac (Random sample consensus) is used to remove the outliers (wrong matches). The next step is to estimate the two homography matrices between then the last step is to estimate the object positions of the GoPro cameras frame. The most time-consuming part of this method is the keypoint extraction, and because of that reason, a faster implementation is needed, for example, an FPGA implementation of the SIFT keypoint extraction.

II. PROPOSED SOLUTION

Figure 1 show this implementation contains Gaussian and Difference of Gaussian calculator modules[2] which calculate the Gaussian and (DoG) Difference of Gaussian pyramids. After three DoG image calculated the scale-space extrema unit

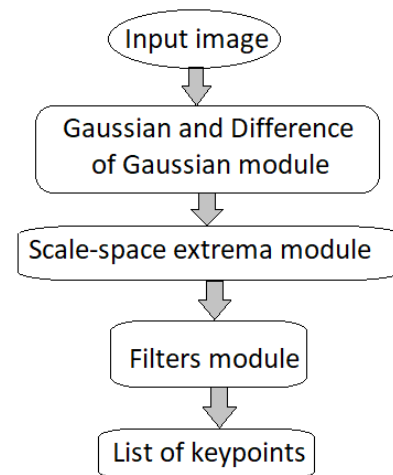


Fig. 1. The flow diagram of the SIFT algorithm FPGA implementation

calculates the given pixel is a possible keypoint or not. If the possible keypoint pass two more filter unit, than the possible keypoint is a valid keypoint.

III. RESULTS AND CONCLUSIONS

Power dissipation of FPGA-s is very low less than 6 Watts [3]. This makes a better choice for wearable device application compare to a CPU or GPU. The bigger computational capacity make a better choice the FPGA than an analog CMOS sensor.

FPGA implementation can extracted SIFT keypoints just as the OpenSift[4] with the same initial values.

IV. ACKNOWLEDGEMENT

The contribution of Mr Zoltán Nagy, Mr Aymar de Rugy and Ms Jenny Benois-Pineau as well as her external supervision are kindly acknowledged.

REFERENCES

- [1] P. P. de San Roman, J. Benois-Pineau, J. Domenger, F. Palet, D. Cattaert, and A. de Rugy, "Saliency driven object recognition in egocentric videos with deep CNN: toward application in assistance to neuroprostheses," *Computer Vision and Image Understanding*, vol. 164, pp. 82–91, 2017.
- [2] A. Fejér, Z. Nagy, J. Benois-Pineau, P. Szolgay, A. de Rugy, and J.-P. Domenger, "Fpga-based sift implementation for wearable computing," in *2019 22nd International Symposium on Design and Diagnostics of Electronic Circuits and Systems (DDECS)*, Dec 2019.
- [3] A. Fejér, Z. Nagy, J. Benois-Pineau, P. Szolgay, A. de Rugy, and J.-P. Domenger, "A comparison of different sift implementation for vision-guides prosthetic arms," in *Jedlik laboratories reports*, vol. VII, pp. 19–20, 2019.
- [4] R. Hess, "An open-source siftlibrary," in *Proceedings of the 18th ACM International Conference on Multimedia*, MM '10, (New York, NY, USA), pp. 1493–1496, ACM, 2010.

Light Field Camera

Mary GUINDY

(Supervisors: Vamsi Kiran ADHIKARLA, Péter SZOLGAY)

Pázmány Péter Catholic University, Faculty of Information Technology and Bionics

50/a Práter street, 1083 Budapest, Hungary

guindy.mary.mohsen.messak@itk.ppke.hu

Abstract—Throughout time and with the advances of technology in the camera field. Many 2D camera animations have been implemented and used in video games, movies, etc. In addition to the camera animation, and with the aid of physics, realistic animations became more achievable. In this paper, we discuss some of the 2D camera animation techniques and we have an insight to some of the physical concepts. Physics simulation is done by means of the "Bullet Physics Library". We then try to achieve realistic camera animations by combining the 2D techniques with the physical concepts. Finally, light field camera types are being introduced with the aim of implementing the realistic camera animations on light field displays and testing them to achieve plausible results.

Keywords-camera animation, realistic camera animation, light field cameras

I. INTRODUCTION

In this paper, we discuss some of the concepts of 2D camera animation, the different light field cameras and the physics behind achieving realistic camera animation. In our work, we use "Bullet Physics" library to simulate the physics for the imported and implemented 3D models. Then, we implement virtual cameras and simulate their physical properties to achieve realistic camera animation. Finally, those animations will be tested on the light field displays.

II. 2D CAMERA ANIMATION BASICS

There are many camera movements, some of which are discussed here. Camera movements include tilt, pan, zoom, dolly, truck, pedestal, punch-in, rack focus and others. Aside from the pan, tilt and zoom, a change in the camera position is required as the camera moves [1] [2].

III. SIMULATING REALISTIC CAMERA ANIMATIONS

In this section, we discuss some of the camera animations that we try to achieve as realistic as possible.

- 1) Dampened harmonic oscillator: Similar to the simple harmonic oscillator but with the addition of the frictional force. Forces acting on mass m in the damped harmonic oscillator are the restoring force and the frictional force which opposes the motion of mass m . The damped oscillator is described as follows:

$$F = -kx - cv = -kx - c \frac{dx}{dt}$$

where k is a positive constant and c is the viscous damping coefficient, x is the displacement of mass m from the equilibrium position and v is the velocity.

- 2) Physics based (Weighted box on a string, simplified rigs)
- 3) Handheld motion
- 4) Jitter (noise models): Adding jitter to the generated camera motions achieves a more realistic effect [6].

IV. LIGHT FIELD CAMERA TYPES

As with the 2D cameras, real and virtual cameras exist for light fields. Numerous light field camera types. In this section, we discuss some of those as follows:

- 1) Plenoptic camera: In 2D cameras, an object space point is being projected into a single pixel. However, in plenoptic cameras a light ray emitted from a point is projected to many positions of the sensor [4]. The plenoptic camera is based on the plenoptic function which defines the "total geometric distribution of light" [5].
- 2) Camera arrays: As the name implies, multiple cameras are arranged in a 2D array to capture the same scene. Arrays could also be arranged in an arc.
- 3) Depth camera: As the name implies, depth cameras are used for depth acquisition. Thus the scenes are easier understood and modelled given the depth values [3].

V. CONCLUSION AND FUTURE WORK

To sum up, camera animations in light field is a new emerging technology that has a lot of room for research. Different camera effects including motion blur, depth of field and lens flare could be further implemented and tested on light fields. Moreover, work on an environment to test the various animations is in progress.

REFERENCES

- [1] Brown, Blain. *Cinematography: theory and practice: image making for cinematographers and directors*. Focal Press, 2016.
- [2] Medoff, Norman, and Edward J. Fink. *Portable Video: Eng & Efp*. Routledge, 2013.
- [3] Jayasuriya, Suren, et al. "Depth fields: Extending light field techniques to time-of-flight imaging." 2015 International Conference on 3D Vision. IEEE, 2015.
- [4] Monteiro, Nuno Barroso, et al. "Depth range accuracy for plenoptic cameras." *Computer Vision and Image Understanding* 168 (2018): 104-117.
- [5] Ng, Ren. *Digital light field photography*. Stanford: stanford university, 2006.
- [6] Kurz, Christian, et al. "Generating Realistic Camera Shake for Virtual Scenes." *JVRB-Journal of Virtual Reality and Broadcasting* 10.7 (2014).

Emulation of a single fault-tolerant memristor with memristor networks

Dániel HAJTÓ

(Supervisor: György CSEREY)

Pázmány Péter Catholic University, Faculty of Information Technology and Bionics

50/a Práter street, 1083 Budapest, Hungary

hajto.daniel@itk.ppke.hu

Abstract—Over the past few years several different materials were used to implement the memristor and other memristive devices. However, most of those suffer from undesirable noises and/or parasitic effects. To be able to design complex circuits using them, one has to deal with these high device-to-device variances. A possible solution was previously introduced which, uses several highly unreliable memristors, interconnected in an array-like circuit emulating a single, more reliable memristor unit. In this work we present measurement results for this solution and provide an explanation on the different, previously introduced circuit topologies.

Keywords—memristor; neuromorphic computing; circuit design

I. INTRODUCTION

Since their recent rediscovery in 2008 [1], memristors are subject of great interest. Many useful applications were created [2], [3], [4], however, these applications require memristors with ideal characteristics. Not only that ideal memristor is not yet presented, but the existing ones have a considerable device-to-device variance in certain parameters, such as effective resistance range and write-erase speed. Furthermore, their production yield is less than 100%, meaning that in some cases the produced devices do not function as memristors. A previously published article [5] introduces a memristor circuit, which is able to deal with the above mentioned problems and the circuit emulate a single, robust memristor.

II. MEASUREMENTS

A measurement environment is designed and created to confirm the previous results by real-device measurements. Every used Ge_2Se_3 memristor was measured to approximate the device-to-device variance of the produced devices. Using both memristors and ordinary resistances, the network measurements did take into account various possible defects such as non-functioning memristor devices.

III. RESULTS

The real-device measurements confirmed most of the hypotheses of the previous simulation results. Except for one aspect, namely the writing-erasing speed, which is reproducible contradicts with the simulation results. This topic requires more investigation to clarify the reason behind this anomaly. A new measurement setup should be designed focusing on writing and erasing characteristics and time measurement.

REFERENCES

- [1] Strukov, Dmitri B., Gregory S. Snider, Duncan R. Stewart, and R. Stanley Williams, *The missing memristor found*, nature 453, no. 7191, 2008.
- [2] Li, Can, Miao Hu, Yunning Li, Hao Jiang, Ning Ge, Eric Montgomery, Jiaming Zhang et al., *Analogue signal and image processing with large memristor crossbars*, Nature Electronics 1, no. 1, 2018.

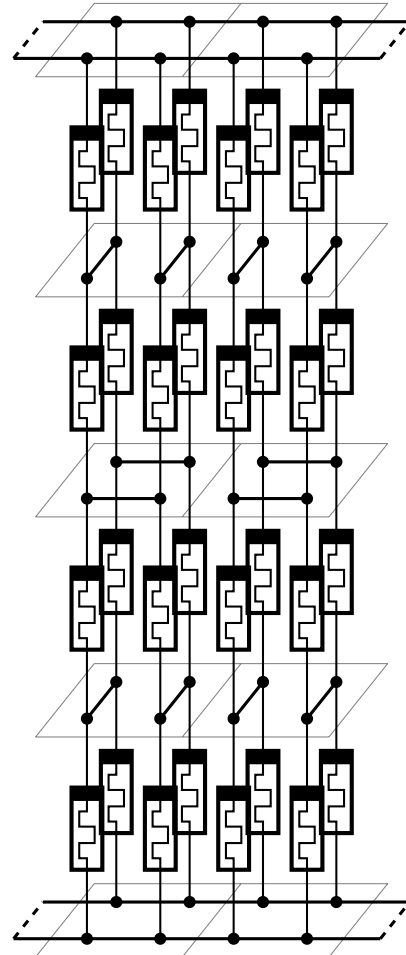


Fig. 1: A proposed three dimensional cell structure, two emulated memristor unit from a $2 \times 2 \times 4$ shaped array.

- [3] Ascoli, Alon, Dominik Baumann, Ronald Tetzlaff, Leon O. Chua, and Manfred Hild, *Memristor-enhanced humanoid robot control system—Part I: Theory behind the novel memcomputing paradigm*, International Journal of Circuit Theory and Applications 46, no. 1, 2018.
- [4] Baumann, Dominik, Alon Ascoli, Ronald Tetzlaff, Leon O. Chua, and Manfred Hild, *Memristor-enhanced humanoid robot control system—Part II: Circuit theoretic model and performance analysis*, International Journal of Circuit Theory and Applications 46, no. 1, 2018.
- [5] Hajtó, Dániel, Adam Rak, and Gyorgy Cserey, *Robust Memristor Networks for Neuromorphic Computation Applications*, Materials 12, 3573., 2019.

Accelerating Charged Single α -helix Detection on FPGA

Sam KHOZAMA

(Supervisors: Zoltán NAGY, Zoltán GÁSPÁRI)

Pázmány Péter Catholic University, Faculty of Information Technology and Bionics

50/a Práter street, 1083 Budapest, Hungary

khozama.sam@itk.ppke.hu, nagy.zoltan@itk.ppke.hu, gaspári.zoltan@itk.ppke.hu

Abstract—Implementing and speeding up the bioinformatics algorithms which need a very fast and accurate results is the main advantage of re-configurable architectures which can be used more efficiently in the comparing of conventional microprocessors with 32 or 64 bit representations.

Keywords—FPGA; FT_CHARGE; CSAH; Charged Single α -helix; alpha helix;

I. INTRODUCTION

Charged single α -helix (CSAHs)[1] form a recently recognized protein structural motif. Its existence and role are characterized in a few proteins only. To get reliable candidate CSAH motifs, we have two conceptually different computational methods that are capable of scanning large databases: SCAN4CSAH and FT_CHARGE. SCAN4CSAH is based on sequence features characteristic, whereas FT_CHARGE applies and utilizes Fourier transformation to charges along with sequences. By using the unanimity of these two approaches, a noteworthy number of proteins were found which contain putative CSAH domains. Field-programmable gate array (FPGA) based systems provide the potential for drastic improvement in the performance of data-intensive applications.

II. FT_CHARGE ALGORITHM

while FT_CHARGE algorithm applies Fast Fourier transformation to charges along with sequences, SCAN4CSAH algorithm is based on the characteristic of sequence features[6]. standard FASTA format is the input format for both algorithms. FASTA file involves of series of characters where each character represents one protein in a sequence. The analysis of biopolymer sequences utilizes Fourier transformation regularly. The processing flow through the third block is to find the maximum amplitude and its frequency which used to fit an Extreme Value distribution (EVD). At last, determining the threshold for signaling a charged single α -helix motif is done by using the fitted distribution.

III. FPGA IMPLEMENTATION

The first way to extend this solution is to create several units in parallel using a larger Xilinx ZYNQ board. In this case, we have the possibility to increase the performance nearly 6 times more on a larger FPGA. Hence, we should take into consideration, having such a huge number of hardware blocks on FPGA. Another consideration should be taken into account is the number of memory interfaces. We have 6 input and 3 output AXI interfaces. And these 9 interfaces will be replicated 6 times. We can say that the area demanded to connect these 4 units on the ZYNQ board requires 54 interfaces of the 6 replications. This is considered as a very huge area

to implement an AXI interconnect.. Therefore, we need to go further to improve computing performance and utilize some of the recent advantages of the High Level Synthesis. So, we should re-write the previous implementation such a way to execute some steps in parallel. Basically, this is the motivation behind trying to improve the speed of computation by parallelizing the algorithm.

IV. FAST FOURIER TRANSFORMATION BLOCK

Fast Fourier Transformation by using The Cooley-Tukey[2] Algorithm is the way of avoiding using the Discrete Fourier Transformation which is incredibly slow!

Previously, the system used Xilinx FFT IP which does the transformation serially. So, 32 or 64 clock cycles are required to load the samples. And the whole computation is done in 32 — 46 clock-cycles. In our case, we modified the charge correlation part to provide these data elements in parallel, which means: computation could be increased by 32 times.

V. SYSTEM DEBUGGING

For the error analyzing step, we went back to detect the output for each block and try to synchronize their results on both sides. We discovered differences in the output of the FFT block. Therefore, we computed the amplitude for every 32 or 64 elements window, exported the results into binary files, read them in Matlab, and plotted them in both hardware and software sides simultaneously. Figures 3 and 4 plot the representation of the amplitude in both cases 32 and 64 elements window computations respectively.

The difference can not be determined by the human eye. It is in the third or fourth decimal number so the difference is very near to zero. More deeply diving with numbers clarify, that we have two equal peaks inside one half of the sequence in the software.

VI. CONCLUSION

We improved, in this paper, the proposed FPGA based system for speeding up α -helix detection algorithm by replicating the main three blocks as much as they fit a larger FPGA board. In addition, implementing these several processing units in parallel enables fast search on larger protein databases and runs the whole system at a speed of 30 times higher. Future work will be implementing the Smith-Waterman (SW) algorithm to find the optimal local alignment between two sequences. Our vision to improve the SW algorithm will be comparing the sequences by dihedral angels.

REFERENCES

- [1] D. Süveges, Z. Gáspári, G. Tóth, L. Nyitray, *Charged single α -helix: a versatile protein structural motif*, *Proteins*, 74 (2009) 905–916.

Physiological Signal Extractor Algorithms Optimized for Embedded System

Ádám NAGY

(Supervisor: Ákos ZARÁNDY)

Pázmány Péter Catholic University, Faculty of Information Technology and Bionics

50/a Práter street, 1083 Budapest, Hungary

nagy.adam@itk.ppke.hu

Abstract—In earlier articles like [1][2][3], we presented that pulse and respiration can be extracted from video records or from the live camera record. These publications assume that we have enough computational power to run these algorithms on more or less arbitrary resolutions in real time. In the case of real applications we have to consider using optimization techniques because unusually we have not computational power big enough. To highlight these kind of problems, we did an experiment with an embedded system. Actually we made a working camera based physiological signal monitoring system for neonatal. This system is capable of monitoring pulse and respiration of newborn babies if they don't move extensively.

nor the segmentation nor the pulse rate estimation were run on every frame. The segmentation was run in every 5 seconds. The pulse rate estimation was run in every 2 seconds.

II. DISCUSSION

We have implemented some pulse and respiration extracting algorithms that were tested in real time scenario. In addition we have optimized these algorithms to the requirements of a very popular embedded system where we also was able to reach real time running.

REFERENCES

- [1] D. Terbe and A. Zarandy *Remote camera based measurement of human-vital signs*, inCNNA 2018; The 16th International Workshop on Cellular Nanoscale Networks and their Applications, 2018, pp. 1–5.
- [2] Ádám Nagy, D. Csetverikov, and Akos Zarándydy. *Novel methods for video-based respiration monitoring of newborn babies*, in KEPAF 2019. Képfeldolgozók és Alakfelismerők Társaságának 12. országos konferenciája, Debrecen, 2019, pp. 1–10. [Online]. Available: <http://eprints.sztaki.hu/9699/>
- [3] Ákos Zarándy, P. Földessy, Ádám Nagy, I. Jánoki, D. Terbe, M. Siket, M. Szabó, and J. Varga *Multi-level optimization for enabling life criticalvisual inspections of infants in resource limited environmen*, in IEEE International Symposium on Circuits and Systems, 2020.
- [4] Ádám Nagy *Monitoring of the physiological signals of newborn babies*, in PhD PROCEEDINGS ANNUAL ISSUES OF THE DOCTORAL SCHOOL FACULTY OF INFORMATION TECHNOLOGY BIONICS 2019, 2019,p. 37.
- [5] W. Wang, A. C. den Brinker, S. Stuijk, and G. de Haa *Algorithmic principles of remote ppg*, EEE Transactions on Biomedical Engineering,vol. 64, no. 7, pp. 1479–1491, July 2017.
- [6] S. Kolkur, D. Kalbande, P. Shimpi, C. Bapat, and J. Jatakia *Human skin detection using rgb, hsv and ycbcr color models*, Proceedings of the International Conference on Communication and Signal Processing 2016 (ICCASP 2016), 2017. [Online]. Available: <http://dx.doi.org/10.2991/iccasp-16.2017.51>
- [7] T. Vogels, M. van Gastel, W. Wang, and G. de Haan *Fully-automatic camera-based pulse-oximetry during sleep*, in 2018 IEEE/CVF Conference on Computer Vision and Pattern Recognition Workshops (CVPRW), June 2018, pp. 1430–14 308.

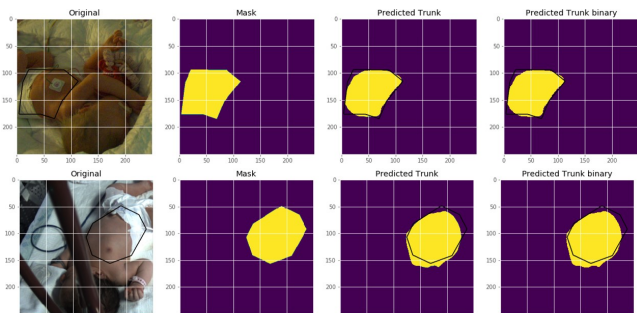


Fig. 1. This figure represents how the UNET based ROI detector find the back of the newborn baby. The unfilled curve is the ground truth. The filled yellow region is what ROI detector found on the image.

I. OPTIMIZATION FOR RASPBERRY PI

The raspberry Pi is an embedded system which have a limited computational power. As we published in [3], we made some modifications on all algorithms to make them able to run on Raspberry Pi.

In the case of respiration monitoring we down-scaled the image to 20x20 to speed up the running of respiration signal extraction. In such small images the running time of Optical Flow is relatively low. In addition, the ROI detector wasn't run on every frame but on every k. frame. In [3], we set k=200. So in the case of 20 FPS, it means that the ROI detector was run in every 10 seconds.

In the case of pulse extraction, we also down-scaled the frames in a certain point of the algorithm. In addition, we used a color based segmentation instead of SVD decomposition which is used very often [7][5] to separate the skin region from the background. We used sliding window approach and

Domain of attraction computation of a unique non-zero equilibrium point of a Lotka-Volterra system

Péter POLCZ

(Supervisor: Gábor SZEDERKÉNYI)

Pázmány Péter Catholic University, Faculty of Information Technology and Bionics

50/a Práter street, 1083 Budapest, Hungary

polcz.peter@itk.ppke.hu

Abstract—A computational approach is presented in this paper to construct a local Lyapunov for Lotka-Volterra system. The Lyapunov function is searched in a parameterized quadratic form of a constant and polynomial terms of the state variables. Sufficient conditions for the Lyapunov function are formulated as polytopic linear matrix inequality (LMI) constraints over a compact polytopic subset of the state space. Compared to other known solution in the literature, a Lyapunov function is computed without translating the system equations into the equilibrium point.

Keywords—Lyapunov function, Lotka-Volterra system, domain of attraction.

I. INTRODUCTION

Computing or at least estimating the domain of attraction (DOA) is an important and also non-trivial task for nonlinear systems. Stability analysis for nonlinear autonomous system is often done by searching for a Lyapunov function, which gives information on the qualitative behavior of the dynamics. Then, a forward invariant domain for the equilibrium point can be given as an appropriate level set of the Lyapunov function.

In the literature, numerous *DOA approximation* results are available, see, e.g., [1]–[7]. In most cases, a Lyapunov function is searched in a general quadratic form giving zero in the origin. These techniques require to translate the equilibrium point to the origin. This model transformation often results in a more complicated dynamic equation, which make the computations more demanding and time consuming.

In this paper, we present a generalized version of the polytopic LMI approach of [7]. Differently from [6], [7], the Lyapunov function is searched in a parameterized quadratic form of a constant and polynomial terms of the state variables.

II. LOTKA-VOLTERRA SYSTEMS

Let us consider a locally stable second order Lotka-Volterra system: $\dot{x} = \text{diag}(x)(Ax + b)$, where $A = \begin{pmatrix} -2 & -3 \\ 1.4 & 1 \end{pmatrix}$, $b = \begin{pmatrix} 5 \\ -2.4 \end{pmatrix}$, $x^* = \begin{pmatrix} 1 \\ 1 \end{pmatrix}$. Point x^* is the unique positive equilibrium point of the system dynamics.

During the analysis we consider only initial conditions, which belong the following simplex: $\mathcal{X} = \text{Co}\{\begin{pmatrix} 0 \\ 0 \end{pmatrix}, \begin{pmatrix} 0 \\ 3.5 \end{pmatrix}, \begin{pmatrix} 5 \\ 0 \end{pmatrix}\}$. A Lyapunov function is search in the following polynomial form: $V(x) = \pi^T(x)P\pi(x)$, where $\pi(x) = (1 \ x_1 \ x_2 \ x_1^2 \ x_1x_2 \ x_2^2)$. Through the proposed optimization, we found that

$$P = \begin{pmatrix} 1.0331 & -0.0303 & 0.0334 & -34.8291 & -33.5266 & 2.8896 \\ -0.0303 & 69.7028 & 32.51 & -0.0075 & -5.3509 & 3.8164 \\ 0.0334 & 32.51 & -5.8531 & 5.7741 & -4.0648 & 0.0178 \\ -34.8291 & -0.0075 & 5.7741 & 0.0019 & -0.049 & -1.7556 \\ -33.5266 & -5.3509 & -4.0648 & -0.049 & 3.7963 & 0.2849 \\ 2.8896 & 3.8164 & 0.0178 & -1.7556 & 0.2849 & -0.0059 \end{pmatrix}.$$

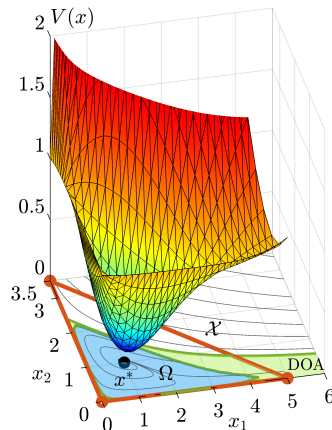


Fig. 1. Computed Lyapunov function and the corresponding maximal invariant level set Ω (blue region) for the Lotka-Volterra model. Polytope \mathcal{X} is illustrated by the orange simplex. The green region constitutes the actual domain of attraction of the equilibrium point x^* . The gray trajectories illustrate the solutions $x(t)$ of the dynamic equation.

In Fig. 1, the shape of the Lyapunov function and that of the obtained invariant domain Ω is presented.

III. CONCLUSIONS

In this paper, we have present a polytopic LMI approach to compute the domain of attraction of a Lotka-Volterra system. The Lyapunov function is searched in the form of a polynomial function with both a constant an linear terms in the state. Though the Lyapunov function is not forced to be zero in the positive equilibrium point (x^*), the Lyapunov function attains a local minima in x^* .

ACKNOWLEDGMENT

P. Polcz gratefully acknowledges the support of the New National Excellence Program scholarship (ÚNKP-19-3-I-PPKE-6).

REFERENCES

- [1] S. F. Hafstein, “An algorithm for constructing Lyapunov functions,,” *Electronic Journal of Differential Equations*, vol. 2007, 2007.
- [2] U. Topcu, *Quantitative local analysis of nonlinear systems*. PhD thesis, University Of California, Berkeley, 2008.
- [3] G. Chesi, *Domain of attraction: analysis and control via SOS programming*, vol. 415. Springer Science & Business Media, 2011.
- [4] G. Chesi, “Rational Lyapunov functions for estimating and controlling the robust domain of attraction,” *Automatica*, vol. 49, no. 4, pp. 1051–1057, 2013.
- [5] R. Bobiti and M. Lazar, “A sampling approach to finding Lyapunov functions for nonlinear discrete-time systems,” in *European Control Conference (ECC)*, pp. 561–566, June 2016.
- [6] A. Trofino and T. J. M. Dezuo, “LMI stability conditions for uncertain rational nonlinear systems,” *International Journal of Robust and Nonlinear Control*, vol. 24, no. 18, pp. 3124–3169, 2013. cited By 14.
- [7] P. Polcz, T. Péni, and G. Szederkényi, “Improved algorithm for computing the domain of attraction of rational nonlinear systems,” *European Journal of Control*, vol. 39, pp. 53–67, 2017.

FPGA Based Onboard Visual Horizon Detection with Partial Camera Lens Distortion Correction

Levente Márk SÁNTHA

(Supervisors: Zoltán NAGY, Ákos ZARÁNDY)

Pázmány Péter Catholic University, Faculty of Information Technology and Bionics

50/a Práter street, 1083 Budapest, Hungary

santha.levente.mark@itk.ppke.hu

Abstract—I shortly introduce a native radial distortion handling fast horizon detection algorithm designed for visual applications. The algorithm is suitable for smaller aerial vehicles. For the implementation I used field programmable gate arrays (FPGA). This module is part of a visual sense-and-avoid (SAA) system, where it is used for the sky-ground separation. The algorithm has low complexity because of the power consumption requirements. Also an initial guess for the horizon is used, which is provided by the attitude heading reference system (AHRS) of the aircraft.

Keywords—UAV; FPGA; sense-and-avoid; horizon; undistortion

I. INTRODUCTION

Unmanned aerial vehicle systems (UAS) are used in more and more applications from the aerial recreational photo shooting, to more complicated semi-autonomous missions [1]. To reduce the risk of collision and to improve the safe usage SAA capability need to be improved. Surveillance mission setups include onboard cameras and a payload computer, which can also be used to perform SAA. Thus, computationally cheap camera-based solutions may need no extra hardware component. Most of the vision-based SAA methods use different approaches for intruders in sky and land backgrounds [2]. Thus, they can utilize horizon detection to produce fast sky segmentation.

Firstly I introduce the camera distortion model and after that the details of the FPGA implementation.

II. EXACT FORMULA OF DISTORTED HORIZON LINES

A two-parameter radial distortion model was selected based on this study [3]. According to this, the relationship between the theoretical perspective coordinates $[x \ y]^T$ and the real ones $[x' \ y']^T$ is given

$$\begin{bmatrix} x \\ y \end{bmatrix} = (1 + k_1 r^2 + k_2 r^4) \begin{bmatrix} x_0 + t d_u \\ y_0 + t d_v \end{bmatrix} \quad (1)$$

where t is the line parameter, $d = [d_u \ d_v]$ the vector of the line's direction, $r^2 = t^2(d_u^2 + d_v^2) + 2t(x_0 d_u + y_0 d_v) + x_0^2 + y_0^2$, and $r^4 = (r^2)^2$. After some transformation (check [3]) we got the followings:

$$\begin{bmatrix} x' \\ y' \end{bmatrix} = \begin{bmatrix} \sum_{i=1}^5 a_i t^i \\ \sum_{i=1}^5 b_i t^i \end{bmatrix} \quad (2)$$

III. FPGA IMPLEMENTATION

The architecture of the system is based on our previous work under [4]. This system is under porting to a new high-end FPGA Evaluation Board, called Xilinx Zynq UltraScale+ Multi-Processor System-on-Chip (MPSoC) ZCU102.

This includes a System of Chip (SoC) FPGA system. That means hard-core processing parts such as traditional Arithmetic Logic Units (ALU) and integrated Input-Output (I/O) moduls (CAN, SPI etc.) can be found on the chip. The main improvement is the Horizon detection module. In [5] the distortion-free version of the horizon detection was introduced. The second algorithm of this version was modified by the followings to handle the distortion:

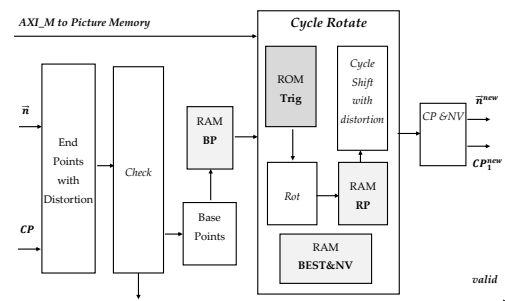


Fig. 1. Post-calculation (gradient sampling) block diagram with radial distortion.

Due to the distortion, it can happen that we have even four intersections with the borders. Therefore, the endpoint calculation module was extended with the functionality of handling this. The cycle shift block was also modified. The other functionalities of the blocks remained the same as the distortion-free case. In all shift cycles for every sample point pairs, the distortion is calculated, and the samples are taken from the distorted pixel coordinates. In the end, a normal vector and the center point of the (tuned) horizon are calculated in CP and NV block. The block diagram of the modified post-calculation submodule is shown in Figure 1.

REFERENCES

- [1] U. Mogili and B. B. V. L. Deepak, "Review on application of drone systems in precision agriculture," *Procedia Comput. Sci.*, vol. 133, pp. 502–509, 2018.
- [2] T. L. Molloy, J. J. Ford, and L. MEJIAS, "Detection of aircraft below the horizon for vision-based detect and avoid in unmanned aircraft systems," *Field Robot.*, vol. 34, pp. 1378–1391, 2017.
- [3] R. Hartley and A. Zisserman, *Multiple View Geometry in Computer Vision*. Cambridge, UK: Cambridge University Press, 2004.
- [4] A. Zarándy, M. Nemeth, Z. Nagy, A. Kiss, L. M. Sántha, and T. Zsedrovits, "A real-time multi-camera vision system for uav collision warning and navigation," *Real-Time Image Process.*, vol. 12, pp. 709–724, 2016.
- [5] A. Hiba, T. Zsedrovits, P. Bauer, and A. Zarandy, "Fast horizon detection for airborne visual systems," in *Proceedings of the 2016 International Conference on Unmanned Aircraft Systems (ICUAS)*, pp. 889–891, 2016.

Bitwise reproducible execution of unstructured mesh applications

Bálint SIKLÓSI

(Supervisors: István Zoltán REGULY, Péter SZOLGAY)

Pázmány Péter Catholic University, Faculty of Information Technology and Bionics

50/a Práter street, 1083 Budapest, Hungary

siklosi.balint@itk.ppke.hu

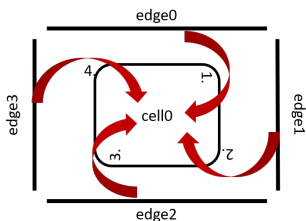


Fig. 1. Example orders of incrementing a cell in airfoil.

I. INTRODUCTION

The IEEE-754 standard defines the behaviour of floating point representation. It is correct, but comes with roundings which cause non-associativity of the operations. The order of calculations, usually relaxed in a parallel environment, affects the results. There are some other approaches to solve this issue. One of these is the ReproBLAS project’s binned representations [1]. Their method causes a $5n$ to $9n$ floating point operations overhead. An other solution can be found in Lulesh [2], although it is applicable only for boundary or halo values. In this paper I present a reproducible ordering for the indirect increments, combined with reproducible reductions. As a result, this method can guarantee full reproducibility, even if it is run on different number of MPI processes.

II. THE OP2 DOMAIN SPECIFIC LANGUAGE

The OP2 (Oxford Parallel library for Unstructured mesh solvers) project is developing an open-source framework for the execution of unstructured grid applications on clusters of GPUs or multi-core CPUs. Although OP2 is designed to look like a conventional library, the implementation uses source-source translation to generate the appropriate back-end code for the different target platforms.

My solution is implemented in this library. Further details at [3].

III. REPRODUCIBLE INDIRECT INCREMENTS

On Figure 1 two example incrementing orders can be seen on a single cell, by executing through the edges set by using an `edge_to_cells` mapping. Since the associative laws of algebra do not necessarily hold for floating-point numbers, $cell0 = e0 + e1 + e2 + e3 \neq cell0 = e1 + e3 + e0 + e2$. This situation might happen over MPI, when OP2’s partition algorithm produces different local IDs for every elements. Thus we had to implement a fixed execution order into OP2, to solve this issue. My method consists of two main parts:

- OP2 needs to determine a consistent fixed ordering
- The code automatically generated for the application needs to use this order

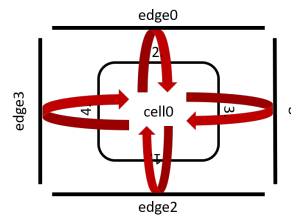


Fig. 2. Swapped structure of execution

My solution can be seen at [3]. My main idea is to swap the execution of the elements. From iterating through edges and increment cells, we iterate through cells and ask for increments from each edges with a fixed global order and apply those on the cell. This idea can be seen on Figure 2.

Obviously in implementation, this produces some overheads in computational time and memory usage. All edges are executed as they were executed originally, but their results are stored in a temporary array. After that an extra loop must be executed to collect all the local increments.

This method works with other type of mappings, not just with `edges_to_cells`.

An other difficulty of combining reproducibility with MPI is reducing into a single variable. To solve this issue, we introduce again a temporary storage for all local increments, and then we use ReploBLAS’s `double_binned` structure which can apply all increments reproducibly.

RESULTS

My results are tested on the ARCHER supercomputer on two mini-applications: (1) Airfoil, a standard finite volume CFD benchmark code and (2) Aero, a finite element 2D non-linear steady potential flow simulation. Both meshes contain 2880000 nodes and 5757200 edges.

As it was expected, reproducibility comes with a significant slowdown effect due to the extra memory movement involved, although if the application is computationally more intensive then the runtime difference decreases. In terms of bandwidth, there is a $1.4\times$ decrease measured on the Airfoil application, due to increased irregularity in memory accesses.

REFERENCES

- [1] J. Demmel, P. Ahrens, and H. D. Nguyen, “Efficient reproducible floating point summation and blas,” Tech. Rep. UCB/EECS-2016-121, EECS Department, University of California, Berkeley, Jun 2016.
- [2] “Hydrodynamics Challenge Problem, Lawrence Livermore National Laboratory,” Tech. Rep. LLNL-TR-490254.
- [3] “OP-DSL: The Oxford Parallel Domain Specific Languages,” 2015. <https://op-dsl.github.io>.

Reachability Analysis of Structurally Bounded Reaction Networks

Gergely SZLOBODNYIK

(Supervisor: Gábor SZEDERKÉNYI)

Pázmány Péter Catholic University, Faculty of Information Technology and Bionics

50/a Práter street, 1083 Budapest, Hungary

szlobodnyik.gergely@itk.ppke.hu

Abstract—In this brief note computational solutions are presented for the reachability problem of discrete state chemical reaction networks (d-CRNs), namely whether there exists a valid state transition (reaction) sequence between a prescribed initial and a target state. Considering sub-and superconservative network structures, we characterize the reachable set of the d-CRN with well-defined simplexes. Upper bounds are also derived for the possible length of cycle-free state transition sequences. We show that the reachability and the related coverability problem in the case of sub-and superconservative d-CRNs can be decided in the form an integer programming feasibility problem of well-decoupled time complexity. The proposed computation model is also employed for determining feasible series of reactions between given (sets of) states. We also provide conditions upon which the reachability problem is equivalent to the existence of a non-negative integer solution of the corresponding state equation characterizing the possible state transitions. Our findings are illustrated on a discrete state compartmental epidemiological model obeying a conservation law.

This paper is equivalent to [1].

Keywords—Discrete state reaction networks, reachability analysis, integer programming feasibility

I. SUMMARY

Dynamical behavior of complex systems of several interacting components can be modeled by either continuous or discrete state models [1]. If the amount of the interacting components is high, it is reasonable to use continuous differential equation based modeling approaches to characterize the dynamical behavior of the system. However, in the case of low abundance of the interacting components, it is worth introducing discrete state models capable of quantitatively describing the discrete state evolution of all the components. In the latter discrete state case, the so-called reachability problem is strongly related to the quantitative dynamical behavior encoded by the underlying network topology: given an initial state X_0 and a target state X' , is it possible to reach X' from X_0 along a finite non-negative state transition sequence? Through reachability analysis several problems of great importance can be analyzed, such as the existence of malicious states in a biochemical system or extinction events, i.e. state transition sequences resulted in the lack of certain components. In this paper we consider discrete state Chemical Reaction Networks (d-CRNs), a commonly used modeling approach employed for (bio)chemical systems when the molecular count of the species is low (e.g. < 100 molecules). We discuss subclasses of d-CRNs obeying conservation laws. We provide a set of conditions under which the reachability realization is equivalent to the existence of a non-negative integer solution of the respective d-CRN state equation. We show how the results can be used in practice to efficiently analyse the dynamical

behavior of d-CRNs in terms of the decidability of reachability problems. Our findings are shown on a representative example.

REFERENCES

- [1] G. Szlobodnyik, G. Szederkényi, "Reachability Analysis in Discrete State Reaction Networks with Conservation Laws", *Complex Networks*, 2019.
- [2] G. Szlobodnyik, G. Szederkényi, MD Johnston, "Reachability analysis of subconservative discrete chemical reaction networks", *MATCH Commun. Math. Comput. Chem.*, Vol. 81(3), pp. 705-736., 2019.
- [3] G. Szlobodnyik and G. Szederkényi, "Reachability Analysis of Low-Order Discrete State Reaction Networks Obeying Conservation Laws", *Complexity*, Vol. 2019, Article ID 1035974, 13 pages, 2019.
- [4] T. G. Kurtz, "The Relationship between Stochastic and Deterministic Models for Chemical Reactions", *The Journal of Chemical Physics*, 57(7), pp. 2976-2978., 1972.
- [5] D. F. Anderson, T. G. Kurtz, "Stochastic analysis of biochemical systems", Berlin Springer, 2015.
- [6] M. D. Johnston, "A Computational Approach to Extinction Events in Chemical Reaction Networks with Discrete State Spaces", *Mathematical Biosciences*, 294., 2017., 130-142.
- [7] H. W. Lenstra Jr., "Integer Programming with a Fixed Number of Variables", *Mathematics of Operation Research*, 8., 1983., 538-548.
- [8] A. J. Barvinok, "A Polynomial Time Algorithm for Counting Integral Points in Polyhedra When the Dimension is Fixed", *Math. Oper. Res.*, 19., pp. 769-779., 1994.

PROGRAM 3
FEASIBILITY OF ELECTRONIC AND OPTICAL
DEVICES, MOLECULAR AND
NANOTECHNOLOGIES,
NANO-ARCHITECTURES, NANOBIONIC
DIAGNOSTIC AND THERAPEUTIC TOOLS

Head: Árpád CSURGAY

Optimization Techniques in Neural Network Architectures

András FÜLÖP

(Supervisors: András HORVÁTH, György CSABA)

Pázmány Péter Catholic University, Faculty of Information Technology and Bionics
50/a Práter street, 1083 Budapest, Hungary
fulop.andras@itk.ppke.hu

Abstract—In convolutional neural networks, nearly 90% of computations are the convolutions. Therefore, the effective realisation of the convolution operation can be crucial in terms of speed and energy consumption in the implementation of convolutional neural networks. During my work the main project was to find an energy and speed efficient implementation of the convolution operation, which can effectively solve machine learning tasks like image processing (classification) problems.

Keywords—neural network; convolution; optimisation

I. INTRODUCTION

The commonly used deep learning methods (deep learning has been successfully applied for example in large-scale automatic speech recognition, in natural language processing and in image processing as well) go through the same process. The algorithms apply a nonlinear transformation on inputs and use what they learn to create statistical models as outputs and the iterations continue until the outputs have reached an acceptable level of accuracy. [1] [2] [3] [4]

II. CONVOLUTIONAL NEURAL NETWORKS

There are four main operations in convolutional neural network:

- 1) convolution
- 2) non-linearity (ReLU)
- 3) pooling (subsampling)
- 4) classification

III. KERVOLUTIONAL NEURAL NETWORKS

The existing convolutional neural networks works mainly leverage on the activation layers, which can only provide point-wise non-linearity, but the kernel convolution (kervolution) operation can solve this problem. The kernel convolution was used to approximate complex behaviors of human perception systems. [5]

The kernel convolution generalizes convolution, enhances the model capacity, and captures higher order interactions of features without introducing additional parameters, via kernel functions. [5]

The kernel convolutional neural networks can achieve higher accuracy and faster convergence than the baseline convolutional neural networks. [5]

The non-linearity that comes from the activation layers, for example rectified linear unit (ReLU) can only provide point-wise non-linearity, but the convolutional neural networks may perform better if convolution can be generalized to patch-wise non-linear operations via kernel trick, and because of the increased expressibility and model capacity, better model generalization could be obtained. [5]

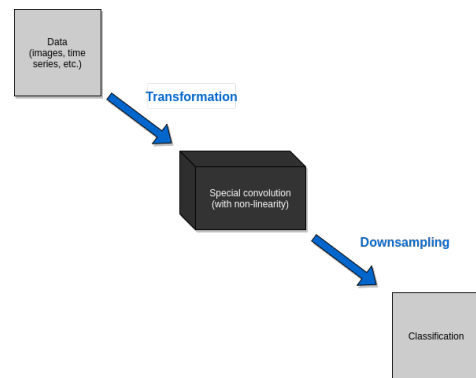


Fig. 1. Nearly 90% of computations in convolutional neural networks are the convolutions. Therefore, the effective realisation of the convolution operation can be crucial in terms of speed and energy consumption in the implementation of convolutional neural networks.

ACKNOWLEDGEMENTS

I would like to thank my supervisors András Horváth and György Csaba for the continuous support of my work and for their expert advice. Without their precious support it would not be possible to conduct this research.

REFERENCES

- [1] Y. Bengio, A. C. Courville, and P. Vincent, “Unsupervised feature learning and deep learning: A review and new perspectives,” *CoRR*, abs/1206.5538, vol. 1, p. 2012, 2012.
- [2] Y. LeCun, Y. Bengio, and G. Hinton, “Deep learning,” *nature*, vol. 521, no. 7553, p. 436, 2015.
- [3] A. Krizhevsky, I. Sutskever, and G. E. Hinton, “Imagenet classification with deep convolutional neural networks,” pp. 1097–1105, 2012.
- [4] Y. LeCun, B. E. Boser, J. S. Denker, D. Henderson, R. E. Howard, W. E. Hubbard, and L. D. Jackel, “Handwritten digit recognition with a back-propagation network,” in *Advances in neural information processing systems*, pp. 396–404, 1990.
- [5] C. Wang, J. Yang, L. Xie, and J. Yuan, “Kervolutional neural networks,” in *Proceedings of the IEEE Conference on Computer Vision and Pattern Recognition*, pp. 31–40, 2019.

A Summary of Tensor Factorisation Techniques for 3D Image Processing

Janka HATVANI

(Supervisor: Miklós GYÖNGY)

Pázmány Péter Catholic University, Faculty of Information Technology and Bionics

50/a Práter street, 1083 Budapest, Hungary

hatvani.janka@itk.ppke.hu

Abstract—The handling of three dimensional image data is essential in many fields. Usually two dimensions are spatial, while the third dimension might be also spatial (computed tomography, 3D ultrasound), temporal (videos, Doppler ultrasound imaging), or spectral (multi- or hyper-spectral imaging). While the third dimension also holds important information about the structure of the data, it is usually discarded and is unfolded into a 2D matrix for further processing. This is convenient, as popular image processing algorithms are using 2D matrix algebra, which are not readily convertible into 3D. However this unfolding leads to huge matrices, heavily increasing the computational cost. Another solution is to keep these data structures in 3D, and to use the appropriate tensor algebra. This, however, needs new mathematical solutions. In this paper such approaches, focusing on tensor factorization will be summarized.

Keywords—tensor factorization, 3D image processing

I. INTRODUCTION

In many fields the information is acquired in a 3D form, referred to as a tensor. The three dimensions might all be spatial, as in CT, MRI, 3D laser scanning, or stereophotogrammetry. In a video or ultrasound flow estimation time is the third dimension. Another example is a spectral dimension, Multi- and hyperspectral, satellite imaging or color images have a third spectral dimension. The image processing task might be reconstruction, super-resolution, artifact reduction, modality fusion, motion tracking, compression, etc. 3D data cubes are often unfolded into 2D matrices in order to employ 2D algorithms on them. This leads to the loss of information, and the computational requirement increases. Matrix algebra is a special case of tensor algebra, meaning that the same solutions do not apply in 3D, therefore they have to be reconsidered. Herein such decomposition algorithms are discussed.

II. TENSOR DECOMPOSITIONS

Most tensor decompositions are different generalizations of the matrix singular value decomposition (SVD). Authors of [1] give a comprehensive summary of such techniques.

Canonical polyadic decomposition (CPD) is the most common decomposition. The smallest number of pure tensors that can sum up to form the tensor \mathbf{X} is called the tensor rank of \mathbf{X} , denoted by F , which is NP-hard to find, and is usually only estimated. The resulting essentially unique factorization of \mathbf{X} is called the CPD of \mathbf{X} . Usually an efficient alternating least squares algorithm is used for finding the CPD, as proposed in [2]. The original algorithm was used in psychometrics, analyzing multiple similarity, dissimilarity matrices. It was also used in the modeling of fluorescence excitation-emission data, the analysis of fMRI data. The algorithm was also used for image compression and classification, data fusion in multi-hyperspectral imaging, and for super-resolution.

The Tucker decomposition (TD) is written as $\mathbf{X} \approx \mathbf{\Sigma} \times_1 V_1 \times_2 V_2 \times_3 V_3$, where $\mathbf{\Sigma}$ is a core tensor, $V_1 \in \mathbb{R}^{I \times R_1}$, $V_2 \in \mathbb{R}^{J \times R_2}$, $V_3 \in \mathbb{R}^{K \times R_3}$ are the bases of the subspaces spanned by the mode- n fibers, and \times_n is the mode product [1]. $\mathbf{\Sigma}$ is not diagonal, but its elements show the level of interaction between the different modes. Singular values similar to the 2D case can also be defined. The algorithm was introduced by Tucker [3]. It might be used for compression, facial recognition, image fusion of limited depth-of-field camera pictures, resolution enhancement of color images, denoising of MRI scans. We are currently working with promising results on a super-resolution algorithm of CT images using the truncated TD.

Higher order robust PCA (HoRPCA) attempts to ease the sensitivity of PCA to outliers and large errors. The tensor \mathbf{X} is decomposed into the sum of a low rank \mathbf{L} and a sparse component \mathbf{S} . The resulting Singleton optimization model is $\min_{\mathbf{L}, \mathbf{S}} \sum_n \|\mathbf{L}^{(n)}\|_* + \lambda \|\mathbf{S}\|_1$ | $\mathbf{X} = \mathbf{L} + \mathbf{S}$. The problem might be solved using alternating direction method of multipliers (ADMM). The algorithm and all its modifications are exhaustively explained in [4], where the algorithms are tested on denoising 3D MRI images, fluorescence data, face databases. Its 2D version was used for ultrasound flow data, and we are currently working on its 3D application.

III. DISCUSSION

The above decomposition techniques can be used efficiently in 3D image processing tasks. The framework of CPD can incorporate further processing steps, but not any. In real-life applications the algorithm converges fast and is robust to the choice of parameters. In TD n times more parameters have to be estimated, than in the CPD, but their setting is easier, similarly to 2D truncation techniques. Further processing tasks might be used only in series with TD. If the data model allows a decomposition into a low rank and a sparse tensor, HoRPCA might be applied. Here the parameters of the ADMM have to be set, which is usually a time-consuming task. However, this is the most flexible framework, further regularizing steps are easy to incorporate. In future work TD in CT image data, and HoRPCA in ultrasound flow data will be explored.

REFERENCES

- [1] T. G. Kolda and B. W. Bader, "Tensor decompositions and applications," *SIAM review*, vol. 51, no. 3, pp. 455–500, 2009.
- [2] J. D. Carroll and J.-J. Chang, "Analysis of individual differences in multidimensional scaling via an n -way generalization of "eckart-young" decomposition," *Psychometrika*, vol. 35, no. 3, pp. 283–319, 1970.
- [3] L. R. Tucker, "Some mathematical notes on three-mode factor analysis," *Psychometrika*, vol. 31, no. 3, pp. 279–311, 1966.
- [4] D. Goldfarb and Z. Qin, "Robust low-rank tensor recovery: Models and algorithms," *SIAM Journal on Matrix Analysis and Applications*, vol. 35, no. 1, pp. 225–253, 2014.

Automated lesion classification on ultrasound images

Péter MAROSÁN

(Supervisor: Miklós GYÖNGY)

Pázmány Péter Catholic University, Faculty of Information Technology and Bionics

50/a Práter street, 1083 Budapest, Hungary

marosan.peter@itk.ppke.hu

Abstract—Sonography has an important role in the analysis of different lesions, such as cancerous skin, liver, breast or thyroid lesions. Interpretation of the ultrasound records often requires experts, but computer-aided diagnostics (CAD) tools also became more and more popular nowadays, since the growing number of subjects and the increasing performance of the available set of techniques. Current paper presents the main automated lesion classification pipeline on ultrasound records and reviews the most relevant differential diagnosis related techniques using a well organised grouping strategy.

Keywords—ultrasound imaging; lesion classification; automated differential diagnosis;

I. INTRODUCTION

Ultrasound imaging became one of the most widely used imaging and diagnostic modalities in the last decades due to its good penetration resolution and depth, non-invasive behaviour, non-ionizing radiation, portability and cost-efficiency. CAD tools can give aid to medical experts during their work. By applying CAD tools on ultrasound images, different kind of human body lesions can be examined, based on their type, malignancy or extension. The most frequently examined lesions are the skin, breast, liver and thyroid lesions. [1], [2] Figure 1. gives an example of ultrasound records of skin lesions.

II. GENERAL PIPELINE FOR CLASSIFICATION PROCESS

The classification pipeline stands from five different steps. These are not all indispensable ones, but they can give some aid in order to set up a diagnosis in a certain medical question. The pipeline starts with potential pre-processing of the examined image data, continues with feature extraction and selection based on some dimensionality reduction technique, which are followed by the classification and ends with the evaluation of the results.

III. REVIEW OF TECHNIQUES

A. Feature extraction and selection

Most commonly used feature extraction techniques are the statistical or intensity-based features (eg.: basic statistical features, probability distribution parameters), textural or sonographic features (eg.: Gray Level Co-occurrence Matrices, Local Binary Pattern...), shape features, such as edge and boundary features, and transform features using Fourier, Gabor and different wavelet transforms (often used Discrete Wavelet Transform).

There are unsupervised and supervised feature selection methods. Supervised ones are Filter Methods, which examine feature relationship with the target, Wrappers, considering the selection of features as a searching problem and Intrinsic

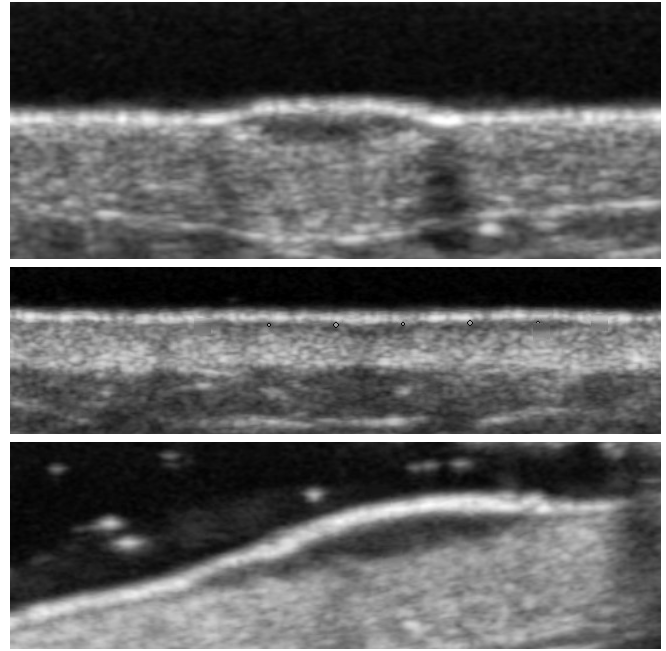


Fig. 1. High-frequency ultrasound images of different types of skin lesions (from up to down: Benign Nevus, Basal Cell Carcinoma and Malignant Melanoma.) In some cases, certain differential features, such as shape, speckle pattern or echogenicity are noticeable even by naked eyes.

or Embedded Methods, such as Tree-based methods perform automatic selection of the features during the training.

B. Classification

Commonly used image classification methods applied on ultrasound lesions are Support Vector Machines, Decision Tree Classifiers and Artificial Neural Networks. Less frequently applied but still mentionable techniques are the Gaussian Mixture Model, Naive Bayes Classifier, AdaBoost Classifier, K-Nearest Neighbour technique and the Fuzzy classifier.

C. Evaluation

Classification performance is usually measured by accuracy, precision, recall, the F1 Score (harmonic mean of the precision and the recall), the AUC (area under the receiver operating characteristic curve) or the Log Loss.

REFERENCES

- [1] K. Andr ekut e, G. Linkevi iut e, R. Rai sutis, S. Valiukevi ien e, and J. Mak stien e, "Automatic differential diagnosis of melanocytic skin tumors using ultrasound data," *Ultrasound in medicine & biology*, vol. 42, no. 12, pp. 2834–2843, 2016.
- [2] D. Csabai, K. Szalai, and M. Gy ngy, "Automated classification of common skin lesions using bioinspired features," in *2016 IEEE International Ultrasonics Symposium (IUS)*, pp. 1–4, IEEE, 2016.

Two-photon microscopical measurement of navigation integration in mouse brain

Zsolt MEZRICZKY

(Supervisor: Balázs RÓZSA)

Pázmány Péter Catholic University, Faculty of Information Technology and Bionics

50/a Práter street, 1083 Budapest, Hungary

mezriczky.zsolt@itk.ppke.hu

Hippocampus is one of the most important brain region in memory processes. It also participates in the navigation: decision making and replay of the spatial map during spatial orientation [1]. Hippocampus represents different type of local field potentials during navigation, like theta waves or sharp wave-ripples [2]. Sharp wave-ripples are typical local field potentials during slow wave sleep and consummatory behavior. The synchronized activity of pyramidal cells and interneurons results as sharp wave-ripples [3].

In early works navigation related hippocampal cell activity was investigated by single-unit recordings. These in vivo electrophysiological measurements have several limitations: identification of different cell types within the tissue, distinguish different intracellular parts of neurons, less spatial resolution. These disadvantages can be solved by in vivo two-photon imaging [4]. The Ca²⁺ signal recordings with genetically encoded sensors are an indirect way to examine the activity of neurons and it is also good for separate different neuron populations based on their molecular pattern [5]. AO two-photon microscopy allows fast three-dimensional imaging. We can simultaneously record the activity of neurons in different layers of a volume. With different scanning techniques population activity or certain parts of neurons – for example, the whole dendritic tree - can be examined [6][7][8].

Previous works proved the role subcellular parts of neuron in the generation of sharp wave-ripples in vitro [8]. We currently working on in vivo validation of sharp wave-ripple associated dendritic activities in parvalbumin containing interneurons. Interneurons together with pyramidal cell network activity result as cell assemblies [9].

Here I will present an alternative way of imaging on pyramidal cell layer of dorsal hippocampus of mice. Our three-dimensional AO system is capable to record Ca²⁺ signal from large volume with high-enough spatial resolution. Previously surgeries for in vivo experiments makes limitations in the field of view and the viewpoint. Our three-dimensional microscopy system is able tilt the field of view along all the three axes. It gives us a huge advantage to set an optimal field of view to maximize the measurable cell number.

In this work I also present a newly developed linear treadmill prototype. It was a necessary step forward in the case of behavior experiment. The earlier treadmill, called gramophone is a well used one to record the movement of the animal. The running surface is grounded, which had limitations in the movement and the body position of the animal in longer experiments. [Fig.1/A].

We developed a new treadmill system, which imitates more natural navigational movement of mice. The system is suitable to connect with virtual reality system and licking port, thus

complex navigational experiments could be accomplished.

I showed a new imaging method for record high cell number in hippocampus. Tilting the field of view gives higher possibility to record more cells when the surgery was not ideal, or the cell distribution is not homogeneous. With this technique we can reach different aspects of certain brain region. In hippocampus we were able to record cell activity from different layers off hippocampus. It can be also useful in the cortex, where dendrites are perpendicular position to brain surface. Tilting the field of view may gives advantages in the measurements of tissues with high cell density. Different scanning methods are more useful in volumes with lower cell density [6], [7].

In next step we want to find the relationship between navigation related local field potentials - especially sharp wave-ripples - and cellular activity of different neuron populations in hippocampus. Describing the role of different cell type in navigation helps us to understand how animals orientate in new environment.

ACKNOWLEDGEMENTS

I would like to thank for the help of Balázs Chiovini, Dénes Pálfi, Gábor Juhász and Linda Sulcz-Judák in my work.

REFERENCES

- [1] O'Neill J, Pleydell-Bouverie B, Dupret D, Csicsvari J. Play it again: reactivation of waking experience and memory. *Trends Neurosci.* 2010 May;33(5):220-9
- [2] Colgin L. Rhythms of hippocampal network. *Nat Rev Neurosci.* 2016 March; 17(4): 239-249
- [3] Stark E, Roux L, Eichler R, Senzai Y, Royer R, Buzsáki. Pyramidal Cell-Interneuron Interactions Underlie Hippocampal Ripple Oscillations. *Neuron* 2014, 83(2): 467-480
- [4] Dombeck DA, Harvey CD, Tian L, Looger LL, Tank DW. 2010. Functional imaging of hippocampal place cells at cellular resolution during virtual navigation. *Nat Neurosci.* 13(11):1433-40
- [5] Tian L, Akerboom J, Schreier ER, Looger LL. Neural activity imaging with genetically encoded calcium indicators. 2012. *Prog Brain Res.* 196:79-94
- [6] Katona G, Szalay G, Maák P, Kaszás A, Veress M, Hillier D, Chiovini B, Vizi ES, Roska B, Rózsa B. Fast two-photon in vivo imaging with three-dimensional random-access scanning in large tissue volumes. 2012. *Nat Methods.* 9(2):201-8
- [7] Szalay G, Judák L, Katona G, Ócsai K, Juhász G, Veress M, Szadai Z, Fehér A, Tompa T, Chiovini B, Maák P, Rózsa B. Fast 3D Imaging of Spine, Dendritic, and Neuronal Assemblies in Behaving Animals. 2016. *Neuron.* 92 (4): 723-738
- [8] Chiovini B, Turi GF, Katona G, Kaszás A, Pálfi D, Maák P, Szalay G, Szabó MF, Szabó G, Szadai Z, Káli S, Rózsa B. Dendritic spikes induce ripples in parvalbumin interneurons during hippocampal sharp waves. 2014. *Neuron.* 82(4):908-24
- [9] Buzsáki G. Neural syntax: Cell assemblies, synassemblies and readers *Neuron.* 2010 Nov 4;68(3):362-85

Two-way logical gates based on nanomagnetic logic devices

Tamás RUDNER

(Supervisor: György CSABA)

Pázmány Péter Catholic University, Faculty of Information Technology and Bionics

50/a Práter street, 1083 Budapest, Hungary

rudner.tamas@itk.ppke.hu

Abstract—Nanomagnetic logic (NML) devices are shown to have low power consumption. The information throughout a NML device is stored and processed through magnetic interactions between magnetic dots. The motivation behind building two-way logic gates is coming from a different computational phenomena, called self-organising logic gates, which is a memcomputing-based architecture.

Keywords—two-way logic functions, nanomagnetic logic devices, majority voting

I. INTRODUCTION

In the recent years, a new paradigm, called memcomputing has risen[1], which puts the memory inside the computational unit to bypass the bottleneck of moving the data between the processing and memory units. Self-organising logic gates are two-way logic gates.[2] They have no set input/output terminals and the data can flow through them in both direction. They are theoretically capable of solving computationally hard (NP) problems using polynomial scaling resources and time. In order to put them into a physical framework, we decided to build logic gates using nanomagnetic devices (NML)[3][4], which are not SOLGs, but they work in a two-way fashion.

II. TWO-WAY NANOMAGNETIC MAJORITY LOGIC GATES

Nanomagnetic logic gates utilise majority voting to calculate the magnetisation of the computing dot, based on the magnetisation vector of the computing cell's neighbours. At 0K the solution to these systems is deterministic, but for complex circuits, stochastic gradient descent algorithm is needed, introducing thermal fluctuations.

III. CONCLUSION

The implemented gates worked within their limitations, but other experiments will be performed, such as in-depth thermal analysis. Another interesting challenge with the nanomagnetic two-way gates is that building more complex circuits might not work properly and they might stuck in metastable states.

IV. RESULTS

To test the majority gates, I have carried out two different experiments. One for the forward and one for backward operating mode of a single NAND gate.

REFERENCES

- [1] F. L. Traversa and M. Di Ventra, "Universal memcomputing machines," *IEEE Transactions on Neural Networks and Learning Systems*, vol. 26, no. 11, pp. 2702–2715, 11 2015.
- [2] F. Traversa and M. Di Ventra, "Polynomial-time solution of prime factorization and np-complete problems with digital memcomputing machines," *Chaos: An Interdisciplinary Journal of Nonlinear Science*, vol. 27, p. 023107, 02 2017.

T. RUDNER, "Two-way logical gates based on nanomagnetic logic devices" in *PhD Proceedings – Annual Issues of the Doctoral School, Faculty of Information Technology and Bionics, Pázmány Péter Catholic University – 2020*. G. Prószéky, G. Szederkényi Eds. Budapest: Pázmány University ePress, 2020, p. 57. This research has been partially supported by the European Union, co-financed by the European Social Fund (EFOP-3.6.3-VEKOP-16-2017-00002).

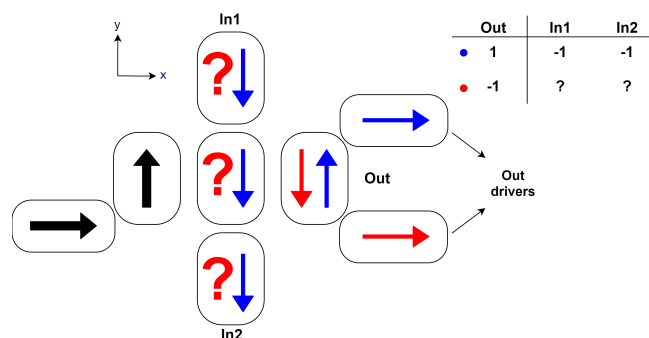


Fig. 1. Structure of a NAND majority gate working backwards. If the structural element's magnetisation vector (indicated by the black arrow inside the magnet left to the central, computing magnet) and the Out labelled magnet's magnetisation vector are parallel (indicated by the blue arrow), then the upper and lower magnets align. However, if the magnetisations of the two magnets next to the computing cell are antiparallel, then the computing cell does not even have a valid outcome from the majority voting, meaning it cannot decide which way it's magnetisation should be facing.

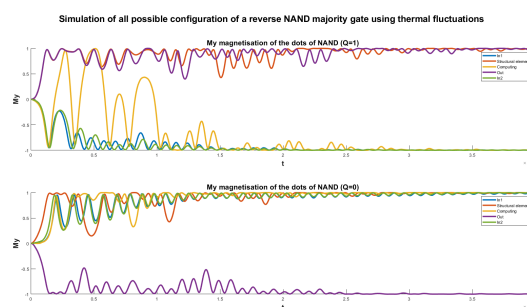


Fig. 2. The layout of the experiment is the same as in Fig. 1. The driver nodes' M_y components are excluded from the plots again. Because of the issue shown in Fig. 1, these simulations were performed considering thermal fluctuation (temperature was set to $T = 300K$).

- [3] G. Csaba, A. Imre, G. H. Bernstein, W. Porod, and V. Metlushko, "Nanocomputing by field-coupled nanomagnets," *IEEE Transactions on Nanotechnology*, vol. 1, no. 4, pp. 209–213, 2002.
- [4] G. Csaba, M. Becherer, and W. Porod, "Development of cad tools for nanomagnetic logic devices," *International Journal of Circuit Theory and Applications*, vol. 41, no. 6, pp. 634–645, 2013. [Online]. Available: <https://onlinelibrary.wiley.com/doi/abs/10.1002/cta.1811>

PROGRAM 4
HUMAN LANGUAGE TECHNOLOGIES,
ARTIFICIAL UNDERSTANDING,
TELEPRESENCE, COMMUNICATION

Head: Gábor PRÓSZÉKY

Investigation of open-set recognition techniques

András Pál HALÁSZ

(Supervisors: Kálmán TORNAI, Péter Norbert SZOLGAY)

Pázmány Péter Catholic University, Faculty of Information Technology and Bionics

50/a Práter street, 1083 Budapest, Hungary

halasz.andras@itk.ppke.hu

Nowadays, various machine learning methods provide excellent results in different classification and recognition tasks, reaching or even exceeding the human level in numerous cases. The experiments yielding these results were conducted in a closed-set scenario, i.e., the assumption that all classes are known during training. A more realistic situation is the open-set case when new classes can appear during testing, and our model has to reject them, which is a great challenge. I review the definition of the problem and the existing solutions to it with the help of the literature.

Scheirer et al. [1] formalized Open-Set Recognition defining Open Space Risk. They immediately presented their solution, an SVM-based method. There were earlier SVM models with reject option. However, those assumed closed world; the rejection was only desired for uncertain classifications.

Another significant milestone was the application of the Extreme Value Theory for open-set recognition. I review its theoretical foundation, according to Rudd et al. [2], who, although were not the first to use it, was the first to ground it to my knowledge formally. They also created their model, the Extreme Value Machine.

Neural networks were also adapted for the open-set scenario. The greatest difficulty to overcome was the SoftMax layer used in classifier networks with its inimitably closed-set nature. One solution was the OpenMax [3] replacing the SoftMax; others used autoencoders in addition to SoftMax classifier to separate known and unknown classes with the reconstruction error. [4]

I have tested some of these methods with the help of available source codes. Only tests on EVM were exhaustive so far, the results qualitatively agreed with the ones published in the article. The setup of larger-scale tests of the other methods is a task for the next period, as well as beginning to implement own ideas.

REFERENCES

- [1] W. J. Scheirer, A. Rocha, A. Sapkota, and T. E. Boulton, "Toward open set recognition," *IEEE Transactions on Pattern Analysis and Machine Intelligence*, vol. 35, pp. 1757–1772, 2013.
- [2] E. M. Rudd, L. P. Jain, W. J. Scheirer, and T. E. Boulton, "The extreme value machine," *IEEE Transactions on Pattern Analysis and Machine Intelligence*, vol. 40, pp. 762–768, 2018.
- [3] A. Bendale and T. Boulton, "Towards open set deep networks," Jun. 2016, pp. 1563–1572. DOI: 10.1109/CVPR.2016.173.
- [4] P. Oza and V. Patel, "Deep cnn-based multi-task learning for open-set recognition," Mar. 2019.

Deep Learning Algorithms for Intelligent Named Entity Recognition

Kamran IBIYEV

(Supervisor: Gábor PRÓSZÉKY)

Pázmány Péter Catholic University, Faculty of Information Technology and Bionics

50/a Práter street, 1083 Budapest, Hungary

ibiyev.kamran@itk.ppke.hu

Abstract—Named Entity Recognition (NER) is one of the primary fields of Natural Language Processing, focused on analyzing and determining the entities in a given text. In this research, our aim is transferring knowledge from one language to others and evaluate the outcomes. For that, we apply the multilingual BERT language model to the NER task using the FLAIR interface. We focus on Azerbaijani, Turkish, Hungarian, English and German. WikiANN, a ‘silver standard’ NER dataset generated from Wikipedia, is used to train and test our models.

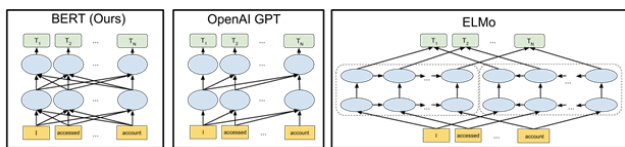
Keywords—keyword; Named Entity Recognition; BERT; FLAIR; WikiANN

I. INTRODUCTION

Named Entity Recognition is a subfield of Information Extraction that can determine the entities in the given text. It is a fundamental part of many NLP tasks and is used in various applications like information extraction [1], question answering, document de-identification, machine translation, conversational models and so on. The task of Named Entity Recognition is to determine and classify the entities in the given text based on the predefined categories like organizations, dates, times, persons, locations and so on.

There are context-free and contextual pre-trained representations, while contextual representations can be unidirectional or bidirectional. Context-free models (word2vec, GloVe) create only one single embedding representation for each word, however the contextual method creates a representation of every single word that is depending upon the other words in that sentence.

BERT, is a contextual and bidirectional language representation model as it is obvious from its abbreviation [2]. The Figure indicates BERT’s neural network structure and compares it with previous state-of-the-art contextual pre-training methods. The arrows show the information flow from one layer to the next. The green section displays the eventual contextualized representation of the input token.



Source: Adapted from [3]

Fig. 1: Comparison of BERT, OpenAI GPT and ELMo

Between these three approaches, just BERT is collectively conditioned on both left and right context in all layers. In this research, we apply the multilingual mBERT (Multilingual BERT) model using the FLAIR framework.

II. EXISTING SOLUTIONS

FLAIR framework provides a simple UI with the possibilities of training and distribution of state-of-the-art sequence labelling, language models, text classification and so on.

Wikipedia is a huge multi-lingual portal with 295 languages, 35 million articles which contains 3 billion words, and it includes inherently annotated markups and plenty of information. Therefore, we use WikiAnn datasets, which were automatically created by extracting and classifying anchor links on Wikipedia for 282 languages,

Overall, regardless of some mistagging and other minor issues, WikiAnn is very useful and only existing NER dataset that contains a huge amount of language.

Although FLAIR interface provides some datasets that make possible to load with one line of code, we will use the WikiAnn datasets to train our model. We can train your model with more than one language, MultiCorpus object. After creating the (multi)corpus we should split our dataset to dev, test and train parts. Then we can start the learning process with the help of FLAIR’s LanguageModelTrainer class. Subsequently, it is possible to do a finetuning on our language model in place of starting a new one without changing any other code.

ACKNOWLEDGEMENTS

This research is supported by the European Union, co-financed by the European Social Fund (EFOP-3.6.3-VEKOP-16-2017-00002).

I express appreciation to my supervisors Gabor Proszeky and Attila Novak for their continuous guidance and professional advice. I would like to acknowledge the support of Pázmány Péter Catholic University for the technological equipment provided which helped a lot during the research.

REFERENCES

- [1] J. Raiman and O. Raiman, “Deeptype: Multilingual entity linking by neural type system evolution;” in *Proceedings of the Thirty-Second AAAI Conference on Artificial Intelligence, New Orleans, Louisiana, USA, February 2-7, 2018* (S. A. McIlraith and K. Q. Weinberger, eds.), pp. 5406–5413, AAAI Press, 2018.
- [2] M. E. Peters, M. Neumann, M. Iyyer, M. G. 0001, C. Clark, K. Lee, and L. Zettlemoyer, “Deep contextualized word representations;” in *Proceedings of the 2018 Conference of the North American Chapter of the Association for Computational Linguistics: Human Language Technologies, NAACL-HLT 2018, New Orleans, Louisiana, USA, June 1-6, 2018, Volume 1 (Long Papers)* (M. A. Walker, H. Ji, and A. Stent, eds.), pp. 2227–2237, Association for Computational Linguistics, 2018.
- [3] J. Devlin, M.-W. Chang, K. Lee, and K. Toutanova, “Bert: Pre-training of deep bidirectional transformers for language understanding;” in *Proceedings of the 2019 Conference of the North American Chapter of the Association for Computational Linguistics: Human Language Technologies, NAACL-HLT 2019, Minneapolis, MN, USA, June 2-7, 2019, Volume 1 (Long and Short Papers)* (J. Burstein, C. Doran, and T. Solorio, eds.), pp. 4171–4186, Association for Computational Linguistics, 2019.

Abstractive Arabic Text Summarization

Mram KAHLA

(Supervisor: Gábor PRÓSZÉKY)

Pázmány Péter Catholic University, Faculty of Information Technology and Bionics
50/a Práter street, 1083 Budapest, Hungary
kahla.mahmoud.mram@itk.ppke.hu

Abstract—The topic of the current paper is the Abstractive Arabic Text Summarization, or in simple terms, how a text can be summarized into a brief essence with the use of machine, the utilization of neural network models, in a way that is not only very appealing for use in natural language problems, but leads to breakthroughs in it, including summarization. While that in its own is anything but an easy task, the current research deals with this in Arabic. That is for a number of reasons, which shall be implied here. In this brief overview the aim is to provide and insight to the field of text summarization, its trajectories and approaches, the methods used for the path taken, the current phase of the research, the obstacles we face, the possible applications for this research field, which has been envisioned. Upon that the uses and urgencies of doing that with Arabic shall be assessed, but also the specific challenges we face with this language text summarization process.

Keywords-abstractive summarization

I. EXTRACTIVE VS. ABSTRACTIVE

When we talk about text summarization that practically means that using certain algorithms, we teach a machine to subtract information from an extensive text and provide a significantly shorter overview of it. And just like in the case of human beings, like a number of cases in our own school experiences, there are two ways of doing that.

The first way is called extractive [1]. In this method the idea is to practically highlight, take out certain key words, phrases, or sentences from the text and put it together. Therefore, the result, the summary will use the exact same words, terms, and sentences as the original, and almost certainly even in the same order.

The second way is the abstractive [2]. In brief, creative reconstruction of a textual message built on its comprehension. It might sound futuristic to achieve this with a machine, but in fact with number of languages progress is good, and the main technical obstacles are indeed successfully tackled. Recently neural approaches in abstractive summarization achieved high performance development and impressive results. The so-called supervised learning model is widely used. A common approach is to use attention mechanism in the sequence-to-sequence framework. The other way relies on the usage of reinforcement learning. Unsupervised training strategies are also suggested.

II. THE ROLE AND THE PROBLEMS OF ARABIC

In fact, Arabic has many features, which on one hand provides us great ways to improve stability, but on the other it presents us challenges, which once surpassed can open up new fields of researches. One of the advantages of Arabic language is that besides its huge variety of dialects and spoken versions - which is a naturally occurring phenomenon - its formal written version (Fusha), a practically dead language, is highly standardized and lacks major regional variety. But it

still has a massive number of primary users and text providers, also a big amount of secondary users. Arabic also has another advantage, both scientifically and in the sense of application. It is one of the only 6 U.N. official language, so we have a big amount of translated official text.

The work for Arabic summarization is very recent and limited. This paper reflects on a specific approach of the abstractive text summarization, which deals with the Arabic language. And because large-scale pre-trained language models (LM), such as BERT [3] obtained new state-of-the-art results through diverse natural language processing tasks, including text summarization. Therefore, an application of BERT-based summarization model shall be attempted on Arabic, especially that they released a multilingual model that includes Arabic.

For that, we need a big enough dataset, enough amount of text and its summaries. And here comes the other logical question. From where should we acquire this corpus? One great source is the press, as many news articles have a lead, a brief - though sometimes misleading - overview of the material broadly spread out in the article, with details only supporting, but not altering the original message. So far, the problem is that news with reliable abstractive lead is very rare to find.

III. THE CURRENT PHASE

Sadly, the work of Arabic abstractive text summarization has hardly begun, the topic was hardly ever scratched. This, however, provides the advantage to open up new research fields and imply possibly new approaches, regardless the obvious difficulties it represents.

Work so far focused on collecting data, texts and summaries, to build up a big enough corpus even for preliminary tryouts. Also, the circle of press sources applying potentially useful summary routines was assessed, which can provide the basis for building the corpus.

In short that has the appearance of very little achievement, and indeed little success was reached. Given the nature of the task, however, and that work is done on a useful, but practically undigested language, the bulk of the work is the data collecting is being done now. Tryouts are promising at this stage, but it might take yet some time to show major results. Presenting a reliable corpus would be the first on the row, which is hopefully not far. The indications are reassuring.

REFERENCES

- [1] S. Narayan, S. B. Cohen, and M. Lapata, "Ranking sentences for extractive summarization with reinforcement learning," *arXiv preprint arXiv:1802.08636*, 2018.
- [2] R. Paulus, C. Xiong, and R. Socher, "A deep reinforced model for abstractive summarization," *CoRR*, vol. abs/1705.04304, 2017.
- [3] J. Devlin, M.-W. Chang, K. Lee, and K. Toutanova, "Bert: Pre-training of deep bidirectional transformers for language understanding," *arXiv preprint arXiv:1810.04805*, 2018.

State Space Reconstruction with Generative Models

András Attila SÜLYOK

(Supervisors: Kristóf KARACS, Péter SZOLGAY)

Pázmány Péter Catholic University, Faculty of Information Technology and Bionics

50/a Práter street, 1083 Budapest, Hungary

sulyok.andras.attila@itk.ppke.hu

I. INTRODUCTION

Partially Observable Markov Decision Processes (POMDPs, [1]) represent situations when it is either impossible or too costly to collect all information about the environment that would be necessary to make a perfect decision. It has been used in medical and healthcare, educational contexts, but simple robot control and automation problems can be described using its formalism.

It is also a challenging problem, since many possible environment states have to be considered, hence straightforward planning or model-based methods cannot be used.

A special type of these problems is when the agent has to collect the information for itself, a type of active learning.

In this work, we describe Reconnaissance Blind Chess [2], an illustrative task of this type, then propose a training approach.

A. Reconnaissance Blind Chess

Reconnaissance Blind Chess (RBC, [2]) is a variant of chess where neither of the two players can see the other's moves. Instead, before each move, they can choose a 3×3 square that is revealed to them (neither the location, nor the contents of this square is not revealed to the opponent). There is no concept of check, the goal is simply to capture the opponent's king.

This makes it necessary to develop an effective exploration strategy: the agent has to figure out the location of opponent pieces; on the other hand, it has to move in such a way so as to minimize prediction on the opponent's part.

This has obvious applications in any artificial or natural competition where there is a limited window to observe the others' strategies.

Note that it is still a symmetric problem: both players have the same limited observation capability based on which to make moves.

Since each player has only a belief over the actual board configuration (the location of all the pieces) and it is in each player's interests to manipulate the other one's belief, the state space effectively consists of not only the board configuration, but the opponent's current belief as well.

Markowitz et al. [2] estimate the number of possible opponent states in any given perceived state to be about $1.3 \cdot 10^{68}$ based on the possible observable histories: this makes RBC as complex as most of the tasks solved by model-free RL algorithms recently, while involving much larger uncertainty.

A further complication is that the board state changes with time: it changes after each sensing by two moves, only one (the player's own) is visible.

II. PROPOSED AGENT

Formulating the task as a simple POMDP problem, and using existing POMDP-solvers have the limitation that due to the large state space, they will either take a long time to learn or would need virtually infinite amount of memory. Likewise, because of the very limited observability, stock MDP-solvers cannot work either.

Instead, we propose an agent architecture that decomposes the task into submodules that we can train separately. There are three main modules: the sensing module to choose the location of the next sensing action, the reconstruction module to predict the current state and the policy module to choose the next move.

ACKNOWLEDGEMENT

This research has been carried out partly in the project Thematic Research Cooperation Establishing Innovative Informatic and Info-communication Solutions, which has been supported by the European Union and co-financed by the European Social Fund under grant number EFOP-3.6.2-16-2017-00013.

REFERENCES

- [1] E. J. Sondik, "The optimal control of partially observable markov processes over the infinite horizon: Discounted costs," *Operations Research*, vol. 26, no. 2, pp. 282–304, 1978. [Online]. Available: <http://www.jstor.org/stable/169635>
- [2] J. Markowitz, R. W. Gardner, and A. J. Llorens, "On the complexity of reconnaissance blind chess."
- [3] R. S. Sutton and A. G. Barto, *Reinforcement learning: An introduction*, 2nd ed. MIT press, 2018. [Online]. Available: <http://incompleteideas.net/book/the-book-2nd.html>

PROGRAM 5

ON-BOARD ADVANCED DRIVER ASSISTANCE SYSTEMS

Heads: Csaba REKECZKY, Ákos ZARÁNDY

The effect of outlier activations in neural networks

Jalal ALAFANDI

(Supervisor: András HORVÁTH)

Pázmány Péter Catholic University, Faculty of Information Technology and Bionics

50/a Práter street, 1083 Budapest, Hungary

alafandi.mohammad.jalal@itk.ppke.hu

Abstract—A Gaussian distribution is assumed for the activations of all layers in neural network. This assumption led to the use of batch normalization yielding faster training with better accuracy. We will demonstrate the flaw of this hypothesis in deeper layers where neurons are more task specific, and a large out-of-distribution activation is more common. Outlier activations will diverge the training from the true data distribution steering the weights towards specificity.

I. INTRODUCTION

Normalization has become a standard procedure in neural networks accelerating training and yielding a better accuracy. The original paper [1] proving the effect of normalization has assigned reducing internal covariate shift as the reason for batch normalization success. Batch normalization is a regularizer altering the parameters to stabilize the training procedure by forcing a smoother loss protecting the network from exploding or vanishing gradients and hyperparameters.

Batch normalization ultimate goal is to produce coherent distribution at each layer. The distribution can be identified by its moments (mean and variance) which can be transformed by batch normalization. Batch normalization modify the distribution to be zero mean and variance of one, then it will scale and shift the distribution according to a trainable parameters.

Although many other normalization approaches have been emerged e.g. [2] [3], the assumption of Gaussian distribution in the activations is unanimous. We will demonstrate that batch normalization will produce out-of-distribution moments even with large batches.

II. ACTIVATION OUTLIERS

Gaussian distribution assumption for all layers in neural network contradict the common belief that kernels in convolutional neural network are task specific only firing for a specific feature. This discrepancy is manifested clearly in the logits (the output of the network before using softmax function) of any classification problem where only one neuron should have a large activation while other neurons should have zero or negative activation.

We have investigated VGG-19 architecture where pretrained weights have been used (we have downloaded the model with its parameters from pytorch library) as in figure 1. We can clearly notice the large out-of-distribution (outside the 3σ band where $\sigma = 1$) activation at the last layer, but even in the earlier layers you will find a lot of outliers which can effect the regularization rule of normalization preventing the network from generalization. To illustrate that this problem of outliers does exist even without normalization, we investigated the activations of VGG-19 without batch normalization as in figure 2 where the variance can be estimated (it is not one any more) to see that a lot of large activations are present. In case of VGG-19 without batch normalization, the largest activations

can be found in the middle of the network while they are more concentrated at the last layer using batch normalization.

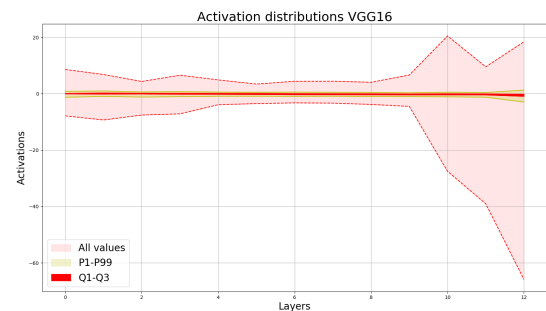


Fig. 1. This figure depicts the distribution of the activations in VGG-19 after the first convolutional layers. Only activations after convolutional layers are present. 98% can be found in the golden band and the middle dark red band contains 75% of the values. We can notice that at the last layer, large activations are present even after normalizing the activation distribution to be zero mean and variance of one.

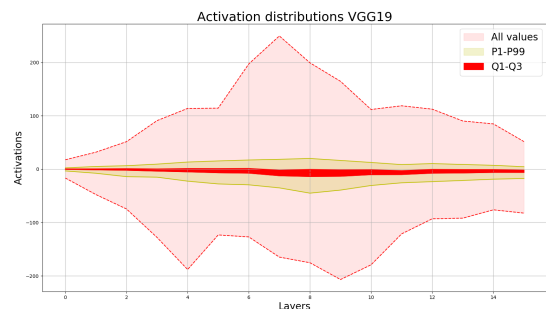


Fig. 2. This figure display the distribution of the activations after each convolutional layers in the VGG-19 architectures without batch normalization. On this figure 98% of the values are in the golden interval, based on this one can estimate the variance of each distribution (it is not normalized to 1 without batch normalization). One can see, that similarly to batch normalization, extreme activations are present in these cases as well.

REFERENCES

- [1] S. Ioffe and C. Szegedy, “Batch normalization: Accelerating deep network training by reducing internal covariate shift,” *arXiv preprint arXiv:1502.03167*, 2015.
- [2] S. Ioffe, “Batch renormalization: Towards reducing minibatch dependence in batch-normalized models,” in *Advances in neural information processing systems*, 2017, pp. 1945–1953.
- [3] Y. Wu and K. He, “Group normalization,” in *Proceedings of the European Conference on Computer Vision (ECCV)*, 2018, pp. 3–19.

Solving K-SAT Problems with Continuous Time Neural Networks

Dóra Eszter BABICZ

(Supervisors: András HORVÁTH, Csaba REKECZKY)

Pázmány Péter Catholic University, Faculty of Information Technology and Bionics

50/a Práter street, 1083 Budapest, Hungary

babicz.dora.eszter@itk.ppke.hu

NP complete problems are efficiently (polynomial time) checkable, but the worst-case complexity of finding a solution is exponential on Turing machines [1]. Because every NP-complete problem can be transformed into a Boolean satisfiability (k -SAT) in polynomial time, it increases the relevance of solving these types of problems [2]. Boolean satisfiability problems are a type of constraint satisfaction problems and are considered to be one of the hardest. Converting an NP-complete problem to a Boolean satisfiability (k -SAT) problem - can be done in polynomial time. k -SAT problems contain conjunctive normal formulas of variables in which every conjunction contains k number of variables. It was shown in [3] that k -SAT problems can be solved with analogue dynamics, avoiding local traps, and also in polynomial time, but with an exponentially increasing power consumption.

The definition of the k -SAT problem is the following: there are given N Boolean variables $x_i \in \{0, 1\}$ and a propositional formula \mathcal{F} which is a conjunction of M constraints C_i . Each constraint is a disjunctive form of k variables x_i or their negations \bar{x}_i . Solving this kind of problem means finding an assignment of the variables where all clauses (constraints) are satisfied. The form of the dynamics used in the circuits are very similar to regular cellular neural network dynamics and are the following:

$$\frac{dx_i(t)}{dt} = -x_i(t) + \sum_j w_{ij} f(x_j(t)) + u_i \quad (1)$$

where x_i is the state value (activation potential) of the cell, $f(x)$ is the output function of the neuron (usually sigmoid), u_i is the input or bias of the neuron and w_{ij} are connection weights between cells i and j .

The Continuous-time recurrent neural network can be defined on a bipartite graph with two type of nodes/cells. One is called the "s-type" and represents the variables of k -SAT. Their state value will be denoted by s_i , $i=1, \dots, N$ and the output function is defined as the following:

$$f(s_i) = \frac{1}{2}(|s_i + 1| - |s_i - 1|) \quad (2)$$

The output of $f(s_i) = 1$ is assigned to x_i Boolean variable when it is *TRUE* ($x_i = 1$) and if the variable is *FALSE* ($x_i = -1$), then $f(s_i) = -1$, but between these two extrema, any continuous value is allowed, meaning $f(s_i) \in [-1, 1]$. The self-coupling parameter will be a fixed value $w_{ii} = A$ and the input is $u_i = 0 \forall i$.

The other type of the cells represent the constraints of k -SAT

with value a_m , $m=1, \dots, M$ and with the output function of:

$$g(a_m) = \frac{1}{2}(1 + |a_m| - |a_m - 1|) \quad (3)$$

The "a-type" cells determine the impact of a clause at a given moment on the dynamics of the state (s) variables. When the clause is true, then $g(a_m) = 0$ and $g(a_m) = 1$ if it is false. For these cells the self coupling $w_{mm} = B$ and the input is $u_m = u = 1 - k$ where k is the number of variables in the clause, in this case $k = 3$.

The dynamics fulfill the following requirements:

- They have continuous-time dynamics
- All states, constraints and variables remain bounded
- The derivative of the dynamics is zero if and only if the formula is satisfied
- Starting from a chosen initial condition the system converges to a solution without getting trapped

The proof of the last two points along with a more detailed description can be found in [4]. An example problem in conjunctive form is the following:

$$\begin{aligned} &(\neg A_1 \vee A_2 \vee V) \wedge (A_1 \vee \neg A_2 \vee V) \wedge (A_1 \vee A_2 \vee \neg V) \\ &\wedge (\neg A_1 \vee \neg A_2 \vee \neg V) \wedge (\neg C \vee H \vee G) \wedge (D \vee H \vee F) \end{aligned}$$

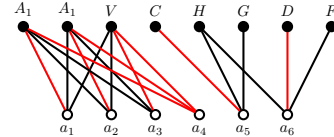


Fig. 1. Bipartite graph of the example problem

REFERENCES

- [1] Michael, R. Garey, and S. Johnson David. "Computers and intractability: a guide to the theory of NP-completeness." WH Freeman and Co., San Francisco (1979).
- [2] Cook, Stephen A. "The complexity of theorem-proving procedures." Proceedings of the third annual ACM symposium on Theory of computing. ACM, 1971.
- [3] Ercsey-Ravasz, Maria, and Zoltan Toroczkai. "Optimization hardness as transient chaos in an analog approach to constraint satisfaction." Nature Physics 7.12 (2011): 966-970.
- [4] Molnar, Botond, Zoltan Toroczkai, and Maria Ercsey-Ravasz. "Continuous-time neural networks without local traps for solving Boolean satisfiability." Cellular Nanoscale Networks and Their Applications (CNNA), 2012 13th International Workshop on. IEEE, 2012.

A Masonry Wall Image Inpainting Method with Adversarial Learning

Yahya IBRAHIM

(Supervisor: Csaba BENEDEK)

Pázmány Péter Catholic University, Faculty of Information Technology and Bionics

50/a Práter street, 1083 Budapest, Hungary

ibrahim.yahya@itk.ppke.hu

Abstract—Existing image inpainting methods use either pre-defined holes or low-level objects to fill in, moreover, these methods are globally-oriented purpose which makes it hard to tune it for a specific application. In this paper, we developed an end-to-end blind inpainting algorithm that specializes in masonry wall inpainting application, this algorithm can define the irregular objects (broken, hidden, occluded) of the wall, and predict the pattern of the original mortar and texture of these areas, which is considered as an initial and important step for many engineering and archeology applications. We propose a three-stage deep learning network that comprises a segmentation method followed by a two-stage adversarial inpainting model. The segmentation step is for detecting the irregular objects area and the pattern of the wall, the inpainting steps are for generating the mortar pattern and the color information that is expected to be in these areas. A new dataset has been created for training our method and it is used for evaluating our model, we show that our approach performs as the state-of-the-art inpainting techniques quantitatively and qualitatively.

Keywords—Inpainting; Adversarial; Masonry

I. INTRODUCTION

During the investigation of building masonry, accurate detection and outlining of their structural components is a key initial step of the documentation process [1]. In some cases the wall structure is invisible in some image segments because of some occlusions by various objects such as decorative elements, wall sculptures and vegetation (see examples in Fig.1), or in damaged wall parts in archaeological applications. We can consider that a way for virtually filling in the missing part is the application of image inpainting techniques.

Existing image inpainting methods can be divided into two main groups called *non-blind* and *blind* techniques. Our selected problem needs a significantly different blind inpainting approach from the existing ones: the occluded or damaged image regions may exhibit a high variety, however, we can assume that the *background*, which is a wall image, follows a regular pattern.

In this report, we propose an end-to-end deep learning based blind inpainting algorithm, which implements a segmentation step as pre-processing, followed by an adversarial model for inpainting. We tailored and tuned the algorithm to the above defined masonry wall completion task, in which the occluding objects are inpainted through modeling and understanding the texture features of the uncovered wall parts.

II. PROPOSED APPROACH

We propose a blind image inpainting network that consists of three stages: 1) image segmentation, 2) generation of hidden features, 3) image completion. We assume that the input of the algorithm is a masonry wall image which might be partially



Fig. 1: Examples of completion results.

occluded by one or several arbitrary shaped and textured foreground objects. The goal is to provide as output a reconstructed wall image, by automatic detection and inpainting of the occluded part.

The goal of the image segmentation step is twofold: extracting the wall structure by separation of the bricks from the mortar regions, and detecting the masks of possibly occluded wall segments which should be inpainted in the consecutive steps. In second step, the features in the hidden areas are predicted, in the last step the color of this missing holes is predicted by using the results of the feature generator.

III. RESULTS

For evaluating the first stage, we measure the detection accuracy of the wall regions occluded by irregular objects. Here we compare the occlusion mask provided by the U-Net to the corresponding reference map. We can confirm, that the U-Net network can detect the occluding objects with high accuracy as all of the virtually added irregular objects have been correctly detected.

At the evaluation stage of the G_1 Hidden Feature Generator, we compare both our reconstructed delineation mask, and as reference the output of the Canny based EdgeConnect algorithm [2], to the ground truth delineation map. Comparative qualitative test results demonstrate the superiority of our proposed method over the Canny based reference technique.

By evaluation of the last stage, we noticed that our measured values (PSNR, SSIM, Relative L_1 error) were similar to ones reported by state-of-the-art inpainting algorithms on public datasets [2].

REFERENCES

- [1] Y. Ibrahim, B. Nagy, and C. Benedek, “CNN-based watershed marker extraction for brick segmentation in masonry walls,” in *Int’l Conf. Image Analysis and Recognition*, 2019, pp. 332–344.
- [2] K. Nazeri, E. Ng, T. Joseph, F. Qureshi, and M. Ebrahimi, “Edgeconnect: Generative image inpainting with adversarial edge learning,” in *Int’l Conf. on Computer Vision Workshop (ICCVW)*, 2019, pp. 3265–3274.

Evaluating the quality of medical images using artificial intelligence

Ákos KOVÁCS

(Supervisors: András HORVÁTH, Tamás BÜKKI)

Pázmány Péter Catholic University, Faculty of Information Technology and Bionics

50/a Práter street, 1083 Budapest, Hungary

kovacs.akos@itk.ppke.hu

Abstract—The aim of my research is to create a neural network that can provide quantitative feedback on the quality of medical images. Neural networks can be used successfully in many areas, but in critical areas such as medical image processing, it is extremely important that the results be reliable and interpretable. The main goal of the research is to develop such networks and methods.

A summary of the different training strategies can show which strategy and error function is best suited to develop a neural network that analyzes image quality. This can not only provide a solution that can be used in medical fields, but can also be used to improve the object recognition capability of self-driving cars, for example.

Keywords-medical imaging; SPECT; AI; artificial intelligence; bone scintigraphy


I. INTRODUCTION

In recent years, solutions based on artificial intelligence have achieved breakthrough results in many areas. In practice, it has also shown that methods using deep learning can approximate the transformation function between data with high accuracy for large amounts of input and output data pairs [1].

Medical imaging methods have played an important role in the accurate diagnosis of certain disease groups for decades. When using traditional, global pixel-based metrics for evaluation, there is a risk that local changes will not adequately contribute to the value of the metric [2], [3], [4]. It is difficult to create a robust, well-functioning solution for the search for local features (such as the detection of the disappearance of cancerous lesions from the image, or the identification of artefacts), and their diversity is also a difficult circumstance. In the medical fields, therefore, phantom tests are performed in advance, and then the functionality of the solutions is evaluated with the involvement of doctors, as part of clinical validation [5]. However, this is an extremely costly and time-consuming process, so a preliminary evaluation using artificial intelligence can be expedient.

In the case of neural networks developed to support imaging procedures and diagnostic, it is especially important to test the robustness and generality of the solution. Thus, the resulting evaluation networks created for quantitative quality evaluation can be useful for testing them as well.

ACKNOWLEDGEMENT

 SUPPORTED BY THE ÚNKP-19-3 NEW NATIONAL EXCELLENCE PROGRAM OF THE MINISTRY OF HUMAN CAPACITIES

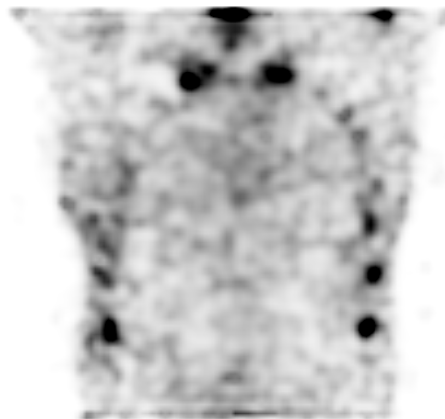


Fig. 1. A noisy bone SPECT measurement with stripe artifacts (bottom and top). We can also see, that it is really hard to quantitatively measure the quality of medical images about real patients. It is also very important that we cannot prepare for all failures, such as the phenomenon shown in the picture.

REFERENCES

- [1] I. Goodfellow, Y. Bengio, and A. Courville, *Deep Learning*. MIT Press, 2016. <http://www.deeplearningbook.org>.
- [2] L. Kang, P. Ye, Y. Li, and D. Doermann, “Convolutional Neural Networks for No-Reference Image Quality Assessment,” in *2014 IEEE Conference on Computer Vision and Pattern Recognition*, (Columbus, OH, USA), pp. 1733–1740, IEEE, June 2014.
- [3] M. A. Villan, “afsalashyana/FakeImageDetection,” Sept. 2019. original-date: 2016-07-14T11:39:32Z.
- [4] X. Jiang, L. Shen, G. Feng, L. Yu, and P. An, “Deep Optimization model for Screen Content Image Quality Assessment using Neural Networks,” *arXiv:1903.00705 [cs]*, Mar. 2019. arXiv: 1903.00705.
- [5] L. S. Graham, “Quality control for SPECT systems.,” *RadioGraphics*, vol. 15, pp. 1471–1481, Nov. 1995.

Change detection in Lidar point clouds

Lóránt KOVÁCS

(Supervisor: Ákos ZARÁNDY)

Pázmány Péter Catholic University, Faculty of Information Technology and Bionics

50/a Práter street, 1083 Budapest, Hungary

kovacs.lorant@itk.ppke.hu

I. INTRODUCTION

The navigation and scene understanding of the currently developed autonomous vehicles in urban areas is often aided by prerecorded maps. These maps can contain georeferenced road structure information and Lidar point clouds. The interest of my research is on the point clouds.

The application of point cloud maps has several challenges. The creation and the update of the maps is an expensive task, but even the information from the maps might become outdated, as the map gets older. For example the street furniture or even the vegetation can be changed easily, leading the affected map regions to become obsolete. There are current methods on object detection and removal in 3D maps [1], [2].

To be able to use the Lidar point cloud map as an a priori information for scene understanding and navigation, usually a very accurate registration and calibration [3], [4] is needed for both the map and the vehicle's Lidar sensor. Besides the calibration, the proper registration and alignment of the clouds is needed as well for point-wise methods. And one might have to handle the different density of the point clouds.

My research focuses on change detection among Lidar point clouds, where the point clouds are recorded in the same environment and roughly at the same position, but they do not have a common registration.

II. DATA COLLECTION

To find the answer to this research task, a significant amount of data is required: Lidar point cloud pairs from the same location at different times. The following data collection pipeline was used: a car was equipped with a Velodyne HDL-64E rotating multi-beam Lidar, and an industrial PC collected the 3D point cloud data by driving multiple times on a selected path in an urban environment. The visible scenes were recorded by cameras and the GPS position of the vehicle was logged as well.

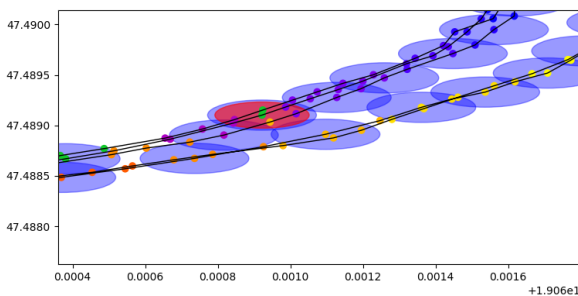


Fig. 1. Example of clustered point cloud measurement locations

III. DATA PREPARATION

The recorded images were helpful for selecting the measurement segments for the sub tasks of the research. The GPS positions were used to cluster the recorded point clouds based on their location - to achieve corresponding measurements (Fig. 1.). The raw Lidar stream was splitted to separate point clouds. The GPS positions were assigned to the point clouds, where the cloud and position acquisition time matched. As the sampling frequency of the Lidar and the GPS are different (15Hz vs. 1 Hz), initially only the minority of the clouds have their GPS positions assigned. For the assessment of the concept, only these located clouds are used, but later the dataset can be extended using interpolation, motion offset estimations for the point clouds without assigned position.

IV. CHANGE DETECTION

To train a system for detecting changes on among unregistered Lidar point clouds, a significant amount of labeled dataset is required. This was achieved by annotating the segments of the recorded point clouds: the points were annotated as they belong to foreground/dynamic objects or to the background/static objects.

The change detection on unregistered point clouds is under investigation, the results are going to be published soon.

ACKNOWLEDGEMENTS

The support of the Széchenyi 2020 Program, of the Human Resource Development Operational Program, of the Program of Integrated Territorial Investments in Central-Hungary and of the European Structural and Investment funds (EFOP-3.6.2-16-2017-00013, 3.6.3-VEKOP-16-2017-00002 and EFOP-3.6.2-16-2017-00002) are gratefully acknowledged. Supported by the ÚNKP-19-3-I-PPKE-86 New National Excellence Program of the Ministry of human capacities.

REFERENCES

- [1] O. Zovathi, L. Kovacs, B. Nagy, and C. Benedek, "Multi-Object Detection in Urban Scenes Utilizing 3D Background Maps and Tracking," *Proceedings - 2019 3rd International Conference on Control, Artificial Intelligence, Robotics and Optimization, ICCAIRO 2019*, pp. 231–236, 2019.
- [2] B. Nagy and C. Benedek, "3D CNN based phantom object removing from mobile laser scanning data," *Proceedings of the International Joint Conference on Neural Networks*, vol. 2017-May, pp. 4429–4435, 2017.
- [3] B. Nagy, L. Kovacs, and C. Benedek, "Online targetless end-to-end camera-lidar self-calibration," in *Proceedings of the 16th International Conference on Machine Vision Applications, MVA 2019*, pp. 1–6, IEEE, may 2019.
- [4] B. Nagy and C. Benedek, "On-the-Fly Camera and Lidar Calibration," *Remote Sensing*, vol. 12, p. 1137, apr 2020.

On-the-fly Camera-Lidar calibration

Balázs NAGY

(Supervisor: Csaba BENEDEK)

Pázmány Péter Catholic University, Faculty of Information Technology and Bionics
50/a Práter street, 1083 Budapest, Hungary
nagy.balazs@itk.ppke.hu

Abstract—In this paper we propose an automatic, online and target-less camera-Lidar extrinsic calibration approach. We turn into a structure from motion (SfM) method to generate 3D point clouds from the camera data and we address the extrinsic calibration problem as a registration task in the 3D domain. The core step of the approach is a two-stage transformation estimation: first we introduce an object level course alignment to transform the source and the target point clouds into a common coordinate system and next we propose a control point based nonrigid transformation to register the point clouds more precisely. We evaluated the method in various real life traffic scenarios in Budapest, Hungary.

Keywords—calibration; LIDAR; point cloud; camera

I. INTRODUCTION

Nowadays, state-of-the-art autonomous system rely on wide range of visual sensors such as *optical cameras*, *radars* and *Lidars*, so robust sensor and data fusion are quickly getting one of the main focus and challenges in the field of self driving vehicles and robotics. While real time Lidars, such as Velodye’s rotating multi-beam (RMB) sensors provide accurate 3D geometric information with relatively low vertical resolution, optical cameras capture high resolution feature rich data with color and texture information enabling to extract low level details from the scene. A common problem with optical cameras that lighting conditions (dark, strong sunlight) may cause a great effect on the captured data while Lidars are able to provide reliable information independently from the illumination.

II. THE PROPOSED APPROACH

To avoid feature (2/3D interest points, line and planar segments) detection, we propose a two-stage calibration approach where first we use a motion based (SfM) [1] approach to generate 3D model from the consecutive image frames recorded by the moving vehicle. In such manner, the calibration task can be defined as a point cloud registration problem. We proposed a robust object based course alignment method [2] to estimates a sufficient initial translation between the Lidar point cloud and the synthesized 3D data. Based on extracted object center points the method is able to calculate the best overlap in object level between the Lidar and the synthesized point cloud. Based on our experiences, we observed that in synthesized point clouds, dynamic object such as vehicles and pedestrians often fall apart into several blobs due to several occlusions and artifacts during the SfM pipeline which fact may cause inaccurate matching between the objects. To handle this issue we eliminate the dynamic objects both from the image and the Lidar point cloud data applying state-of-the-art object detectors: Mask R-CNN [3] provide an instance level semantic segmentation on images while Point pillars method [4] is able to detect dynamic objects in the Lidar point cloud.

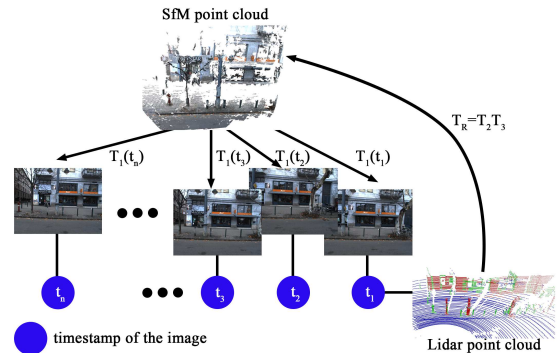


Fig. 1. Workflow of the projection calculation process.

After the initial transformation estimation step we refine the registration error using the ICP point level method and we propose a NURBS curve based method to deform the Lidar point cloud according to the local properties of synthesized point cloud.

Finally, the proposed approach ensures three matrices to project the 3D Lidar points onto the 2D image pixels: T_1 is calculated during the SfM method which is able to project the synthesized 3D points to the corresponding pixel coordinates, T_2 transforms the Lidar point cloud to the coordinate system of the synthesized one using the object level alignment, T_3 perform an ICP based registration refinement and T_4 which is a non-rigid body transformation scales and deforms the local point cloud parts. After applying T_2 and T_3 and T_4 transformations to the Lidar point cloud T_1 can be used to projects the Lidar points onto the image.

Fig. 1 demonstrate the workflow of the proposed approach.

III. ACKNOWLEDGMENT

This work was supported by the National Research, Development and Innovation Fund (grants NKFI K-120233 and KH-125681), and by the Széchenyi 2020 Program (grants EFOP-3.6.2-16-2017-00013 and 3.6.3-VEKOP-16-2017-00002). Balázs Nagy was also supported by the ÚNKP-19-3 New National Excellence Program of the Ministry of Human Capacities.

REFERENCES

- [1] P. Moulon, P. Monasse, R. Marlet, *Global Fusion of Relative Motions for Robust, Accurate and Scalable Structure from Motion*, IEEE International Conference on Computer Vision (ICCV), 2013.
- [2] B. Nagy, C. Benedek, *Real-time point cloud alignment for vehicle localization in a high resolution 3D map*, Workshop on Computer Vision for Road Scene Understanding and Autonomous Driving (ECCV), 2018.
- [3] K. He, G. Gkioxari, P. Dollár, R. Girshick, *Mask R-CNN*, IEEE International Conference on Computer Vision (ICCV), 2017.
- [4] Lang, Alex H., Vora, *PointPillars: Fast Encoders for Object Detection From Point Clouds*, The IEEE Conference on Computer Vision and Pattern Recognition (CVPR), 2019.

Different aspects of learning in biological and mathematical systems

Franciska Sára RAJKI

(Supervisor: András HORVÁTH)

Pázmány Péter Catholic University, Faculty of Information Technology and Bionics

50/a Práter street, 1083 Budapest, Hungary

rajki.franciska.sara@itk.ppke.hu

Abstract—With the help of Deep Dream algorithm [1], we can visualize what a neural network sees. We need a convolutional neural network that is trained to classify a big dataset. For this we used an InceptionNet V1 [2] that is pretrained on ImageNet. [3] The first layers learn simple features, while going deeper in the network we can see complex, recognisable structures, like animal heads.

I. SUMMARY

During the Deep Dream algorithm our networks weights are frozen, and the input image is changed in a way to give maximal answer to the chosen layers or neurons. For this to generate nice images, the networks weights has to be already trained. Also we have to cut the input image to tiles, and optimize these tiles to the chosen neuron one by one. The tiles has to be chosen randomly, so their border is not too visible. After having the optimized tiles, these need to be blended together nicely. I used an available implementation of the Deep Dream algorithm. [4]

The InceptionNet V1 has twelve layers. To generate these images (1 2) I used the tenth layer of the network. This is why the first image shows a recognisable dog head. This is a deep enough layer to learn such complex structures. The input image was a simple color gradient image, with one darker blot in the middle, to have an obvious spot to optimize.

REFERENCES

- [1] K. Simonyan, A. Vedaldi, and A. Zisserman, “Deep inside convolutional networks: Visualising image classification models and saliency maps,” *preprint*, 12 2013.
- [2] C. Szegedy, Wei Liu, Yangqing Jia, P. Sermanet, S. Reed, D. Anguelov, D. Erhan, V. Vanhoucke, and A. Rabinovich, “Going deeper with convolutions,” in *2015 IEEE Conference on Computer Vision and Pattern Recognition (CVPR)*, pp. 1–9, 2015.
- [3] J. Deng, W. Dong, R. Socher, L.-J. Li, K. Li, and L. Fei-Fei, “ImageNet: A Large-Scale Hierarchical Image Database,” in *CVPR09*, 2009.
- [4] M. E. Hvas Pedersen, “TensorFlow-Tutorials GitHub.”

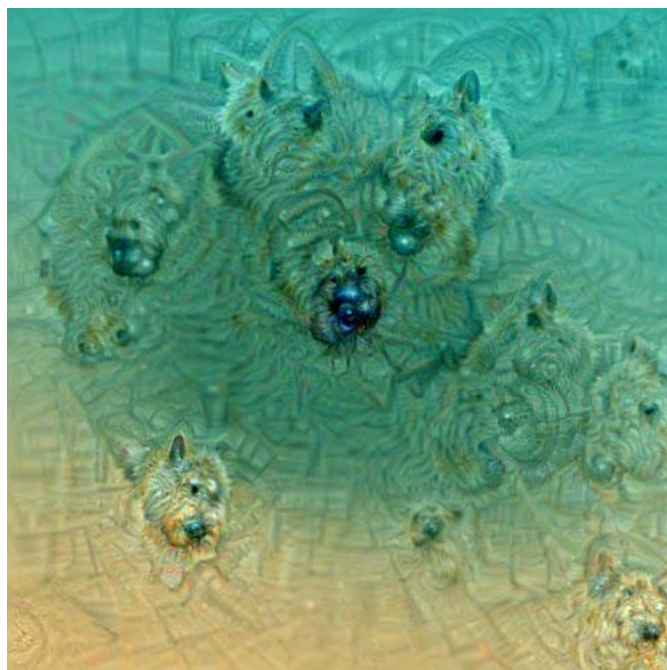


Fig. 1. Image generated with deep dream algorithm, showing recognisable structures.

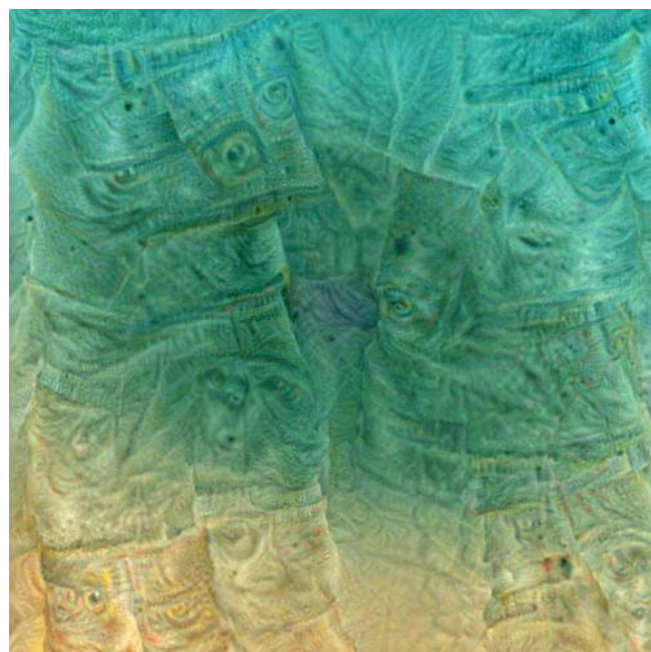


Fig. 2. Image generated with deep dream algorithm, showing learned features.

Improving 3D Object Detection in Lidar Point Clouds

Örkény Ádám H. ZOVÁTHI
(Supervisor: Csaba BENEDEK)

Pázmány Péter Catholic University, Faculty of Information Technology and Bionics
50/a Práter street, 1083 Budapest, Hungary
h.zovathi.orkeny.adam@itk.ppke.hu

Abstract—In this paper we propose a general method for improving the performance of real time dynamic object detection methods operating on point clouds captured by Rotating Multi-Beam (RMB) Lidar sensors, using nowadays widely available high resolution city maps obtained by Mobile Laser Scanning. The algorithm takes the predictions of a state-of-the-art object detector as input and refine its results using the following consecutive core steps: accurate alignment of the RMB measurements to the city map, a grid based probabilistic step to filter out *falsely detected* object regions and a point level change detection and recognition step to find *erroneously missed objects*. Exploiting the information stored in the city maps, we are able to omit typical misdetections and therefore improve the overall performance and reliability.

Keywords—Lidar; Point cloud; Object detection

I. INTRODUCTION

Recent scientific and engineering progress in autonomous driving make us believe that cars will be able to drive without human intervention in the near future. Modern autonomous vehicles are often equipped with Rotating Multi-beam (RMB) Lidar sensors, since they are robust through different weather and lightning conditions and provide strong geometric information about their surrounding. However, due to the spatial sparsity and inhomogeneity of the sensor data, dynamic object detection [1] on such point clouds still remains a key challenge, especially in urban environment with many traffic participants and various occlusion effects.

On the other hand, Mobile Laser Scanning (MLS) technologies can nowadays efficiently obtain high resolution 3D maps of cities, providing dense, accurate and homogeneous point clouds from the static environment. Our main idea is to exploit all the information stored in these 3D maps in order to overcome the typical errors of the state of the art object detection algorithms.

A. Related work

Propagating low level information from 3D maps to object detection is a quite new area in the literature. A promising method is [2], which uses a prior *road map* with local *ground-height* data as reference, helping the elimination of false object candidates detected out of the road, or above/under the ground level. However, it does not deal with the confusion of dynamic objects with static regions from the map, which is the main address of our paper.

II. PROPOSED METHOD

Initially, we apply a state-of-the-art object detection algorithm [1] to detect object candidates on the raw RMB Lidar frames. Then, we refine this output in three key steps: First, we accurately register the input RMB Lidar point cloud frame

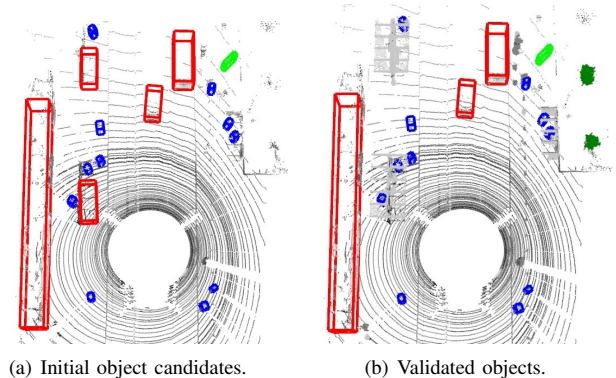


Fig. 1. Detected objects without (a) and with (b) map information.

to the MLS based high resolution city map with an object level coarse [3] and point level fine alignment [4]. Then, we apply a probability map based validation step [5] where we compare all object candidates to regions of the city map and remove *false positive* predictions. Finally, we apply a point level change detection between our captured RMB frame and the city map using a Markov Random Field based segmentation, and identify *previously undetected* object candidate blobs in the extracted changed regions.

ACKNOWLEDGEMENTS

This work was supported by the Széchenyi 2020 Program grants EFOP-3.6.2-16-2017-00013.

REFERENCES

- [1] A. Lang, S. Vora, H. Caesar, L. Zhou, J. Yang, and O. Beijbom, “PointPillars: Fast Encoders for Object Detection from Point Clouds,” in *IEEE Conference on Computer Vision and Pattern Recognition (CVPR)*, 2019.
- [2] B. Yang, M. Liang, and R. Urtasun, “HDNET: Exploiting HD Maps for 3D Object Detection,” in *Conference on Robot Learning*, vol. 87 of *Proceedings of Machine Learning Research*, pp. 146–155, 29–31 Oct 2018.
- [3] B. Nagy and C. Benedek, “Real-time point cloud alignment for vehicle localization in a high resolution 3D map,” in *Workshop on Computer Vision for Road Scene Understanding and Autonomous Driving at ECCV’18*, vol. 11129 of *LNCS*, pp. 226–239, 2019.
- [4] P. Biber and W. Strasser, “The Normal Distributions Transform: A New Approach to Laser Scan Matching,” in *IEEE International Conference on Intelligent Robots and Systems*, vol. 3, pp. 2743 – 2748 vol.3, 11 2003.
- [5] Ö. Zováthi, L. Kovács, B. Nagy, and C. Benedek, “Multi-object detection in urban scenes utilizing 3D background maps and tracking,” in *2019 International Conference on Control, Artificial Intelligence, Robotics Optimization (ICCAIRO)*, pp. 231–236, 2019.

APPENDIX

PROGRAM 1: Bionics, Bio-inspired Wave Computers, Neuromorphic Models

Name	Supervisor
András ADOLF	István ULBERT MD DSc
Luca Anna BORS	Franciska ERDŐ PhD
Suchana CHAKRAVARTY	Attila CSIKÁSZ-NAGY DSc
Veronika CSILLAG	Imre FARKAS MD PhD, Zsolt LIPOSITS MD DSc
Ward FADEL	István ULBERT MD DSc, Lucia WITTNER MD PhD
Bianka Vivien FARKAS	Zoltán GÁSPÁRI PhD, Tamás HEGEDŰS PhD
Anna HAJDARA	Balázs MAYER PhD, Miklós GYÖNGY PhD
Zita HARMAT	Zoltán GÁSPÁRI PhD
Regina KALCSEVSZKI	Sándor PONGOR MHAS
Zsófia Etelka KÁLMÁN	Zoltán GÁSPÁRI PhD
Máté KÁLOVICS	Kristóf IVÁN PhD
Bence Márk KEÖMLEY-HORVÁTH	Attila CSIKÁSZ-NAGY DSc, István Zoltán REGULY PhD
Márton Zsolt KISS	Ákos ZARÁNDY DSc
Barnabás KOCSIS	István ULBERT MD DSc
Csaba Márton KÖLLŐD	István ULBERT MD DSc
Dániel Zoltán KOLPASZKY	Kristóf IVÁN PhD
Adrienn Lilla MÁRTON	Kristóf IVÁN PhD
Gergely MÉSZÁROS	István ULBERT MD DSc, Dániel HILLIER PhD
Marcell MISKI	Attila CSIKÁSZ-NAGY DSc
Máté MOHÁCSI	Tamás FREUND MHAS, Szabolcs KÁLI PhD
Eszter NAGY-KANTA	Zoltán GÁSPÁRI PhD
Bence NÉMETH	András HORVÁTH PhD
Anna SÁNTA	Zoltán GÁSPÁRI PhD
Ágnes SZABÓ	Zoltán FEKETE PhD
Mihály SZŰCS	Kristóf IVÁN PhD
Luca TAR	Tamás FREUND MHAS, Szabolcs KÁLI PhD
Zsófia VARGA-MEDVECZKY	Franciska ERDŐ PhD
Moutz WAHDOW	István ULBERT MD DSc

PROGRAM 2: Computer Technology Based on Many-core Processor Chips, Virtual Cellular Computers, Sensory and Motoric Analog Computers

Name	Supervisor
Nawar AL-HEMEARY	Gábor SZEDERKÉNYI DSc, György CSEREY PhD
Gábor Dániel BALOGH	Péter SZOLGAY DSc, István Zoltán REGULY PhD
Attila FEJÉR	Péter SZOLGAY DSc
Mary GUINDY	Péter SZOLGAY DSc, Vamsi Kiran ADHIKARLA PhD
Dániel HAJTÓ	György CSEREY PhD
Sam KHOZAMA	Zoltán NAGY PhD, Zoltán GÁSPÁRI PhD
Ádám NAGY	Ákos ZARÁNDY DSc
Péter POLCZ	Gábor SZEDERKÉNYI DSc
Levente Márk SÁNTHA	Ákos ZARÁNDY DSc, Zoltán NAGY PhD
Bálint SIKLÓSI	Péter SZOLGAY DSc, István Zoltán REGULY PhD
Gergely SZLOBODNYIK	Gábor SZEDERKÉNYI DSc

PROGRAM 3: Feasibility of Electronic and Optical Devices, Molecular and Nanotechnologies, Nano-architectures, Nanobionic Diagnostic and Therapeutic Tools

Name	Supervisor
András FÜLÖP	György CSABA PhD, András HORVÁTH PhD
Janka HATVANI	Miklós GYÖNGY PhD
Péter MAROSÁN	Miklós GYÖNGY PhD
Zsolt MEZRICZKY	J. Balázs RÓZSA PhD
Tamás RUDNER	György CSABA PhD

PROGRAM 4: Human Language Technologies, Artificial Understanding, Telepresence, Communication

Name	Supervisor
András Pál HALÁSZ	Péter SZOLGAY DSc, Kálmán TORNAI PhD
Kamran IBIYEV	Gábor PRÓSZÉKY DSc
Mram KAHLA	Gábor PRÓSZÉKY DSc
András Attila SULYOK	Péter SZOLGAY DSc, Kristóf KARACS PhD

PROGRAM 5: On-board Advanced Driver Assistance Systems

Name	Supervisor
Mohammad Jalal ALAFANDI	András HORVÁTH PhD
Dóra Eszter BABICZ	Csaba REKECZKY PhD, András HORVÁTH PhD
Yahya IBRAHIM	Csaba BENEDEK PhD
Ákos KOVÁCS	Tamás BÜKKI PhD, András HORVÁTH PhD
Lóránt KOVÁCS	Ákos ZARÁNDY DSc
Balázs NAGY	Csaba BENEDEK PhD
Franciska Sára RAJKI	András HORVÁTH PhD
Örkény Ádám H. ZOVÁTHI	Csaba BENEDEK PhD
